EUROPEAN ORGANIZATION FOR NUCLEAR RESEARCH

NP Internal Report 75-3
3 July 1975

FINAL REPORT ON THE EXPLORATORY EXPERIMENT ON THE INVESTIGATION OF HIGH MULTIPLICITY GAMMA-RAY EVENTS

G.F. Dell, H. Uto and L.C.L. Yuan
CERN, Geneva, Switzerland

and

Brookhaven National Laboratory*), Upton, NY, USA

E. Amaldi, M. Beneventano, B. Borgia, L. Luminari,
P. Pistilli and I. Sestili
CERN, Geneva, Switzerland

and

Istituto di Fisica dell'Università di Roma
and INFN, Sezione di Roma, Italy

J. Dooher
Adelphi University, New York, NY, USA

G E N E V A
1975

---

*) Work performed under the joint auspices of the U.S. Energy Research & Development Administration in collaboration with the U.S. National Aeronautics & Space Administration and the Research Corporation of New York.

SUMMARY

An experiment investigating high-multiplicity gamma-ray events in a region covering 18% of 4π around 90° in the centre of mass has been performed at the CERN ISR by sharing the detector of the CERN-Columbia-Rockefeller group. Information on the dependence of the cross-section on gamma-ray multiplicity as well as the dependence of the average gamma-ray and charge multiplicities on the centre-of-mass energy has been obtained. Studies have been made of correlations between the number of gamma-rays and charged particles, as well as between the total number of gamma-rays plus charged particles and the total measured energy per event. Two-body inclusive rapidity distributions in the rapidity interval 0.86 to -0.86 covered by the detector are also presented.

The main corrections to the data, as well as considerations of background effects, are extensively discussed in the appendices. Also discussed in the appendices are a Monte Carlo calculation of the gamma-ray multiplicity distribution expected from π^0 decay and a calculation based upon an independent emission model of π^0 production. Both calculations give identical results, which are found to be several orders of magnitude lower than the experimental results for gamma multiplicities ≥ 10.

CONTENTS

1. INTRODUCTION

In the fall of 1970, the Brookhaven-Grumman-Rome (BGR) Collaboration presented a proposal for an experiment aiming to detect multigamma events by means of a set-up designed to cover about 60% of the total solid angle around an intersection region of the ISR[1]. The proposal was motivated by two kinds of physical problems: a) Since the great majority of the gamma-rays originate from the decay of π^0, a study of events with many photons would provide information on the multiplicity of the parent pions, their correlations, etc. b) Around 1955 a few events were observed, in stacks of nuclear emulsions exposed to cosmic rays at high altitude, which show that between 16 and 24 gamma-rays were converted into electron-positron pairs in a length varying between 1 and 2 radiation lengths[2]. These observed events could not be accounted for either by conventional electromagnetic showers originating from a single high-energy gamma (or electron) or by conventional nuclear interactions with the production of many π^0's.

Since the estimated energies of the primaries of these events are very close to the equivalent energy of the ISR colliding beams it seemed to us that a multigamma-ray search experiment at the ISR would provide a unique opportunity for recognizing whether events of this type are simply caused by extreme fluctuations of the usual multiple production of pions or due to a different physical origin.

In August of 1971 the ISR Committee suggested to us to try first an exploratory experiment by sharing an existing detector system of some other group already working at the ISR, mainly to see if there were present a sufficiently large number of multigamma events which had not been looked for before.

Since the CERN-Columbia-Rockefeller (CCR) detector system appeared to be most suitable for this type of experiment[3], the BGR group discussed with the CCR group the possibility of sharing the use of their equipment for a preliminary search for multigamma events. The CCR group kindly agreed to this proposition and suggested that we could add our trigger to their electronics, to trigger our own electronic system, provided that the connection of the outputs of their counters to the BGR circuit would not disturb their experiment.

Besides sharing the detector system and the associated electronics, the BGR shared also the recording system of the CCR group. This was done by having all the BGR events recorded on the same tape with a special code, so that, later, they could easily be transferred to separate tapes.

It was clear from the beginning that for the search for multigamma events, the CCR counter arrays had the considerable disadvantage of covering only a small fraction, namely 18%, of the total solid angle and of being concentrated around 90° with respect to the direction of motion of the two colliding protons in their centre-of-mass system, so that the forward and backward cones were completely uncovered.

Moreover, since the CCR group focused its interest and effort on investigating comparatively rare events associated with high-energy gammas or electrons, the apparatus was not well suited for the study of processes with many low-energy photons. Nevertheless, a satisfactory and valuable exploratory experiment has been carried out with the shared detector equipment described above and some rather interesting results have been obtained.

A few preliminary results have been already made known elsewhere[4]. In Section 2 we shall briefly describe the main features of the detector and the kind of triggers we have used. After a few general remarks on the nature of the recorded events and their analysis (Section 3) we discuss the spectrum of the gamma-rays observed in a single lead-glass counter -- in particular its slope -- as well as the cross-section for production of at least one gamma-ray at 90° with respect to the direction of the pp collision. We find that both the slope and cross-section agree with the values obtained by other authors (Section 4).

We shall then discuss a number of pairs of regression lines from which one can conclude that (Section 5): (a) the multiplicity of the observed gamma-ray does not depend, or depends very weakly, on the transverse momentum or energy of a single photon; (b) the total energy observed in gamma-rays increases by increasing the multiplicity.

The two-body inclusive rapidity correlations will also be discussed and found to be in reasonable agreement with similar results of other authors (Section 6).

Finally, we shall discuss the multiplicity distribution, the average multiplicity (Section 7) and the influence of the trigger mode on these observed quantities (Section 8). The average multiplicity of neutral secondaries (mainly gamma-rays) as well as the tails of the corresponding distributions, observed in a rather narrow region around 90°, are considerably larger than those computed from π^0 uncorrelated production (Section 9).

2. THE EXPERIMENTAL EQUIPMENT AND THE TRIGGER

Figures 1 and 2 show a top and a longitudinal view of one of the two identical detectors of the CCR group placed on the two opposite sides of the intersection region. Its details have been discussed on various occasions[5] and will not be repeated here.

The gamma-rays are detected by 16 + 16 lead-glass Čerenkov counters, about 3 radiation lengths ($3X_0$) thick, denoted by HV, behind which there are 60 + 60 Čerenkov counters, about $15X_0$ thick, denoted by LB.

The values of the variable[6)]

$$\eta = -\ln \operatorname{tg} \frac{\theta^*}{2} \qquad (2.1)$$

for particles emitted from the centre of the interaction region (i.r.) in the direction of the contour of the HV counters are shown in Fig. 3. Since for gamma-rays this variable is identical to the c.m. rapidity, one can keep in mind that the deviation from linearity of the rapidity, as a function of x and y, is small over the whole surface of the detectors and is negligible within each HV counter. The interval of c.m. rapidity covered by each HV counter is shown in Table 1, from which it follows that the total interval covered by the detector out (in) extends from +0.86 (+0.66) to -0.86 (-0.66).

The scintillators A, Z and B (5, 10 and 6 in each detector) add information to that provided by the spark chambers, which allow the recognition and reconstruction of the tracks crossing the detector.

Besides the counters shown in Figs. 1 and 2, two types of beam counters in coincidence were used in the trigger. They allowed a reduction in the background by requiring that in each event the timing of the pulses corresponded to fast particles produced within the interaction region (i.r.). Their geometry is summarized in Table 2. Downstream in each beam there was a single Σ_i counter and two B_i counters. The $\Sigma\Sigma$ counters were designed for detecting a large fraction of the interactions (Table 2), while the counting rate of the BB counters was about 5 times lower.

The trigger can be described symbolically as

$$M_t \cdot \Sigma\Sigma \cdot \bar{V} \quad \text{or} \quad M_t \cdot BB \cdot \bar{V}$$

where $\bar{V}$ is a veto against pick-ups and other disturbances, $\Sigma\Sigma$ (or BB) is the coincidence between the Σ_1 $(B_1 \cdot B_1')$ and Σ_2 $(B_2 \cdot B_2')$ counters, and M_t means that at least t out of the 32 HV counters were fired in coincidence, each with a threshold of E^e_{th}. The threshold of the HV triggers was originally set at $E^e_{th} = 0.160$ GeV, which is more than twice the average energy deposited by a fast charged particle in an HV counter. Such a value would most likely ensure that the HV counts forming the trigger are due mainly to gamma events. The value of E^e_{th}, however, changed during the experiment, mainly because of the radiation damage undergone by the lead glass (Section 4).

Once an event was obtained by such a trigger, the energies and positions of all the Čerenkov counters fired, as well as the information on all the charged tracks given by the scintillators and wire spark chambers, were completey recorded.

Runs were made at various values of the momentum p_0 of the protons circulating in the ISR, and with different trigger modes (Table 3). In the majority of the runs, the value of t was set equal to 4 because we wanted a high multiplicity and we wanted to avoid too high a counting rate, which would affect the CCR event rate. But, even under this condition, our counting rate was still so large at high beam energies that it was necessary to introduce an artificial dead-time of up to 3 sec that was adjusted to keep the counting rate about 1/10 of that of the CCR group.

Only a few runs were made with t = 3, 2 and 1, respectively (Table 3). Those at t = 1 were essential for converting our counting rates into cross-sections for production of gamma-rays that could be compared with results of other authors (Section 4). The comparison of the data obtained with different trigger modes provides a very useful check of their internal consistency (Section 8).

3. GENERAL REMARKS ON THE ANALYSIS OF THE EVENTS

The HV fired in each event have been divided into two classes[4]: charged HV (HV^c) are defined as those HV fired with a pulse greater than the adopted cut-off energy E_{cf} and with one (or more) reconstructed wire chamber track(s) crossing them.

The neutral HV (HV^n) are those HV that show a pulse ($\geq E_{cf}$), but do not have any track of charged particles crossing their entrance surface. The majority of the neutral HV are fired by neutral particles such as gamma-rays, n, or $\bar{n}$, while the majority of the charged HV are fired by charged particles. Such a distinction, however, is not rigorous but the over-all correction is small. For example, the class of (HV^n) includes a certain number of HV fired by charged particles, whose track has not been reconstructed, either because of the limited efficiency of the wire chambers, or because the computer was confused by the presence of too many sparks.

These are two of the five main corrections (Appendix A) to be applied to the observed numbers of HV^n and HV^c. Their estimated values are summarized in Table A.1, from which we can conclude that each correction is rather small, and that they compensate each other almost exactly giving an over-all correction of the order of 1%. Such a correction has not been applied to the observed numbers which are affected by statistical as well as systematic errors which are appreciably greater. Here by systematic errors we mean errors arising from normalization errors (Section 4) and background (Appendix B).

The background was determined, for both BB and $\Sigma\Sigma$ trigger modes by three types of measurements: (a) single-beam runs; (b) delayed coincidences (such as $[M_t^{del} \cdot \Sigma\Sigma]$ or $[M_t \Sigma_1 \cdot \Sigma_2^{del}]$); (c) events triggered at random (pedestal events).

In the case of BB trigger modes, the estimated background is of the order of 1%, while for ΣΣ trigger modes it is not more than 10%. Finally the HV multiplicity of the events triggered at random amounted, in the worst case, to 0.3 count/event.

The results presented in the following have not been corrected for the background. We have, however, compared systematically the ΣΣ data with the BB data and, since we found, in general, a satisfactory agreement, we concluded that the background should not affect our results appreciably. This statement will be clarified by a few specific examples.

Another effect for which we did not introduce any correction could arise from spurious gamma-rays, i.e. gamma-rays due to the decay of π^0 produced in the walls of the vacuum chamber -- and other objects in the surroundings -- by charged particles generated in the pp collision. From the considerations summarized in Appendix C we arrived at the conclusion that the contribution of these gamma-rays is small even in the case of high multiplicity events.

The energy E_{HV} deposited in an HV counter ($3X_0$ thick) by a gamma-ray initiated shower amounts, on the average, to a fraction of the order of 30% of its total energy and fluctuates considerably around its mean value[7]. The energy k of the initiating photon is given by the relation

$$k = E_{HV} + \sum E_{LB} \ , \tag{3.1}$$

where the second term is the sum over all LB counters (6 or 9) located behind the HV in which the energy E_{HV} was observed*).

The scale of energy of single photons (3.1) (or of the corresponding transverse momentum k_t) is uncertain because of two reasons: the calibration of the lead-glass counters, which is affected by systematic errors of about 15%, and the

---

*) We assume that when two near-by HV counters are fired in coincidence, they are due to two gamma-rays, for the following reason. The coincidence due to a single shower developing in a lead-glass counter and passing in part in the next counter, is in general negligible, except in the case of counter 7 "dragging" counter 5 ($\lesssim$ 5%), counter 5 "dragging" counter 3 ($\lesssim$ 10%), counter 3 "dragging" counter 1 ($\lesssim$ 15%) and other geometrically equivalent pairs of counters. We had however, to solve the problem of the ambiguity in the determination of the energy k_i and k_j of each of these two gamma-rays originating from the LB counters. We adopted the recipe of adding to the energies E_i and E_j observed in the two HV counters, the energies in the LB counters placed behind both of them proportionally to E_i and E_j, i.e.

$$k_i = E_i + \frac{E_i}{E_i + E_j} \sum E_{LB}, \quad k_j = E_j + \frac{E_j}{E_i + E_j} \sum E_{LB} \ .$$

The results do not change appreciably by adopting the extreme simple recipe of adding to E_i (E_j) the energies observed only in the LB's placed behind HV_i (HV_j).

uncertainty deriving from the recipe adopted for distributing the energy deposited in the LB counters located behind two fired HV whenever these were close to one another*).

In the analysis of the data we used a cut-off in the energy deposited in a single HV (E_{cf}) equal to 30 MeV (or more). This value, according to pedestal measurements (Appendix B), was adequate to eliminate completely the pedestal fluctuations, although it should be considered as a "nominal" value, because of the uncertainty in the absolute scale of energy.

The fluctuations of the background for the photon energy (3.1) are much larger than for an HV, because one should add -- incoherently -- the fluctuations of all counters involved (about 10).

Finally, two further remarks about the trigger. Apart from the variation undergone with time of the pulse amplitude due to radiation damage (Sections 2 and 4), the threshold E^e_{th} of the trigger is not "sharp", i.e. its transmission increases from zero to full acceptance in a rather wide energy interval. This is an instrumental effect that introduces some complications in certain analyses of the data. In order to avoid these complications, we often use an analysis threshold E^a_{th}, appreciably greater than the electronic threshold E^e_{th}

$$E^a_{th} > E^e_{th} \ . \qquad (3.2)$$

Secondly, in order to obtain a better defined class of events, we have introduced, in some analyses of the data, what we call a neutral trigger, defined by requiring that the trigger mode M_t is due to at least t HV^n (and no HV^c). This was obtained by requiring that the t HV with greatest deposited energy were HV^n. This trigger clearly introduces a small bias against the HV^c.

4. ENERGY SPECTRUM OF SINGLE GAMMA-RAY AND INCLUSIVE CROSS-SECTION AT 90° IN THE c.m.

As an example, we show in Fig. 4 the distribution of the energy deposited per event by neutral secondaries in a single HV (HV 1 out) observed at $s^{\frac{1}{2}} = 53.2$ GeV, with the trigger mode M_4. The general trend of the distribution is the same for all other HV counters and is the same when the trigger mode is changed from M_4 to M_3, M_2 or M_1. The black dots shown in the figure are the distribution of the pulses of the events in which 4, and only 4, counters were fired. They allow an *a posteriori* determination of the threshold E^e_{th} of the discriminator which, in the case of Fig. 4, turns out to be around 0.240 GeV. This value does not differ too much from the original value of 0.160 GeV (Section 3), but for a few other HV counters the variation undergone by E^e_{th} because of radiation damage was appreciably larger, with a maximum of about $\Delta E_{th} \simeq 0.200$ GeV.

---

*) See footnote on preceding page.

The distributions of the type of that of Fig. 4 are the result of the superposition of two distributions: (a) The distribution of the energy deposited in the HV by photons that contribute to the trigger. This distribution increases rapidly around E^{e}_{th}, from zero to a maximum and then decreases exponentially. (b) The distribution of the energy deposited by the photons recorded in all other HV counters, which starts at the value of E_{cf} adopted in the analysis and decreases exponentially. Figures 5 and 6 show these two distributions in the case of the four HV counters placed at 90° lumped together (Nos. 7 + 8 + 9 + 10 separately for the "OUT" and "IN" detectors). These data were taken at $s^{\frac{1}{2}} = 53.2$ GeV with the trigger mode $[M_4\Sigma\Sigma]$.

We tried to parametrize the distributions of the type of that of Fig. 4 in terms of two Gaussian distributions representing the fluctuations of both the energy deposited by a shower in the HV and the value of the threshold E^{a}_{th} of the discriminator. The adjustable parameters were the widths of both Gaussians and the mean value $\bar{E}^{a}_{th}$ of the threshold. The values of these three parameters corresponding to the best fit in all cases turned out to be very close to the expected values.

In order to obtain the slope of the gamma-ray spectrum, we have plotted, after subtraction in each event of the photon responsible for the trigger, the data in Fig. 5, as a function of the photon energy in the c.m.

$$k^{*} = \gamma_{cm}(1 \mp \beta_{cm} \cos \alpha)k \qquad \begin{pmatrix} - \text{ OUT} \\ + \text{ IN} \end{pmatrix}, \tag{4.1}$$

where k is the energy of the photon in the laboratory frame [Eq. (3.1)], $\beta_{cm} = 0.1287$ and $\gamma_{cm} = 1.0085$, the velocity and the corresponding γ of the c.m. of the two colliding protons originating from the angle (14.8°) between the two beams of the ISR. The angle α appearing in Eq. (4.1) is the angle between $\vec{\beta}_{cm}$ and the line from the centre of the i.r. to the centre of any one of the counters placed at 90°, i.e. the HV, Nos. 7, 8, 9 and 10.

The subtraction, in each event of the photon responsible for the trigger, has been made for eliminating (or at least reducing) the deformation of the spectrum introduced by the trigger itself.

Best fits of these plots were made for the "OUT" ($k^{*} > 155$ MeV) and "IN" ($k^{*} > 200$ MeV) detectors by folding in an exponential spectrum, $\exp[-k^{*}/k_0]$ with a Gaussian representing the energy resolution of lead-glass counters. The free parameters were k_0 and the variance of the Gaussian. From the best fit we obtain

$$\begin{aligned} k_0 &= 180 \pm 10 \text{ MeV} \qquad \left(\frac{\chi^2}{f} = 1.3, \text{ OUT}\right) \\ k_0 &= 160 \pm 10 \text{ MeV} \qquad \left(\frac{\chi^2}{f} = 1.8, \text{ IN}\right), \end{aligned} \tag{4.2}$$

where the errors are purely statistical. Also the values deduced for the variance of the counter resolutions are in very good agreement with those measured directly by us as well as by other authors.

The values (4.2) are in very good agreement with the value obtained by other authors[8,9]

$$k_0 = 161 \pm 8 \text{ MeV}$$
$$k_0 = 157 \pm 8 \text{ MeV} , \tag{4.3}$$

especially if one considers the uncertainty inherent in the calibration of the lead-glass counters (Section 3).

We have then proceeded to verify whether our counting rates are in agreement with the cross-section for producing gamma-rays at 90° measured by other authors. We have used two procedures, the first of which is based on the data shown in Fig. 5, while the second utilizes the data of Fig. 6.

The first procedure is the following. We have made semilogarithmic plots of the data of Fig. 5 as a function of k^* and we have summed the number of events observed in the linear part of the semilogarithmic plot ($k^* \geq k^a_{th}$). We obtain a number $M_1\Sigma\Sigma(90°;\ k^* \geq k^a_{th})$ which is connected to the cross-section by the obvious relation

$$\frac{1}{\sigma_{in}} \frac{d\sigma_\gamma}{d\Omega^*} = \frac{M_1\Sigma\Sigma(90°;\ k^* \geq k^a_{th})}{\Sigma\Sigma} \frac{1}{\exp\left[-k^a_{th}/k_0\right] \Omega^*} \frac{1}{F} \tag{4.4}$$

where the exponential factor is introduced in order to extrapolate the cross-section to $k^* \simeq 0$, and Ω^* is 4 times the solid angle for gamma-rays in the c.m., covered by any one of the four counters at 90° in the "OUT" or "IN" detector (Table D.3). Finally, F is a correction factor close to one originating from the bias due to the beam counters (Appendix F). The first factor on the right-hand side of Eq. (4.4) is conveniently factorized as follows

$$\frac{M_1\Sigma\Sigma(90°;\ k^* \geq k^a_{th})}{\Sigma\Sigma} = \left(\frac{M_1\Sigma\Sigma(90°;\ k^* \geq k^a_{th})}{M_1\Sigma\Sigma}\right)\left(\frac{M_1\Sigma\Sigma}{\Sigma\Sigma}\right), \tag{4.5}$$

where the first ratio on the right-hand side is the ratio of the trigger mode $[M_1\Sigma\Sigma]$ due to gamma-rays firing "the 90° counters" to the total number of triggers due to gamma-rays firing any one of the HV counters. The second factor is the ratio of this same number to the total number of $\Sigma\Sigma$, the physical meaning of which is

$$\frac{M_1\Sigma\Sigma}{\Sigma\Sigma} = \frac{1}{\sigma_{inel}} \int_{\Omega^*_{tot}} \frac{d\sigma_\gamma}{d\Omega^*} (k^* \geq k^a_{th})\ d\Omega^* = 0.106\ (\pm\ 7\%) . \tag{4.6}$$

where Ω^*_{tot} is the solid angle of the whole gamma-ray detector.

From Eqs. (4.4) and (4.5) we obtain: for the detector out

$$\frac{1}{\sigma_{inel}} \frac{d\sigma_\gamma}{d\Omega^*} = \frac{0.0198 \times 0.106}{0.0146 \times 0.457} = 0.30, \qquad k_{th}^a = 760 \text{ MeV}, \; k_0 = 180 \text{ MeV} \quad (4.7a)$$

for the detector in

$$\frac{1}{\sigma_{inel}} \frac{d\sigma_\gamma}{d\Omega^*} = \frac{0.0081 \times 0.106}{0.0159 \times 0.275} = 0.20, \qquad k_{th}^a = 660 \text{ MeV}, \; k_0 = 160 \text{ MeV} \quad (4.7b)$$

with an error of about ±40% originating mainly from the exponential factor $\exp\left[-k_{th}/k_0\right]$.

These values agree as much as can be expected with the results of other authors:

$$\frac{1}{\sigma_{inel}} \frac{d\sigma_\gamma}{d\Omega^*} = 0.24 \pm 0.02 \; ^{8)} \quad \text{and} \quad 0.21 \pm 0.02 \; ^{9)} \; . \qquad (4.8)$$

The second procedure for comparing our counting rates with the measured cross-section utilizes the data of Fig. 6 as a function of E_{HV}. Since a determination of E_{th} is rather uncertain because of various causes (including the radiation damage of the lead glass), we use the slopes (E_0) of the two straight lines of Fig. 6 for extrapolating the distributions to $E_{HV} = 0$ and for determining the value of E_{th} that gives a preassigned value of $\sigma_{inel}^{-1} \times d\sigma_\gamma/d\Omega^*$. One starts from a relationship similar to (4.4) with k^*, k_{th}^a and k_0 replaced by E_{HV}, E_{th}^a and E_0, which is solved with respect to E_{th}. Introducing for $\sigma_{inel}^{-1} \, d\sigma_\gamma/d\Omega^*$ the value 0.22 [average of the values in (4.8)], we obtain

$$\begin{aligned} E_{th} &\simeq 200 \text{ MeV } (\pm 20\%) \quad \text{for the "OUT" detector} \\ E_{th} &\simeq 190 \text{ MeV } (\pm 20\%) \quad \text{for the "IN" detector} \; , \end{aligned} \qquad (4.9)$$

which are in very good agreement with the mean values of E_{th} for the counter Nos. 7, 8, 9 and 10. The large error originates again mainly from the uncertainty in the energy determination.

Thus we can conclude that our counting rates give the correct value of the slope of the gamma-ray spectrum at 90° [Eq. (4.2)] as well as the value of the cross-section (4.7), although the latter is affected by a large error.

5. REGRESSION LINES

We present here a few results obtained by the method of regression lines very popular among statisticians[10]. Given a distribution $p(x,y)$ in two stochastic variables x,y, one defines as regression lines the two functions

$$\bar{y}(x) = \frac{\sum_y yp(x,y)}{\sum_y p(x,y)} \tag{5.1a}$$

$$\bar{x}(y) = \frac{\sum_x xp(x,y)}{\sum_x p(x,y)} , \tag{5.1b}$$

where x and y are assumed to take on a set of definite values and the sums are extended over all of them.

The significance of plots of the two lines (5.1) is clarified by considering two extreme cases. If the two variables x and y are stochastically independent, the regression lines are straight lines, one parallel to the x-axis and the other to the y-axis. If, on the contrary, x and y are completely dependent on each other, both regression lines coincide with the one curve which represents the corresponding x- and y-values. Finally, for the normal distribution

$$p(x,y) = \text{const.} \times \exp\left[-\frac{1}{2} Q\right], \quad Q = a_{11}x^2 + 2a_{12}xy + a_{22}y^2 ,$$

one finds

$$\bar{y}(x) = -\frac{a_{12}}{a_{22}} x, \quad \bar{x}(y) = -\frac{a_{12}}{a_{11}} y ,$$

i.e. in this case the regression lines are straight lines passing through the mean value with slopes (relative to the x and y directions, respectively) equal to $-a_{12}/a_{22}$ and $-a_{12}/a_{11}$. This property should, however, be taken with caution: the plots of the regression lines of many non-normal distributions appear to be linear in spite of their completely different analytic nature.

The following remark may contribute to clarifying the meaning of the regression lines (5.1). If x and y are not completely dependent on each other, one can ask for a function $y = g(x)$ of x which gives the best possible estimation of the other variable y. Interpreting the term "best possible" in the sense of the principle of least squares, the problem becomes that of determining $g(x)$ so as to minimize the expression

$$\sum_x \sum_y [y - g(x)]^2 \, p(x,y) .$$

From the minimum property of the variance it follows that, for each x,

$$\sum_y [y - g(x)]^2 \, p(x,y)$$

becomes a minimum when $g(x) = \bar{y}(x)$, which is the mean value (or conditional probability) of y for given x

$$p_2(y|x) = \frac{p(x,y)}{\sum_y p(x,y)} .$$

In the same way

$$\sum_x \sum_y [x - h(y)]^2 \cdot p(x,y)$$

obtains its minimum for $h(y) = \bar{x}(y)$.

A few regression lines obtained from our data are presented here in the form of graphs. They all refer to runs made at $s^{\frac{1}{2}} = 53.2$ GeV. The indicated errors are statistical and have been computed by taking into account the subtraction of the pedestal fluctuations.

The first set of pairs of regression lines (Figs. 7 to 12) regard the variables x = total (out + in) multiplicity of $HV^n = m(HV^n)$ and y = m(tracks) = = the total (out + in) multiplicity of reconstructed tracks. In Figs. 7, 10 and 11 all HV^n have been considered, while Figs. 8, 9 and 12 are constructed by using the neutral trigger (Section 3) and subtracting, in each event, the HV that contribute to the trigger. This was obtained by excluding the t HV^n in which the photons deposit the largest energy.

This recipe eliminates a trivial correlation which produces an apparent higher value of m(tracks) when $m(HV^n)$ is very small. From a comparison of the two sets of figures this effect is very clear.

From Figs. 8, 9 and 12 it seems that, within the statistical errors, $\langle m_{tracks} \rangle$ increases very slowly for t = 1 and 2, and remains practically constant for t = 4, when the abscissa increases from 1 to 8 or 9. This difference, however, remains within the statistical errors over the whole interval of observed values of $[m(HV^n) - t]$. The same figures show a tendency of $\langle [m_t(HV^n) - t] \rangle$ to increase as m_{tracks} increases. Furthermore, for $m_{tracks} = 0$ the values of $\langle [m_t(HV^n) - t] \rangle$ increases when t increases from 1 to 2 and 4, while for $m_{tracks} > 1$ the values of $\langle [m_t(HV^n) - t] \rangle$ observed with different t are always equal within the statistical error.

Since the gamma-rays originating from particles different from π^0 (K^0, $\bar{K}_0$ and in part $K^{\pm}$) at $s^{\frac{1}{2}} = 53.2$ GeV contribute about 20% of the total gamma-rays observed, the behaviour discussed above is a clear indication of a positive correlation between the numbers of charged ($n_{\pm}$) and neutral (n_0) pions.

The derivation of general conclusions from these observations is made rather uncertain by the fact that our data refer to a very small solid angle. This geometrical feature of our detector is particularly inconvenient for such a comparison,

because the angular distribution and spectrum of the gamma-rays are smeared out with respect to the angular distribution and spectra of the charged particles by the decay process of the parent particles. Furthermore, one has to keep in mind the following remarks:

i) At $s^{\frac{1}{2}} = 53.2$ GeV, on the average[11] about 20% [as well as at 90° and $p_t \simeq 0.5$ GeV/c [12,13]] of the charged particles are not $\pi^{\pm}$ and about 20% of the observed gamma-rays originate from the decay of mesons different from π^0 (K_S^0, K_L^0, $K^{\pm}$). This rough estimate is based on the following considerations: (a) we assume for the average numbers of $\pi^{\pm}$, $K^{\pm}$, p, $\bar{p}$ produced at $s^{\frac{1}{2}} = 53$ GeV, the values given in Ref. 11; (b) we take for $\langle n_{\pi^0} \rangle$ the arithmetic averages of $\langle n_{\pi^+} \rangle$, $\langle n_{\pi^-} \rangle$; (c) we assume that the K^0 and $\bar{K}^0$ are produced with the same partial cross-sections as K^+ and K^-. Then by considering the various decay modes of K_S^0 and K_L^0, we obtain the following results:

Parent particle	τ (sec)	$\langle n_{\pi^0} \rangle$
K_S^0	0.886×10^{-10}	0.229
K_L^0	5.179×10^{-8}	0.279
$K^{\pm}$	1.237×10^{-8}	0.240
		$\langle n_{\gamma} \rangle$
K_S^0		0.007
K_L^0		0.149 .

The last two lines refer to gamma-rays that do not originate from π^0 decay.

ii) The observed $m(HV^n)$ differ from n_{γ} because of the five main corrections listed in Table A.1 to which here one should consider adding three more: (a) the probability that a shower produced by a gamma-ray in an HV counter fires also the near-by HV counter; (b) the probabilities that two gamma-rays, originating from the same π^0, cross two different counters, or the same HV counter, or that one crosses one of the HV counters while the other does not cross the detector; (c) the possible contribution of spurious gamma-rays.

We have made an estimate of point (a) starting from a rather detailed study of showers in lead glass[7] and found that the probability for a shower initiated by a gamma-ray in an HV counter to produce a pulse greater than $E_{cf} = 30$ MeV in a second counter is negligible in all cases, i.e. whenever the second HV counter is placed below or above the first one, except in the case of the HV counter placed at the same level as the first one, along its vertical side. In this case, the effect was different from counter to counter, but always between 5% and 10%. This result agrees with the Monte Carlo computation that gives an average effect of 8%.

We have made estimates also of point (b). The result depends, however, in a rather complicated way, on the angular and spectral distribution of the π^0 and the geometry of the detectors.

An over-all estimate of both these effects lumped together is obtained from the Monte Carlo computation (Appendix D), which gives

$$\frac{\langle m(HV^n)\rangle}{\langle m_{\pi^0}\rangle_{\geq 1\gamma}} = 0.99 \pm 0.01 \ , \qquad (5.2)$$

where $\langle m_{\pi^0}\rangle_{\geq 1\gamma}$ is the number of pions per event giving at least one gamma-ray crossing the detectors.

Finally, point (c), i.e. the possible contribution of spurious gamma-rays, is discussed in Appendix C, where we arrive at the conclusion that it can be neglected.

iii) The observed m_{tracks} is lower than the charged particles, because of the efficiency of the wire chambers as well as that of the procedure of track reconstruction. Both losses may increase with increasing multiplicity. We estimate that for events of average charge multiplicity the correction for the first of these effects is about +10% (see Table A.1), while for the second it amounts to about +20%.

A linear dependence of the average number $\langle n_{\pi^0}\rangle$ of neutral pions observed over the whole solid angle on the number of charged particles n_{ch} has been observed by other authors working at lower as well as at the ISR and at NAL energies:

$$\langle n_{\pi^0}\rangle = A + Bn_{ch} \ . \qquad (5.3)$$

A summary of the experimental results and their discussions in the frame of a simple model can be found elsewhere[14].

At ISR energies A seems to be small and $B \sim \frac{1}{2}$. However, our results refer to a small solid angle around 90° and are taken with trigger modes M_t, which impose always the condition $A \geq t$. What was not expected and is shown rather clearly by Figs. 8, 9, and 12, is that in the pionization region $(\langle n_{\pi^0}\rangle_t - t)$ is appreciable for $t = 1$ and increases considerably by increasing t from 1 to 4.

We will come back to the discussion of this point in Section 7, where the data on the mean values of $m(HV^n)$ and m_{tracks} will be reexamined.

As a final remark on this set of regression lines, we notice that the data of Figs. 10 and 12 always agree within the statistical errors, although three of the $\Sigma\Sigma$ points are slightly higher than the corresponding BB points. This is a good indication that the background is not very large even in the $\Sigma\Sigma$ data.

The second set of pairs of regression lines (Figs. 13 to 18) regard the variable $x = m_{IN}$ = total multiplicity (= $HV^n + HV^c$) in the detector IN, and $y = m_{OUT}$ = total multiplicity (= $HV^n + HV^c$) in the detector OUT. In Figs. 13, 16 and 17 all HV have been considered, while Figs. 14, 15 and 18 are constructed by using the neutral trigger (Section 2) and subtracting in each event the HV that contribute to the trigger. Since in this case we do not know how many of the t HV should be subtracted from $m(HV^n_{IN})$ and $m(HV^n_{OUT})$, we have labelled m with an asterisk.

Figures 16 and 17 differ only because the corresponding trigger is $[M_4 BB]$ instead of $[M_4 \Sigma\Sigma]$. Only in a few cases are the $\Sigma\Sigma$ points slightly higher than the BB data. The difference, however, is about one statistical error. This is another example of the agreement we found in general between the BB and $\Sigma\Sigma$ data. It confirms the conclusion that neither the BB data nor the $\Sigma\Sigma$ data are affected by a large background of accidentals.

A third group of figures (Figs. 19 to 22) illustrates the dependence of the average multiplicity $\langle m(HV^n)\rangle$ on the transverse momentum k_t [or momentum k = energy: see Eq. (3.1)] observed in a single HV and the LB's behind it. In all these figures we do not show the companion regression line [$x = \langle k_t\rangle$ (or $\langle k\rangle$), $y = m(HV^n)$], because the values of $\langle k_t\rangle$ (or $\langle k\rangle$), always rather low, are appreciably affected by the fluctuations of the pedestal events which arise from all lead-glass counters involved: one HV plus about eight LB counters placed behind it. We recall the remarks made in Section 4 about the energy scale of k and k_t and the fluctuations of the background.

In the first three figures we have plotted the mean value of $m(HV^n)$ versus k_t at $s^{\frac{1}{2}} = 53.2$ GeV, by separating the observations made in the two detectors. The three figures differ only for the trigger mode, and the multiplicities are computed with $E_{cf} = 30$ MeV.

The broken horizontal lines correspond to the over-all mean multiplicity. They have been drawn for facilitating the recognition of possible general trends of $\langle m(HV^n)\rangle$ when k_t increases. The data of Fig. 19 can be compared with the results of the Pisa-Stony Brook group[15], who observe an increase (decrease) of about 30% (5%) in the normalized total multiplicity of charged particles observed in the hemisphere away from (towards) the direction of a single photon emitted at about 90°, when its transverse momentum increases from 0.3 GeV/c to 4 GeV/c. We recall that, according to the Monte Carlo computation (Appendix D), $m(HV^n)$ is practically equal to the number of π^0 that generate at least a gamma-ray crossing the detector [Eq. (5.2)]. Therefore the data of Fig. 19 show a different behaviour which probably arises from the fact that the solid angles within which we observe $\langle m(HV^n)\rangle$ and k_t are small (9% of 4π) and fixed around 90°, while in the Pisa-Stony Brook experiment the solid angle in which the multiplicity is observed is 50% of 4π taken in each event with its axis opposite to $\vec{k}$.

The data of Figs. 20 and 21 cannot be easily compared with those of Fig. 19, because the difference in the trigger mode introduces a selection of different classes of events.

In the three previous figures the meaning of $\langle m(HV^n)\rangle$ as a function of k_t is not very clear because, as long as the pions have a very low energy, k_t represents the transverse momentum of a single decay photon, while for pions of sufficiently high energy, very often both decay photons cross the same HV, so that the measured k_t represents the transverse momentum of the parent neutral pion. In order to clarify this point we have plotted, in Fig. 22, the mean value of $m(HV^n$ out), observed at $s^{\frac{1}{2}} = 53.2$ GeV with the trigger mode $[M_4\Sigma\Sigma]$, versus the value of k observed in any HV + LB behind it belonging to the "OUT" detector. In the same figure we show a curve $\phi_{\pi^0}(k)$ representing the percentage of the cases in which the observed energy k is due to both gamma-rays originating from the same π^0. The curve should be considered only as an indication since its computation involves two approximations: (a) the π^0 giving a gamma-ray in the detector are emitted isotropically; (b) all π^0 decay emitting the two gamma-rays at

$$\theta_{min} = 2 \arcsin \frac{m_{\pi^0}}{E_{\pi^0}} . \tag{5.4}$$

The probability $\phi_{\pi^0}(k)$ is zero as long as $k < 0.58$ GeV since for $\theta_{min} > 28°$ the two gamma-rays can never cross the same HV counter. If we wish to replot a curve like that of Fig. 22 as a function of the energy k of a single gamma-ray, one should decrease the value of $\langle m(k)\rangle$ for $k \geq 0.58$ by the factor $[1 - \phi_{\pi^0}(k)]$ and at the same time multiply $\langle m(k/2)\rangle$ by the factor $[1 + 2\phi_{\pi^0}(k)]$.

The last set of figures (Figs. 23 to 28) concerns multiplicity and total transverse momentum

$$K_t = \sum k_t \tag{5.5}$$

or total energy

$$K_{tot} = \sum k . \tag{5.6}$$

In Fig. 23 we have plotted the mean value of $m(HV^n)$ versus k_t both observed in both detectors (OUT + IN) for two trigger modes at $s^{\frac{1}{2}} = 53.2$ GeV. The points beyond 3.1 GeV (4.1 GeV) observed with the trigger mode $M_1\Sigma\Sigma$ ($M_4\Sigma\Sigma$) are slightly more uncertain than those at lower k_t for the following reason. Each point in this figure is computed from the event distribution observed -- at a fixed value of k_t -- as a function of $m(HV^n)$. Since, in practice, we did not observe many events with $m(HV^n) > 10$, we were forced to extrapolate these distributions in the region of $m(HV^n) > 10$ for large values of k_t, before computing the mean value of $m(HV^n)$. Such an extrapolation introduces an uncertainty in the value of $\langle m(HV^n)\rangle$,

which increases with k_t, but is not greater than 20% even for the last point of each of the two curves shown in Fig. 23.

Figure 24 is related to the previous figure: it shows, for a few fixed values of $m(HV^n)$, the distribution of the events as a function of k_t.

Figure 25 shows the dependence of the transverse momentum k_t observed (at $s^{\frac{1}{2}} = 53.2$ GeV) in any HV on the multiplicity m of the HV fired with a pulse $\geq E_{cf} = 30$ MeV. The dots refer to all fired HV ($= HV^n + HV^c$), the triangles to the HV^n. The slope of a line drawn through the triangles is equal to 0.35 GeV/c per unit multiplicity, in very satisfactory agreement with all other evaluations of the mean transverse momentum.

The next two figures (Figs. 26 and 27) show, for two different trigger modes, the regression lines corresponding to x = the total multiplicity m(HV) (where $HV = HV^n + HV^c$) and $y = K_{tot}$ = total energy per event observed in all HV.

The mean value of K_{tot} increases regularly with the multiplicity up to m = 12 and the mean value of the multiplicity also increases regularly as a function of K_{tot} reaching a value of about 8 at $K_{tot} = 5.5$ GeV for $[M_2\Sigma\Sigma]$ and 9-10 at $K_{tot} = 7$ GeV for $[M_4\Sigma\Sigma]$.

Figure 28 is related to Fig. 27, since it represents the distribution of the events as a function of K_{tot} observed at $s^{\frac{1}{2}} = 53.2$ GeV with the trigger mode $[M_4\Sigma\Sigma]$. The increase undergone by the distribution from zero to a maximum, when K_{tot} increases from 1.5 to 4.25 GeV, is due to the trigger mode. By requiring that there are at least 4 gamma-rays with an energy $\geq E_{th} = 0.25$ GeV in the HV, we select events with a total energy in the HV + LB of at least

$$4 \times 0.25 \times 3 \simeq 3 \text{ GeV} ,$$

where the factor ~ 3 is due to the fact that a high-energy gamma-ray deposits between 1/2 and 1/3 of its energy in the HV counters[7].

6. TWO-BODY INCLUSIVE RAPIDITY CORRELATIONS

The two-body inclusive rapidity correlation function is defined as

$$C(\eta_1,\eta_2) = \frac{1}{\sigma_{inel}} \frac{d^2\sigma}{d\eta_1 d\eta_2} - \frac{1}{\sigma_{inel}} \frac{d\sigma}{d\eta_1} \frac{1}{\sigma_{inel}} \frac{d\sigma}{d\eta_2} . \qquad (6.1)$$

In the case of our detector we can write

$$\frac{1}{\sigma_{inel}} \frac{d\sigma}{d\eta_i} = \frac{N_{HVi}}{[M_t\Sigma\Sigma]} \frac{[M_t\Sigma\Sigma]}{\Sigma\Sigma} \frac{2\pi}{\Delta\phi_i} \frac{1}{\Delta\eta_i}$$

$$\frac{1}{\sigma_{inel}} \frac{d^2\sigma}{d\eta_i d\eta_j} = \frac{N_{HVij}}{[M_t \Sigma\Sigma]} \frac{[M_t \Sigma\Sigma]}{\Sigma\Sigma} \frac{2\pi}{\Delta\phi_i} \frac{2\pi}{\Delta\phi_j} \frac{1}{\Delta\eta_i} \frac{1}{\Delta\eta_j} , \tag{6.2}$$

where the symbols have the following meanings:

N_{HVi} = counting of the HV counter No. i above the adopted value of E^a_{th};

N_{HVij} = counting rate of coincidences between the HV counters No. i and No. j, with both pulses $\geq E^a_{th}$;

$\Delta\phi_i$ = azimuthal angle covered by the HV No. i;

$\Delta\eta_i$ = rapidity interval covered by the HV No. i.

From Eq. (6.2) we deduce, for the relative correlation

$$R(\eta_1,\eta_2) = C(\eta_1,\eta_2) \Big/ \frac{1}{\sigma_{inel}} \frac{d\sigma}{d\eta_1} \times \frac{1}{\sigma_{inel}} \frac{d\sigma}{d\eta_2} , \tag{6.3}$$

the expression

$$R_t(\eta_1,\eta_2) = \frac{N_{HVij}/[M_t \Sigma\Sigma]}{\{N_{Hi}/[M_t \Sigma\Sigma]\}\{N_{Hj}/[M_t \Sigma\Sigma]\}} \frac{\Sigma\Sigma}{[M_t \Sigma\Sigma]} - 1 , \tag{6.4}$$

when we have added the subscript t to recall that our data are obtained with trigger mode M_t.

In order to obtain values of R regarding all inelastic events without bias originating from the adopted trigger mode M_t, it would be necessary to adopt -- for all HV counters -- an analysis threshold $E^a_{th} \geq$ 400-500 MeV. With this recipe, however, the data turn out to be statistically inadequate.

Therefore we have derived the rapidity correlations from the data provided by the "IN" detector ($\geq E_{cf}$ = 30 MeV) only for those events that fulfil the requirement imposed by the adopted trigger mode in the "OUT" detector ($\geq E^a_{th}$).

Furthermore, we have tried to eliminate the trivial effect deriving from the fact that, in 8% of the cases (Appendix C), a gamma-ray producing a shower in one HV counter also fires the HV counter placed at its side but not those below or above it with respect to the horizontal plane (Figs. 1 and 2). With such an aim we have derived the value of R corresponding to $\Delta\eta = |\eta_1 - \eta_2| = 0$ by using the coincidences of each "odd" HV_i counter (covering the azimuthal angle from $\phi = 0°$ to $\phi = +26°$) with the "even" counter HV_{i+1} (covering the azimuthal angle from $\phi = 0°$ to $\phi = -26°$) placed below it. This means that we have used the coincidences between the pairs of counters (1,2) (3,4) ... (15,16). In order to improve the rather poor statistics, we have lumped all these data together so that the corresponding value of R is averaged over the interval extending from $\eta_1 = \eta_2 = 0$ to $\eta_1 = \eta_2 = \pm 0.6$.

A similar procedure has been used for the data at $\Delta\eta = 0.16$ which are obtained from the coincidences between each one of the odd (even) HV_i (HV_j) with the even (odd) HV_{i+3} (HV_{j+1}) which has a corner in common with HV_i (HV_j). To be more specific we have used the coincidences between the pairs of counters (1,4) (3,6) ... (2,3) ... (13,16) (14,15).

The data at $\Delta\eta = 0.51$ are obtained from the coincidences between one or the other of the two groups of four counters placed away from 90° (i.e. 1 + 2 + 3 + 4: $\eta_1 = 0.585 \pm 0.075$) and (13 + 14 + 15 + 16: $\eta_1 = -0.585 \pm 0.075$) and the four counters placed at 90° (7 + 8 + 9 + 10: $\eta_2 = 0.00 \pm 0.18$).

Finally the data at $\eta_1 = 1.02$ are derived from the coincidences of the two groups of four counters placed away from 90° (i.e. 1 + 2 + 3 + 4: $\eta_1 = 0.585$) and (13 + 14 + 15 + 16: $\eta_2 = -0.585$).

The results, summarized in Table 4, do not agree completely with those obtained by other authors for the correlations of charged-charged[16] and charged-neutral (γ) [17], because: (a) for $\eta_1 = \eta_2 = 0$ our value of R is identical with that of the other two groups while we should get, in addition, the gamma-gamma correlations originating from the decay of a single π^0 [18]; (b) by increasing $\Delta\eta = |\eta_1 - \eta_2|$ from 0 to 1 our values of R seem to decrease faster than found by other authors.

7. MULTIPLICITY DISTRIBUTIONS

Figure 29 shows the integral distribution of the multiplicity of the fired HV^n for four colliding beam energies ranging from 11.7 GeV to 26.6 GeV in each beam. These results were obtained with a trigger mode $[M_4\Sigma\Sigma]$, with a threshold of the HV that we estimate was around $E_{th} = 0.200$ GeV (Section 4), and was sufficient to ensure that these triggered events are due mainly to gamma-ray events. It should be emphasized again, however, that once an event was obtained by such a trigger, the respective energies and positions of all the counters fired, as well as the information on all the charged tracks given by the scintillators and wire spark chambers, were completely recorded. The cut-off in energy deposited in the HV adopted for the plot of Fig. 29 was taken equal to 25 MeV. This value, according to pedestal measurements, was adequate to eliminate practically completely the HV background. Because of the change of the calibration of the HV due to accumulated radiation damage effect, we estimate that the actual cut-off was at 30-35 MeV *).

Figure 30 shows the distribution of the number of fired neutral HV for various trigger modes from ≥ 1 to ≥ 4 at a centre-of-mass energy of 53.2 GeV and for the same cut-off energy as in Fig. 29.

---

*) We wish to point out again that the value of E_{cf} should be considered only a nominal value as stated in Section 3.

The distributions shown in Figs. 29 and 30 are expressed in cross-section per steradian assuming $\sigma_{inel} = 35.6$ mb. Summing the values given in Fig. 30 for the trigger mode $[M_1 \Sigma\Sigma]$, we obtain

$$\sum_{m=1}^{\infty} \left(\frac{d\sigma_\gamma}{d\Omega}\right)_m = 1.25 \text{ mb} . \qquad (7.1)$$

This value, divided by $\sigma_{inel} = 35.6$ mb, gives 0.035, which is about 7 times smaller than the larger of the two values (4.7). This is due simply to the factor $\exp\left[-E^e_{th}/k_0\right]$, where E^e_{th} is the electronic threshold of the trigger. If we assume $k_0 \sim 0.16$ GeV -- as an average for the "IN" and "OUT" HV -- we obtain $E^e_{th} \simeq 0.3$ GeV, in reasonable agreement with what we know from the calibration of the lead-glass counters, especially if we consider that in these plots the $HV^c + HV^n$ are lumped together.

The tails of these distributions show about the same slope irrespective of the trigger mode. This is just the behaviour one would expect for multiplicities m appreciably greater than the trigger t.

Table 5 shows the mean values of the average multiplicity $\langle m(HV^n)\rangle$, their variance σ and the maximum value of $m(HV^n)$ we observed in the BB data, which have been analysed with three different values of the cut-off energy E_{cf}.

In the lower part of the table we give also the mean values of the number of reconstructed tracks. The values of $\langle m(HV^n)\rangle$ and $\langle m_{tracks}\rangle$ obtained with the trigger mode $[M_4 \Sigma\Sigma]$ and $E_{cf} = 30$ MeV are plotted in Fig. 31 as a function of the energy $s^{\frac{1}{2}}$ in the c.m. of the colliding protons and in Fig. 32, for $s^{\frac{1}{2}} = 53.2$, as a function of the trigger t. The results obtained from the BB data agree always, within the indicated errors (statistical), with those derived from the $\Sigma\Sigma$ data.

Figures 33 and 34 show the dependence of the average multiplicity as a function of the cut-off energy for the trigger mode $[M_4 \Sigma\Sigma]$ and $s^{\frac{1}{2}} = 53.2$ GeV. In Fig. 33 the fired HV^n and HV^c have been separated, while in Fig. 34 they are lumped together ($HV = HV^n + HV^c$).

Some of the analyses reported above have been repeated with the neutral trigger (end of Section 3) and we think that these should correspond to better defined conditions. The results of such an analysis are shown in Fig. 35 and in Table 6.

Figure 35 is similar to Fig. 30 except that in the analysis of the data we have imposed the "neutral trigger" and the counting rates normalized to unity over the whole range of values of the abscissa are plotted versus the variable

$$\left[m_t(HV^n) - t\right] .$$

From Fig. 30 it clearly appears that by increasing t, i.e. by selecting events with a greater number of photons with $E_{HV} \geq E^a_{th} \simeq 0.2$ GeV, we obtain a class of events which shows a greater multiplicity.

The corresponding mean values, as well as a few higher moments, are shown in Table 6. The comparison of these results with those obtained with normal trigger suggest the following remarks:

i) Passing from normal to neutral (analysis) trigger, the values of $\langle m_{tracks} \rangle$ slightly decrease and, in the case of the trigger $[M_1 \Sigma\Sigma]$, approach the value one derives by integrating the inclusive cross-section over the solid angle covered by the detectors

$$\langle m_{ch} \rangle \simeq 0.6 \ . \tag{7.2}$$

ii) The mean values of $m(HV^n)$, on the contrary, increase appreciably as we should expect, because with the neutral trigger we exclude from the computation of the mean values the events that we recorded in spite of the fact that $m(HV^n) < t$, because at least one HV^c contributed to the trigger.

iii) By increasing t, i.e. by selecting events with a greater number of photons with $E_{HV} \geq E^a_{th} \simeq 0.2$ GeV, we also select events with a greater number of photons with $0.03 \leq E_{HV} \leq 0.2$ GeV.

8. THE INFLUENCE OF THE TRIGGER

In this section we try to analyse, in more detail, the influence of the trigger on the mean value of $m(HV^n)$. In a run with a fixed mode M_t, the lead-glass counters provide a table of "two-index" numbers

$$N^{(t)}_{n_1,n_2} \ , \tag{8.1}$$

i.e. the number of events with n_1 HV^n with a deposited energy $E > E_{th}$ and n_2 HV^n with a deposited energy $E_{cf} \leq E < E_{th}$. If N is the number of pp inelastic collisions (i.e. BB or $\Sigma\Sigma$ coincidences) recorded during the same run, we can define the two-index frequencies

$$d^{(t)}_{n_1,n_2} = \frac{N^{(t)}_{n_1,n_2}}{N} \ . \tag{8.2}$$

If the electronic trigger were a step function at $E = E_{th}$, the frequencies (8.2) would have the property

$$d^{(t)}_{n_1,n_2} = \begin{cases} d_{n_1,n_2} & \text{whenever } n_1 \geq t \\ 0 & \text{whenever } n_1 < t \ , \end{cases} \tag{8.3}$$

where d_{n_1,n_2} is the frequency of the events, belonging to the class (n_1,n_2), that would be observed in a measurement without trigger.

The meaning of the frequencies d_{n_1,n_2} is clarified by the following remark. If the solid angle of each HV counter were so small that the probability to have more than one gamma-ray crossing the same counter were negligible, then

$$\sum_{n_1+n_2=n} d_{n_1,n_2} = \omega_n \tag{8.4}$$

where ω_n is the probability for n photons produced in an inelastic pp collision to cross the detectors[19].

This is equivalent to saying that ω_n is the integral over the phase-space volume defined by the detectors of the n photons exclusive cross-section (divided by σ_{inel}).

From the observed values of the frequencies d_{n_1,n_2} we compute the mean values of n_1,n_2 and $n = n_1 + n_2$. These mean values depend on the adopted trigger mode (i.e. $n_1 \geq t$), even in the case of an ideal trigger, i.e. a trigger satisfying condition (8.3).

In order to understand such an influence, let us start by expressing the average number of photons (with $E \geq E_{cf}$) that are observed without a trigger. This is given by

$$\langle n \rangle = \frac{1(N_{10} + N_{01}) + 2(N_{20} + N_{11} + N_{02}) + 3(N_{30} + N_{21} + N_{12} + N_{03}) + \ldots}{N_{00} + (N_{10} + N_{01}) + (N_{20} + N_{11} + N_{02}) + \ldots} =$$

$$= \frac{1(N_{10} + N_{01}) + 2(N_{20} + N_{11} + N_{02}) + 3(N_{30} + N_{21} + N_{12} + N_{03}) + \ldots}{N} =$$

$$= 1(d_{10} + d_{01}) + 2(d_{20} + d_{11} + d_{02}) + 3(d_{30} + d_{21} + d_{12} + d_{03}) + \ldots . \tag{8.5}$$

In the limit of validity of (8.4), the relationship (8.5) becomes the well-known relation between the one-particle inclusive integral $[\phi^{(1)} = \langle n \rangle]$ and the exclusive integrals ω_k.

When the trigger mode M_1 is imposed we obtain

$$\langle n_1 \rangle = \frac{1(N_{10} + \cancel{N_{01}}) + 2(N_{20} + N_{11} + \cancel{N_{02}}) + 3(N_{30} + N_{21} + N_{12} + \cancel{N_{03}}) + \ldots}{\cancel{N_{00}} + (N_{10} + \cancel{N_{01}}) + (N_{20} + N_{11} + \cancel{N_{02}}) + \ldots} =$$

$$= 1 + \frac{(N_{20} + N_{11}) + 2(N_{30} + N_{21} + N_{12}) + \ldots}{M_1} \text{ , because } N_{0i} \equiv 0 \text{ with } M_1 .$$

By multiplying the second term by N/N we finally obtain

$$\langle n\rangle_1 = 1 + \frac{N}{M_1}\{(d_{20} + d_{11}) + 2(d_{30} + d_{21} + d_{12}) + 3(d_{40} + d_{31} + d_{22} + d_{13}) + \ldots\} . \tag{8.6a}$$

By the same procedure one obtains for the average numbers of photons observed with the trigger modes M_2, M_3 and M_4

$$\langle n\rangle_2 = 2 + \frac{N}{M_2}\{(d_{30} + d_{21}) + 2(d_{40} + d_{31} + d_{22}) + \ldots\} \tag{8.6b}$$

$$\langle n\rangle_3 = 3 + \frac{N}{M_3}\{(d_{40} + d_{31}) + 2(d_{50} + d_{41} + d_{32}) + \ldots\} \tag{8.6c}$$

$$\langle n\rangle_4 = 4 + \frac{N}{M_4}\{(d_{50} + d_{41}) + 2(d_{60} + d_{51} + d_{42}) + \ldots\} . \tag{8.6d}$$

These expressions can be summarized by the following relationship

$$\left[\langle n\rangle_t - t\right]\frac{M_t}{N} = 1(d_{(t+1)0} + d_{t1}) + 2(d_{(t+2)0} + d_{(t+1)1} + d_{t2}) + \ldots , \tag{8.7}$$

which can be recast in a form more convenient for showing the dependence on the measured numbers

$$\langle n\rangle_t = t + \frac{1}{M_t}A, \qquad A = \sum_{n=1}^{\infty} nN_n, \qquad N_n = \sum_{s=0}^{n} N_{t+n-s,s} . \tag{8.8a}$$

The expressions (8.6) have the following interesting properties:

i) The average number $\langle n\rangle_t$ of photons observed with the trigger $\geq t$ is given by t plus a term depending on the frequencies d_{n_1,n_2}. Therefore the most interesting quantity is $\left[\langle n\rangle_t - t\right]$ rather than $\langle n\rangle_t$.

ii) All the frequencies d_{n_1,n_2} appearing in expressions (8.6) are multiplied by an enhancement factor N/M_1. We recall that its inverse has a simple meaning, i.e.

$$\frac{M_1(> E_{th})}{N} = \frac{1}{\sigma_{inel}}\int_{\Omega^*_{tot}} \frac{d\sigma_\gamma(\geq E_{th})}{d\Omega^*}\, d\Omega^* . \tag{8.9}$$

This expression is formula (4.6) with the dependence on E_{th} stated explicitly.

iii) The frequencies d_{n_1,n_2} appearing in expressions (8.6) obviously are only those with $n_1 \geq t$.

iv) The great sensitivity to rare high-multiplicity events obtained by using a trigger mode M_t with large t, is in some ways paid for by the danger of background contamination, since, if present, this is also multiplied by the same enhancement factor.

The average values of the number n_1 and n_2, mentioned at the beginning of this section, are given by expressions similar to (8.6) or (8.8a). These are

$$\langle n_1 \rangle_t = t + \frac{A_1}{M_t} , \qquad A_1 = \sum_{n_1=t}^{\infty} (n_1 - t) \sum_{n_2=0}^{\infty} N_{n_1,n_2} \tag{8.8b}$$

$$\langle n_2 \rangle_t = \frac{A_2}{M_t} , \qquad A_2 = \sum_{n_2=0}^{\infty} n_2 \sum_{n_1=t}^{\infty} N_{n_1,n_2} \tag{8.8c}$$

$$\langle n_1 \rangle_t + \langle n_2 \rangle_t = \langle n_t \rangle . \tag{8.10}$$

Table 7 shows, as an example, the values of d_{n_1,n_2} for the trigger mode $[M_1BB]$, $s^{\frac{1}{2}} = 53.2$ GeV and $E_{cf} = 30$ MeV, and two values of E^a_{th}.

In Table 8 we have collected the values of the enhancement factors corresponding to the averages given in Tables 5 and 6.

Figure 36 shows, for two values of the threshold E^a_{th} adopted in the analysis, the average number of $\langle n_1 \rangle$ as a function of m_1 [see Eq. (8.11) below]. The points are obtained from data collected with three different trigger modes M_t: $t = 1$, 2 and 4 and by computing for each value of t, the mean value $\langle n_1 \rangle$ obtained from events satisfying the condition

$$n_1 \geq m_1 = t + i , \tag{8.11}$$

where the integer i varies from 0 to the maximum value that still allows a statistically significant result.

The excellent agreement between the values of $\langle n_1 \rangle$ obtained from runs made with different triggers t, but the same m_1, provides a very satisfactory test of the internal consistency of the data. The broken straight line shown in Fig. 36 corresponds to the first term in Eq. (8.8b), i.e. the minimum value of $\langle n_1 \rangle$ imposed by the adopted trigger condition. The difference between the experimental points and these lines corresponds to the second term of Eq. (8.8b), which is the quantity of physical interest (Fig. 37).

Figure 38 shows, again for two values of E^a_{th}, the average number $\langle n_2 \rangle$ as a function of m_1 [see Eq. (8.11)]. Here again the satisfactory agreement between the values obtained for different values of t, but for the same value of m_1, shows the internal consistency of the data.

We expect that the data obtained with $E^a_{th} = 300$ MeV are "cleaner" than those at $E^a_{th} = 200$ MeV, because the influence of the variation undergone by the electronic trigger should be appreciably lower. In any case, both curves in Fig. 38 show that $\langle n_2 \rangle$ increases appreciably by increasing m_1. This trend reveals a correlation between the number of high-energy photons and the average number of low-energy photons.

9. DISCUSSION OF THE OBSERVED MULTIPLICITY AND COMPARISON WITH UNCORRELATED MODELS

The results that drew our attention from the beginning were the multiplicity distributions (Figs. 29, 30 and 35) and the large mean values of the number of fired HV^n (Tables 5 and 6, and Fig. 31). These are not due, in our opinion, to background or secondary effects. As we point out in Section 3 (and Appendix B), the background cannot seriously affect our results for the following reasons: (a) The HV multiplicity of the events triggered at random amounted in the worst case to 0.3 HV counters/event. (b) The very good agreement between the mean values derived from ΣΣ and BB data (Fig. 31) provides *a posteriori* a proof that the background does not seriously affect even the ΣΣ data. We recall that the estimated background in the case of the BB data is about ten times smaller than for the ΣΣ data. (c) The mean values of $m(HV^n)$ obtained with the neutral trigger (Table 6) tend to be greater -- and not smaller -- than with the usual trigger.

The most important secondary effect is represented by spurious gamma-rays originating in the walls of the vacuum chamber or other objects in the surroundings, where a charged secondary undergoes an inelastic collision with emission of neutral pions. According to a rather generous estimate, this effect should produce an increase of $\langle m(HV^n) \rangle$ certainly not larger than 1% (Appendix C).

Assuming that such a conclusion is correct, we can proceed to derive from $\langle m(HV^n) \rangle$ the average number $\langle n_\gamma \rangle$ of gamma-rays observed in the detector. With such an aim, a few further effects should be taken into consideration. Firstly, we should introduce a (negative) correction of about 8% (see Section 5 and Appendix D) for gamma-rays crossing one HV counter and that fire also the near-by HV counter, because the corresponding shower deposits in both of them an energy greater than E_{cf}. Further negative corrections originate from the fact that in a few per cent of the cases the two gamma-rays originating from the π^0 fire two different HV counters.

On the contrary, a positive correction is required, because in high-multiplicity events two gamma-rays originating from two different π^0 can cross the same HV counter. Such a probability depends on any possible correlation between the emitted π^0. If we assume that, within the solid angle covered by the detector, the gamma-rays are emitted without any angular correlation and with almost constant angular density, the mean number of gamma-rays $\langle n_\gamma \rangle$ is connected to $\langle m(HV^n) \rangle$ by the relationship

$$\langle n_\gamma \rangle = -d \ln \left[1 - \frac{\langle m(HV^n) \rangle}{d} \right] ,$$

where d is the number of HV counters constituting the detector: in our case d = 32.

Such a correction increases logarithmically with $\langle m(HV^n)\rangle$ and reaches about 10% for $\langle m(HV^n)\rangle = 6$. This means that this correction compensates within a few per cent the sum of the two previous corrections. In other words, the mean values $\langle m(HV^n)\rangle$ we have observed should provide without corrections a rough estimate of the mean value $\langle n_\gamma\rangle$ of the gamma-rays crossing the detector.

As we have shown in Section 8, in great part the large values of $\langle m(HV^n)\rangle$ originate from the trigger mode M_t and what we should try to interpret is only the difference between $\langle m(HV^n)\rangle_t$ and t, divided by the enhancement factor N/M_t (Table 8).

In order to clarify in which sense the mean values $\langle m(HV^n)\rangle$ are large, two orders of consideration may be useful. The first one is based on the relationship (8.7) that we may apply for example to the BB data taken at $s^{\frac{1}{2}} = 53.2$ GeV. One has (for the electronic threshold E_{th})

$$\left[\langle m(HV^n)_1 - 1\rangle\right] \frac{M_1}{N} = 0.14 \pm 0.01,$$

$$\left[\langle m(HV^n)_4 - 4\rangle\right] \frac{M_4}{N} = \frac{2.51}{2.85} \times 10^{-4} = (0.9 \pm 0.1) \times 10^{-4} .$$

Thus we clearly see how the large values of $\langle m(HV^n)\rangle_t$ originate from high-multiplicity events representing a fraction of the cross-section, which becomes about 10 times smaller each time we increase by 1 the number of photons required by the trigger.

As pointed out in Section 8, this very high sensitivity to rare events of high multiplicity unavoidably regards also any -- even small -- possible contamination of background and/or spurious photons.

The second type of consideration is based on the direct comparison of the observed values of $\langle m(HV^n)\rangle_t$ with the values of $\langle n_\gamma\rangle$ computed from some simple models. We can start from the mean multiplicity computed by integrating the inclusive one-particle angular distribution over the geometry of the detector and the photon spectrum from $k = E_{cf} = 30$ MeV to infinity:

$$\langle n_\gamma\rangle_\Omega \simeq \langle n_{ch}\rangle_\Omega \simeq 0.6 .$$

This computed value, however, cannot be compared directly with the data of Table 5, even in the case of the trigger mode M_1, since they correspond to different definitions.

For this reason we have made two computations. The first one is a Monte Carlo, based on the following assumptions (Appendix D): i) the emission of the π^0 is independent of the emission of the charged pions; ii) the observed single-particle inclusive spectrum is assumed to hold for any value of the multiplicity

and in the whole angular range; iii) the observed inclusive angular distribution is assumed for any value of the number of emitted π^0; iv) the multiplicity distribution of the π^0 is assumed to be Poissonian in the value of the number of emitted π^0, with the average value

$$\langle n_{\pi^0} \rangle = \frac{1}{2} \left[\langle n_{\pi^+} \rangle + \langle n_{\pi^-} \rangle \right] .$$

The computation was made by taking into account, besides the Lorentz transformations to the laboratory frame, the geometry of the detector and the conditions imposed by the trigger mode M_1. Also the pulse-height fluctuations[7] in the HV and the absorption of the Čerenkov light in the lead glass were taken into account. From such a calculation we obtained, with $E_{cf} = 30$ MeV,

$$\langle m(HV^n) \rangle_{MC} = 1.49 \pm 0.01, \quad \sigma = 0.71$$

by neglecting the lateral spread of the showers in the lead-glass counters. If this effect is taken into account, the mean value increases to

$$\langle m(HV^n) \rangle_{MC} = 1.61 ,$$

which still is almost one half the observed value. This seems to be an indication that the assumption of the uncorrelated model over the whole phase-space volume, with values of the parameters fixed according to the results of the one-particle inclusive cross-section measurements, does not allow a satisfactory representation of the multiple production we observe in the detector.

The same conclusion is reached if, instead of the mean values, we compare the distribution of multiplicity of the fired HV observed experimentally with the results of the Monte Carlo computation, as well as of what we call an independent emission model (Appendix E).

In Fig. 39 we have plotted the integral distribution (i.e. summed from m to infinity) versus m obtained with the trigger mode $[M_1 BB]$ with the result of these two models. The difference between the two computed curves originates from the fact that in the Monte Carlo we take into account the shower's spread and fluctuations, as well as a few instrumental features such as the so-called "transit factor", which are not considered in the IEM. Both theoretical curves fall down with increasing m much faster than the observed distribution.

As the next step, we have tried to see if, by leaving as free parameters the mean values of the numbers of particles emitted within the phase-space volume defined by the detector, it was possible to fit the observed data by means of an uncorrelated model. This can be indicated as "locally uncorrelated", since its basic assumptions are required to be valid (at least approximatively) only within the phase-space volume defined by the detector.

Such an attempt should be considered mainly as an exercise in order to see how far the observed distributions and the corresponding mean multiplicities fit together in a simple computational scheme.

In order to disentangle the effect of the trigger mode, two different types of fit have been made, each of which involves four variables. In the first one the numbers of neutral (N) and charged (C) HV that one would observe in the absence of the condition M_t are lumped together (N + C), but those belonging to the "OUT" detector are separated from those belonging to the "IN" detector. In the second type of fit the "OUT" and "IN" detectors are lumped together (OUT + IN), while the neutrals HV(N) are separated from the charged ones (C). In both cases the subscript 1 refers to an energy deposited in a single HV greater than E^a_{th} = 200 MeV, while the subscript 2 refers to an energy deposited in a single HV between E_{cf} = 30 MeV and E^a_{th}. The model incorporates the trigger mode.

A fit of each of these two types has been made to the $[M_2\Sigma\Sigma]$ and $[M_4\Sigma\Sigma]$ data, separately. The values of the free parameters corresponding to the best fit are collected in Table 9. In three out of four cases the agreement between the results for the two trigger modes is satisfactory. But if one tries an over-all best fit of the $[M_2\Sigma\Sigma]$ and $[M_4\Sigma\Sigma]$ data taken together, the value of χ^2 increases considerably. Therefore, we can say that the observed distributions are close to those computed from the locally uncorrelated model provided large mean values -- different for each trigger mode -- are accepted for the average multiplicities one would observe in absence of any trigger. These mean values are connected to the mean values of the HV multiplicities observed under the condition M_t by the relationships (F.10) and (F.11) of Appendix F. These have been used for computing the average values of the HV^n multiplicity we expect to observe in our detector and compare them with the values actually observed (Table 10). The good agreement indicates the consistency of the analysis.

It should be noticed that the difficulty to fit with the same set of values of the free parameters the data obtained with different trigger modes M_t is related to the remark made in Sections 7 and 8: the difference $[\langle m(HV^n)\rangle - t]$ obtained with the neutral trigger (Figs. 8, 9, 12, 35, 36 and 37) increases by increasing t. These experimental observations seem to originate from the fact that by selecting events with a greater multiplicity of photons of large energy, we select a class of events that have also a greater multiplicity of low-energy photons.

In conclusion, we can summarize our results on the multiplicities of the fired HV^n as follows:

i) The various multiplicity distributions obtained with different trigger modes in a narrow region around 90° have multiplicity tails considerably larger than that computed from uncorrelated π^0 production.

ii) These distributions can be analytically represented as Poissonians and in each case the corresponding mean value, obtained from the best fit, turns out to agree with the observed mean value.

iii) Such a fit is rather good for the results obtained with a single trigger mode, while it becomes less satisfactory if one tries to fit, with a unique set of free parameters, the results obtained with different trigger modes.

iv) The rather large tails of the distributions can be due, completely or in part, to correlations between high-energy and low-energy photons of the type indicated by Figs. 36 to 38: if one selects events with a larger number of high-energy photons ($k \gtrsim 3\ E_{th} \simeq 0.6$ GeV), the mean number of low-energy photons ($30 \leq k \lesssim 600$ keV) also turns out to be large.

Acknowledgements

We are deeply indebted to the CERN-Columbia-Rockefeller group for their generous help in sharing their detector, as well as their data recording system, with us, without which our exploratory experiment reported here would not have been possible. We also wish to express our grateful appreciation and thanks to Messrs. G. Muratori, F. Doughty and K. Ley for the design and construction of the multiwire proportional chambers, to Messrs. H. Verweij, F. Cesaroni and J. Tarlé for the design and construction of the electronic logic system; to Messrs. P. Scharff-Hansen, B. Taylor, H. Wendler and B. Baldo for their help in setting up our computer system and programming; to Messrs. G. Basti and S. Guerra for all the necessary constructions and assembly of our experiment. We wish particularly to express our thanks to Mr. B. Couchman, Dr. K. Potter and members of the operating crew of the ISR for their generous help in making our exploratory experiment a successful one.

Table 1

Intervals of rapidity $\Delta\eta$ covered by the HV counters

HV	1	3	5	7	9	11	13	15
	2	4	6	8	10	12	14	16
OUT	0.20	0.21	0.22	0.23	-0.23	-0.22	-0.21	-0.20
IN	0.15	0.16	0.17	0.18	-0.18	-0.17	-0.16	-0.15

Table 2a

Data concerning the downstream counters

Beam counters	Area (cm^2)	Distance from centre i.r.	Typical counting rates/sec
B_1, B_2	40 × 40	4.50	$\sim 4 \times 10^3$
B_1, B_2		5.30	
Σ_1, Σ_2	100 × 100	5.65	$\sim 2 \times 10^4$

Table 2b

Efficiency of the downstream counters at various energies

p_0 (GeV)	$\dot{N}_{BB}/L\sigma_{inel}$ (%)	$\dot{N}_{\Sigma\Sigma}/L\sigma_{inel}$ (%)
11.0	10	44
15.3	10	51
22.6	15	70
26.6	18	73

Table 3

Summary of runs

p_0 (GeV/c)	11		15		22		26		31	
Trigger mode	No. runs	No. events	No. runs	No. events	No. runs	No. events	No. runs	No. events	No. runs	No. events
M_t										
M_1							5	14,172		
M_2			1	5,426			25	48,196		
M_3			1	3,110			11	19,599		
M_4	20	7,058	8	4,257	45	65,291	94	156,495	5	724

Table 4

Rapidity relative correlations: $R(\eta_1,\eta_2)$; $s^{\frac{1}{2}} = 53.2$ GeV

$\Delta\eta$	η_1	η_2	$\Delta\phi_1$	$\Delta\phi_2$	$M_1\Sigma\Sigma$	$M_4\Sigma\Sigma$	
					E_{th} = 300	E_{th} = 300	E_{th} = 400 MeV
0.00	0.090 ± 0.090 0.265 ± 0.085 0.430 ± 0.080 0.585 ± 0.075	η_1	0° to +26°	0° to −26°	0.60 ± 0.2	0.62 ± 0.13	0.60 ± 0.30
0.16	the same as above	η_1 ± 0.16	0° to +26°	0° to −26°	0.35 ± 0.20	0.53 ± 0.10	0.84 ± 0.30
0.51	+0.51 −0.51	0	−26° to +26°	−26° to +26°	0.38 ± 0.10	0.43 ± 0.06	0.62 ± 0.12
1.02	+0.51	−0.51	−26° to +26°	−26° to +26°	0.23 ± 0.15	0.14 ± 0.08	0.30 ± 0.17

Table 5

Mean values of the multiplicities $\langle m(HV^n) \rangle$ and $\langle m_{tracks} \rangle$

		E_{cf} = 30 MeV *)			E_{cf} = 210 MeV *)			E_{cf} = 600 MeV *)		
p_0 (GeV/c)	Trigger mode	$\langle m(HV^n) \rangle$	σ	m_{max}	$\langle m(HV^n) \rangle$	σ	m_{max}	$\langle m(HV^n) \rangle$	σ	m_{max}
26.6	M_1BB	2.68 ± 0.04	1.50	10	1.07 ± 0.02	0.64	5	0.19 ± 0.01	0.40	2
11.8	M_4BB	5.08 ± 0.36	1.26	7	3.17 ± 0.20	0.69	4	0.25 ± 0.12	0.43	1
15.4	M_4BB	5.93 ± 0.34	1.84	9	3.52 ± 0.19	1.04	5	0.62 ± 0.14	0.76	3
22.5	M_4BB	6.16 ± 0.07	1.89	13	3.20 ± 0.05	1.20	7	0.58 ± 0.03	0.80	5
26.6	M_4BB	6.51 ± 0.04	2.00	16	3.57 ± 0.02	1.07	9	0.72 ± 0.02	0.85	5
31.0	M_4BB	6.51 ± 0.22	1.91	12	3.73 ± 0.12	1.06	6	0.68 ± 0.08	0.68	2

p_0 (GeV/c)	Trigger mode	$\langle m_{tracks} \rangle$	σ	m_{max}
26.6	M_1BB	1.09 ± 0.03	1.22	8
26.6	M_4BB	2.57 ± 0.05	2.31	17

*) E_{cf} = cut-off energy

Table 6

Mean values of the multiplicities obtained with the neutral trigger and subtracting the photons responsible for the trigger from each event: $s^{\frac{1}{2}} = 53.2$ GeV

	$\langle n - t \rangle$	$\langle (n - t) \rangle^2$	$\langle (n - t)^2 \rangle$	$\langle (n - t)(n - t - 1) \rangle$	$\langle m \rangle_{tracks}$
$[M_1 BB]$	1.78 ± 0.02	3.16 ± 0.61	5.48 ± 0.73	3.70 ± 0.92	0.870 ± 0.025
$[M_2 BB]$	2.27 ± 0.04	5.15 ± 1.59	8.45 ± 1.60	6.18 ± 1.95	0.98 ± 0.02
$[M_4 BB]$	3.35 ± 0.05	11.22 ± 3.42	15.98 ± 3.20	12.63 ± 3.71	1.11 ± 0.025

Table 7

Two-index frequencies*) $d^{(1)}_{n_1,n_2}$ ($\times 10^3$) observed at $s^{\frac{1}{2}}$ = 53.2 GeV with the trigger mode $[M_1 BB]$, E_{cf} = 30 MeV

n_1 \ n_2	0	1	2	3	4	5	6	7	8
	E^a_{th} = 200 MeV								
1	14.6 (5.7%)	16.6 (5.4%)	11.2 (6.5%)	6.65 (8.5%)	2.60 (14%)	1.04 (21%)	0.66 (27%)	0.14 (58%)	0.094 (70%)
2	3.3 (12%)	4.3 (11%)	2.74 (13%)	1.84 (16%)	0.71 (26%)	0.47 (32%)	0.05 –	0.05 –	0.05 –
3	0.19 (50%)	0.50 (30%)	0.38 (35%)	0.19 (50%)	0.14 (58%)	0.05 –	– –	– –	– –
4	0.05 –	0.14 (58%)	0.05 –	0.05 –	– –	– –	– –	– –	– –
5	–	0.05	–	0.05	0.05	0.05	–	–	–
	E^a_{th} = 300 MeV								
1	11.5 (6.5%)	15.4 (5.6%)	10.9 (6.6%)	6.98 (8%)	3.26 (12%)	1.27 (19%)	0.85 (24%)	0.05 –	0.094 –
2	1.04 (21%)	1.46 (18%)	1.13 (20%)	0.80 (24%)	0.33 (38%)	0.28 (41%)	0.05 –	0.094 (70%)	0.05 –
3	– –	0.094 (70%)	0.094 (70%)	0.094 (70%)	0.05 –	– –	– –	– –	– –
4	–	0.05	–	–	0.05	–	0.05	–	–

*) Numbers in parentheses show relative error: d_{n_1,n_2} = 0.05 corresponds to a single count (relative error: 100%).

Table 8

Enhancement factors: N/M_t $[E^a_{th}$ *) and $E_{cf} \simeq 30$ MeV$]^t$

Trigger	N/M_t
M_1BB	12.4 (± 7.9%)
$M_1\Sigma\Sigma$	9.4 (± 7.5%)
M_4BB	2.85×10^4 (± 13%)
$M_4\Sigma\Sigma$	2.15×10^4 (± 7.2%)
M_1^nBB **)	11.3 (± 9%)
M_4^nBB **)	1.88×10^4 (± 15%)

*) In the case of the trigger mode $[M_1BB]$, the value of N/M_1 becomes 14.5 (± 8.7%) for E^a_{th} = 200 MeV, 17.9 (± 8.8%) for E^a_{th} = 300 MeV.

**) Neutral trigger.

Table 9

Values of the free parameters determined by the best fit

	$[M_2BB]$	$[M_4BB]$
$(N_1 + C_1)_{IN}$	0.43 ± 0.05	0.68 ± 0.07
$(N_2 + C_2)_{IN}$	0.78 ± 0.05	1.40 ± 0.01
$(N_1 + C_1)_{OUT}$	2.74 ± 0.36	2.31 ± 0.05
$(N_2 + C_2)_{OUT}$	0.20 ± 0.28	1.46 ± 0.04
χ^2/f	2.2	4.3
$(C_1)_{OUT+IN}$	0.21 ± 0.07	0.41 ± 0.05
$(C_2)_{OUT+IN}$	0.46 ± 0.09	0.68 ± 0.06
$(N_1)_{OUT+IN}$	0.29 ± 0.07	1.41 ± 0.20
$(N_2)_{OUT+IN}$	3.37 ± 0.08	4.01 ± 0.03
χ^2/f	0.39	1.48

Table 10

Comparison of the multiplicities of the HV^n and HV^c deduced from the locally uncorrelated model with the observed multiplicities in the two sections of the detector ("IN" and "OUT") and globally

	$[M_2BB]$		$[M_4BB]$	
	Locally uncorr. model	Observed	Locally uncorr. model	Observed
$(HV)^{n+c}_{IN}$	1.28 ± 0.09	1.38 ± 0.06	2.52 ± 0.06	2.50 ± 0.04
$(HV)^{n+c}_{OUT}$	3.3 ± 0.5	3.38 ± 0.1	5.24 ± 0.03	5.22 ± 0.04
$(HV)^{c}_{IN+OUT}$	0.69 ± 0.14	0.71 ± 0.03	1.20 ± 0.1	1.22 ± 0.03
$(HV)^{n}_{IN+OUT}$	4.04 ± 0.15	4.05 ± 0.1	6.5 ± 0.3	6.51 ± 0.05

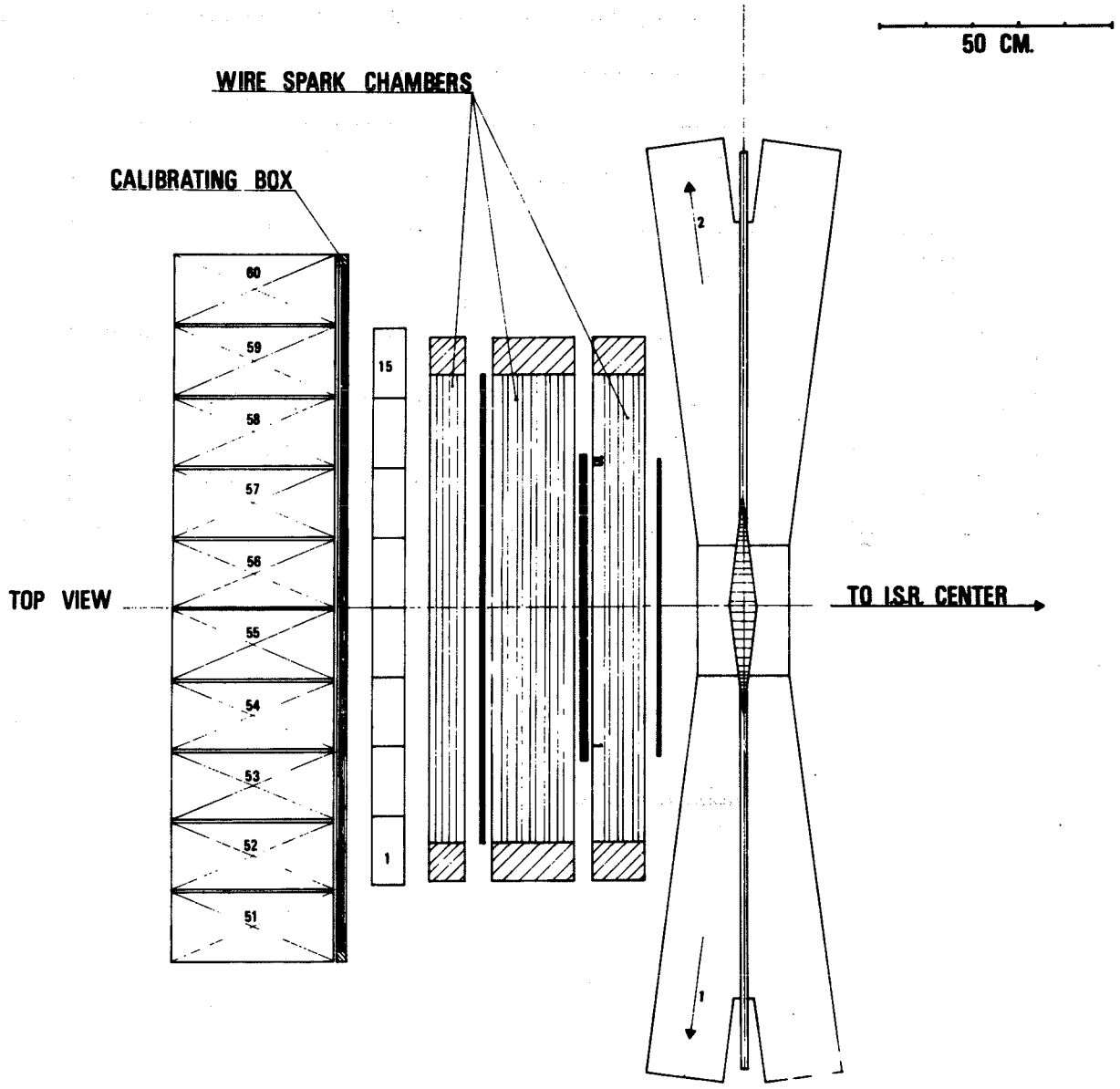

Fig. 1 Top view of one of the two symmetrical detectors

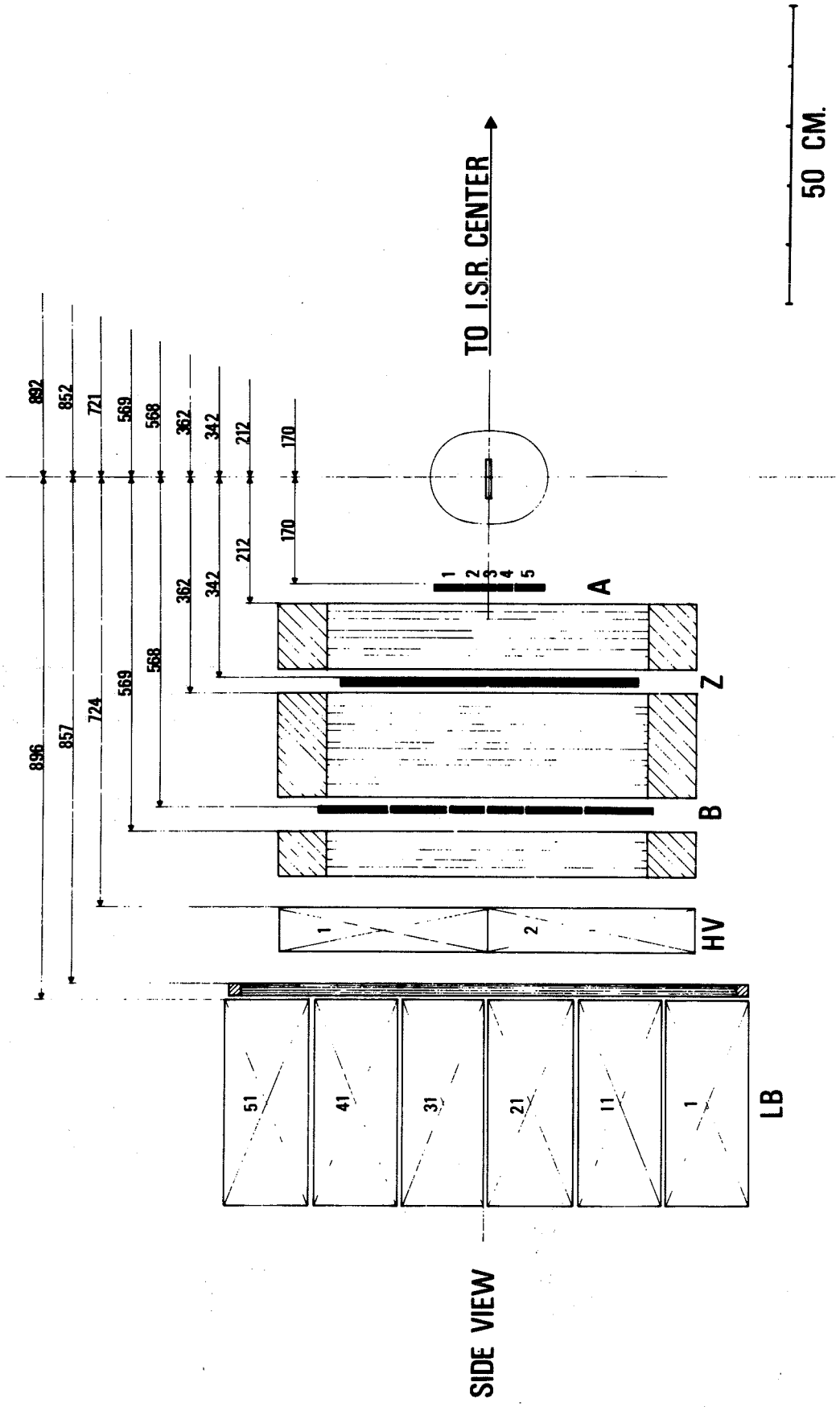

Fig. 2 Longitudinal view of one of two symmetrical detectors

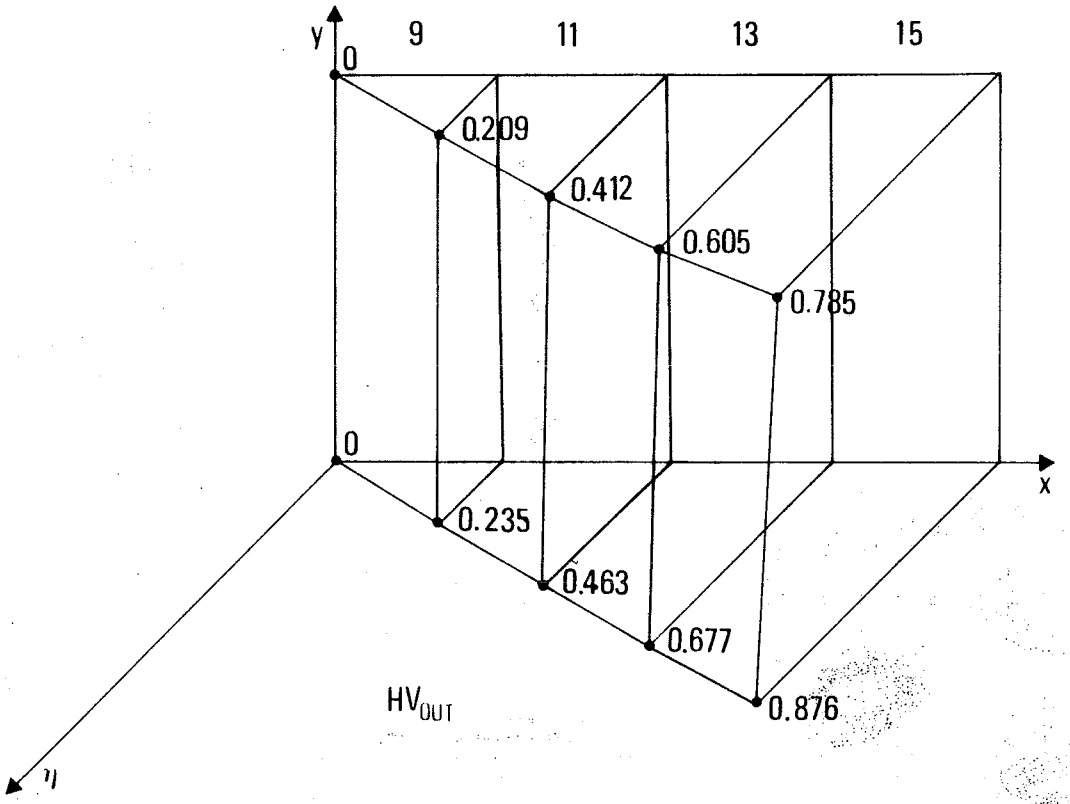

Fig. 3a Centre-of-mass rapidity of gamma-rays emitted from the centre of the interaction region in the direction of the contour of the HV counters (Numbers 9, 11, 13, and 15) of the "OUT" detector. The x-axis is the direction of the incoming protons, the y-axis is vertical.

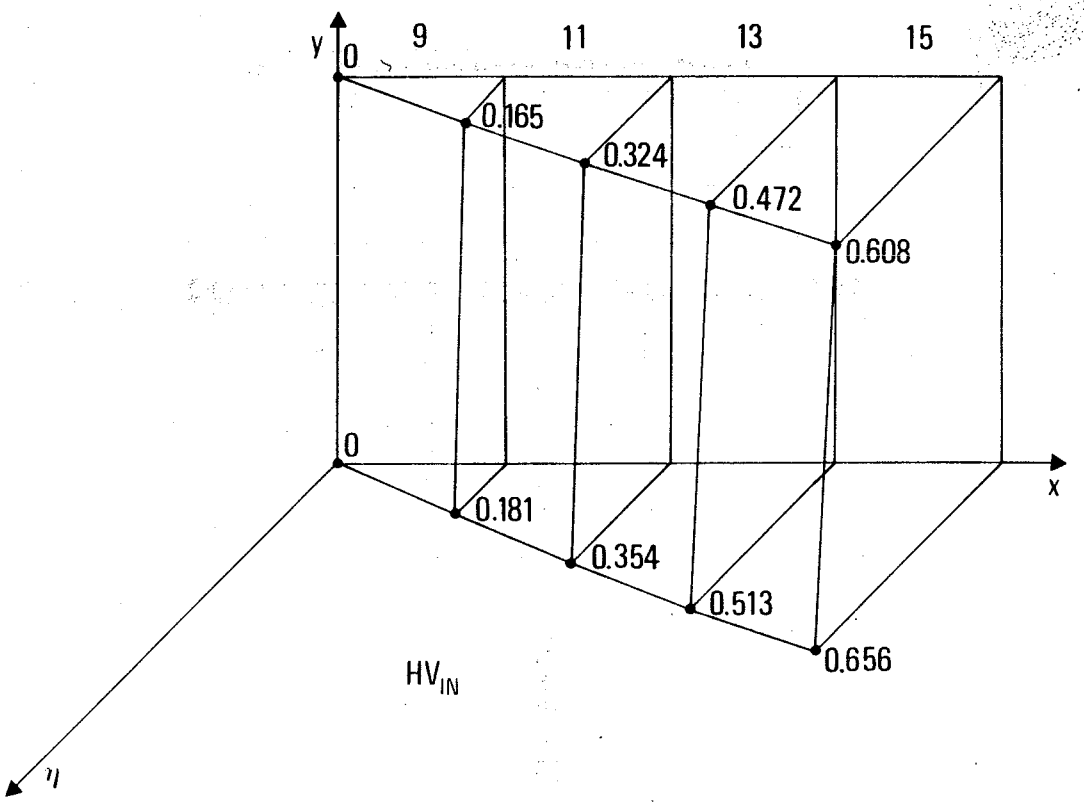

Fig. 3b Centre-of-mass rapidity of gamma-rays emitted from the centre of the interaction region in the direction of the contour of the HV counters (Numbers 9, 11, 13, and 15) of the "IN" detector. The x-axis is the direction of the incoming protons, the y-axis is vertical.

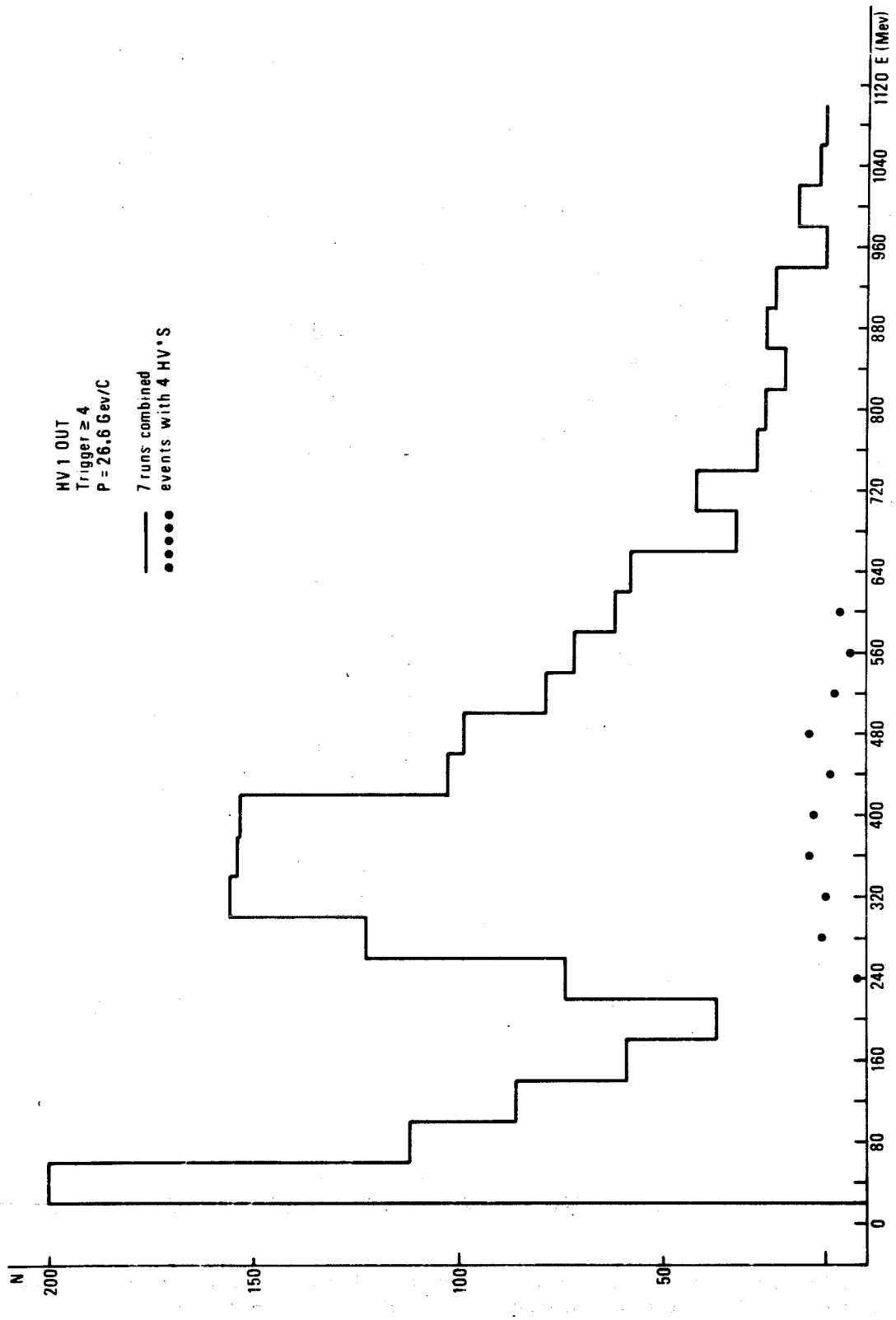

Fig. 4 Distribution of the energy deposited by neutral secondaries in $HV1_{OUT}$, obtained with the trigger mode $[M_4\Sigma\Sigma]$ at a c.m. energy $s^{\frac{1}{2}} = 53.2$ GeV. The black dots show the energy spectrum due to events in which four and only four HV^n were fired.

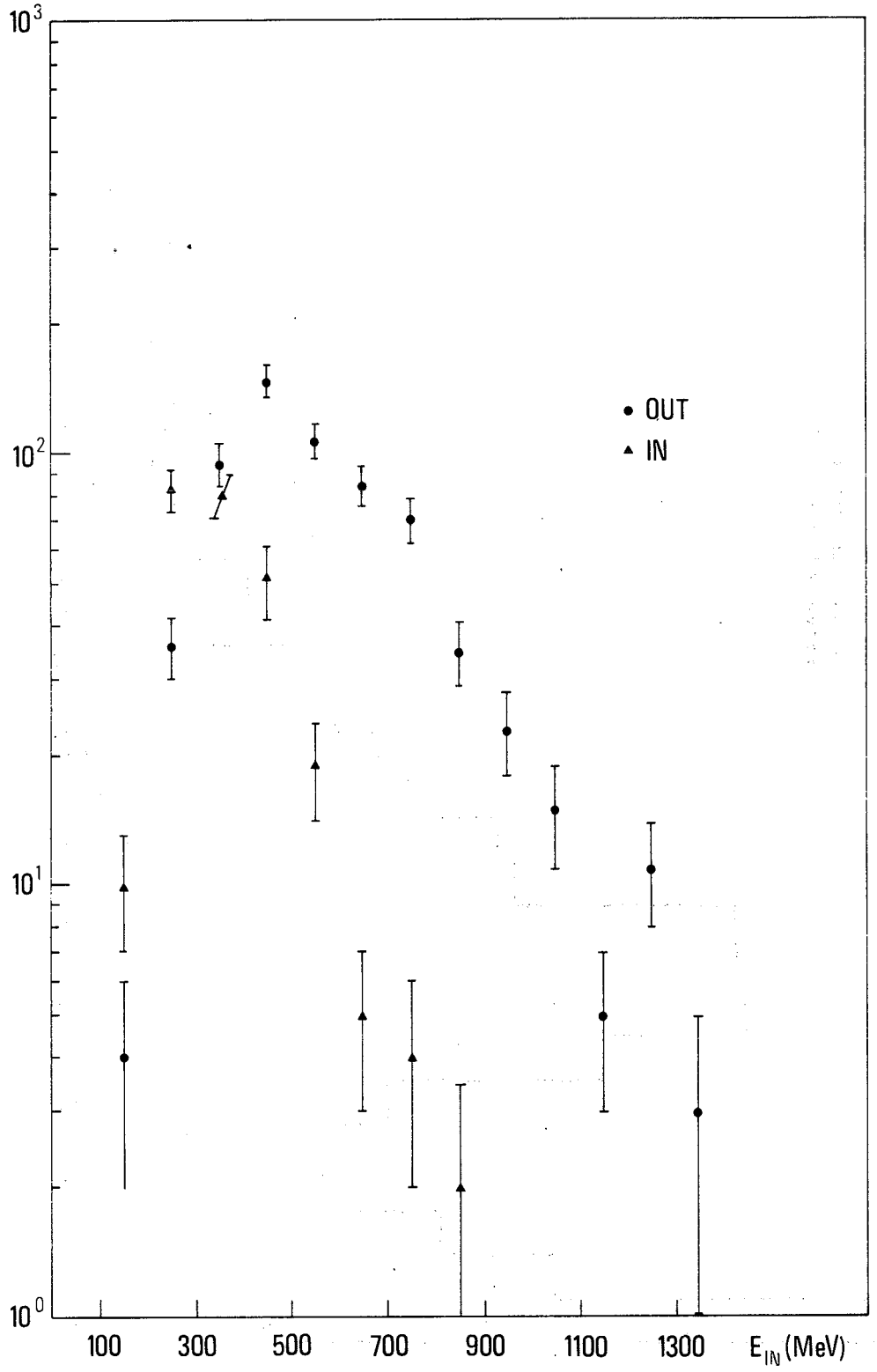

Fig. 5 Distribution of the energy deposited by the photons that contribute to the trigger $[M_1BB]$ in the HV counters at 90° (Nos. 7 + 8 + 9 + 10): $s^{\frac{1}{2}} = 53.2$ and $E^a_{th} = 0.200$ GeV.

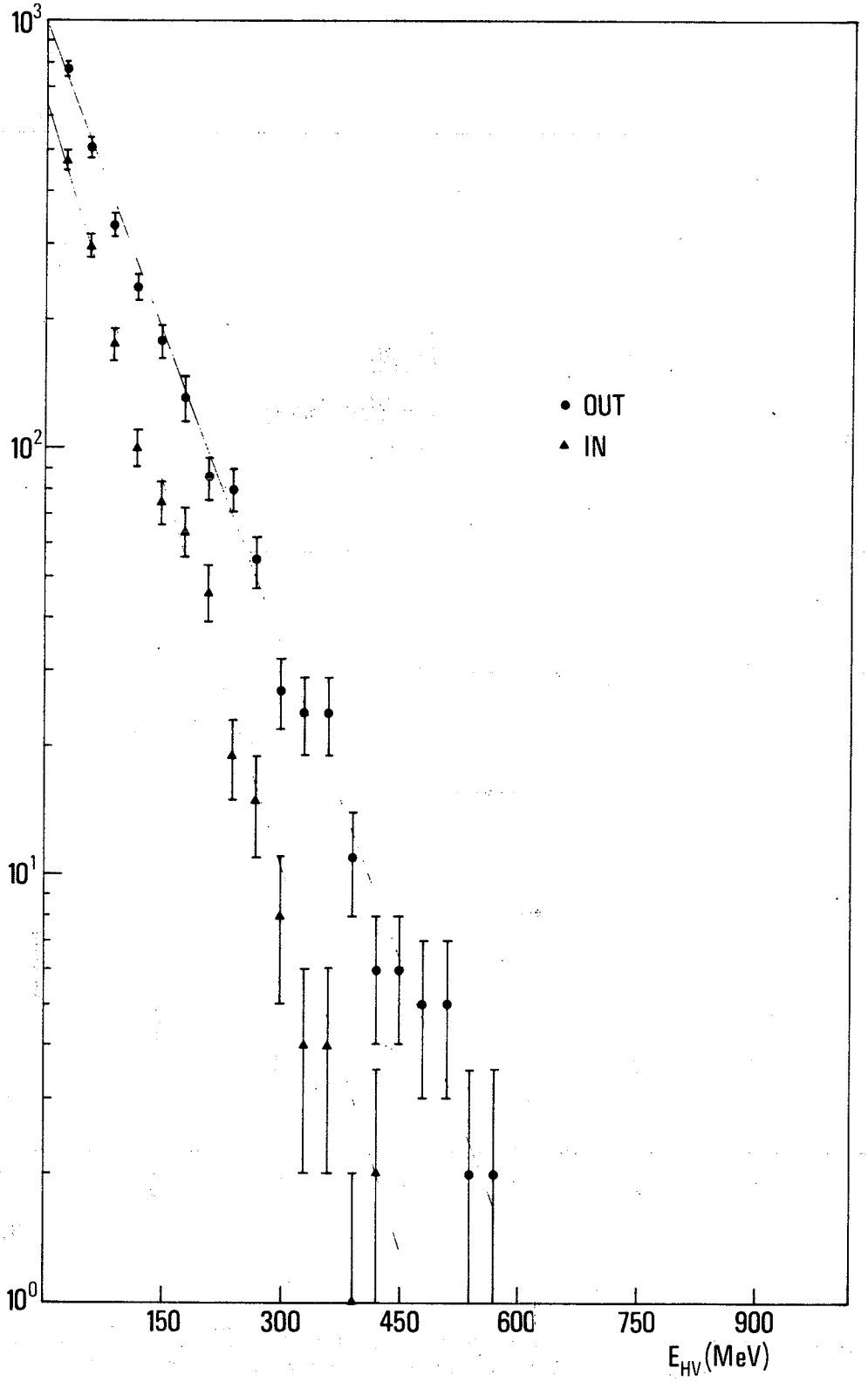

Fig. 6 Distribution of the energy deposited by the photons that do not contribute to the trigger $[M_1BB]$ in the HV counters at 90° (Nos. 7 + 8 + 9 + 10): $s^{\frac{1}{2}}$ = 53.2 GeV and E^a_{th} = 0.200 GeV.

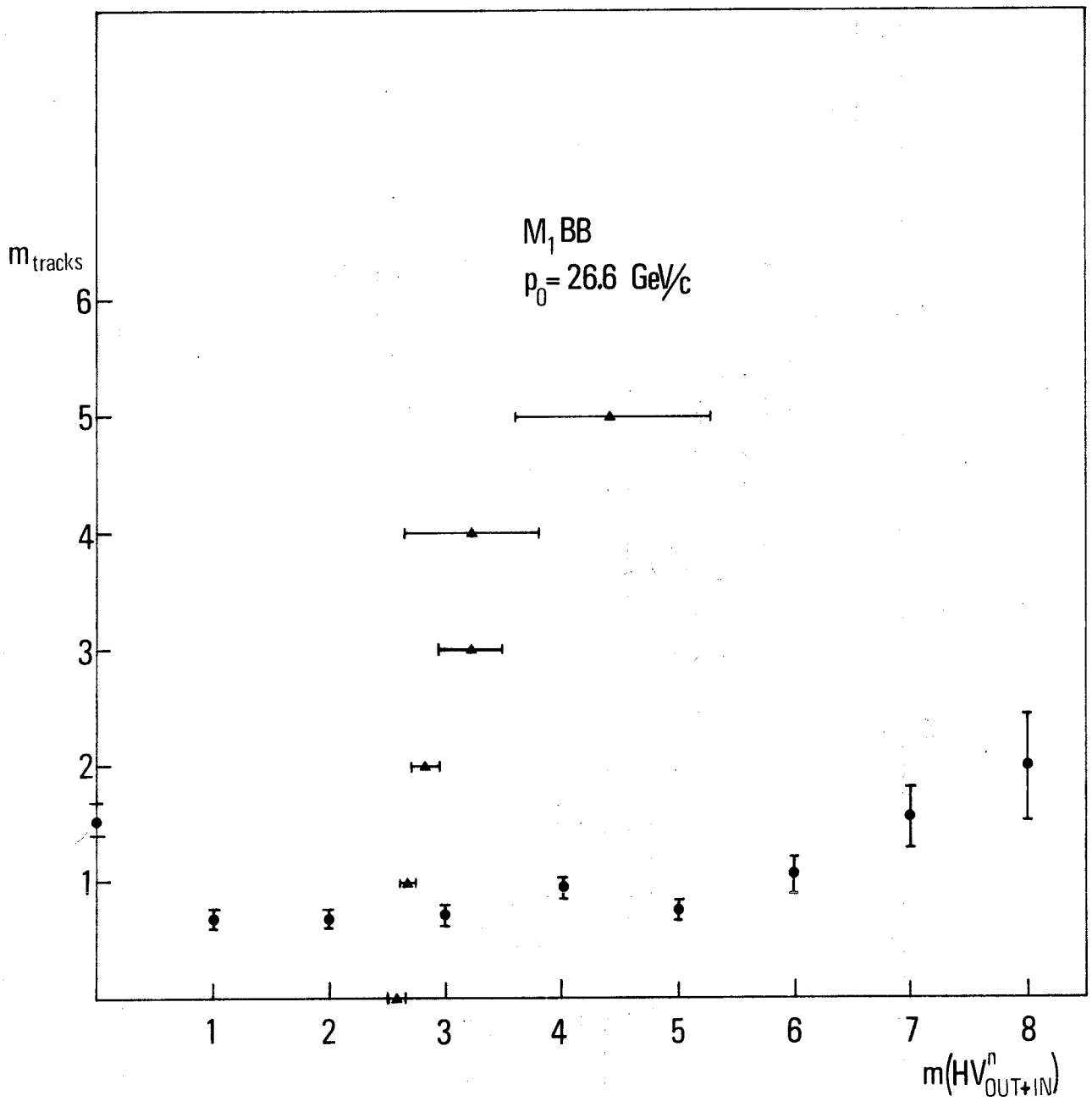

Fig. 7 Regression lines relative to the variables x = m (HV^n: OUT + IN) and y = m_{tracks} = number of reconstructed tracks (OUT + IN). All HV^n fired with $E \geq E_{cf}$ = 30 MeV are taken into account: $s^{\frac{1}{2}}$ = 53.2 GeV; [M_1BB].

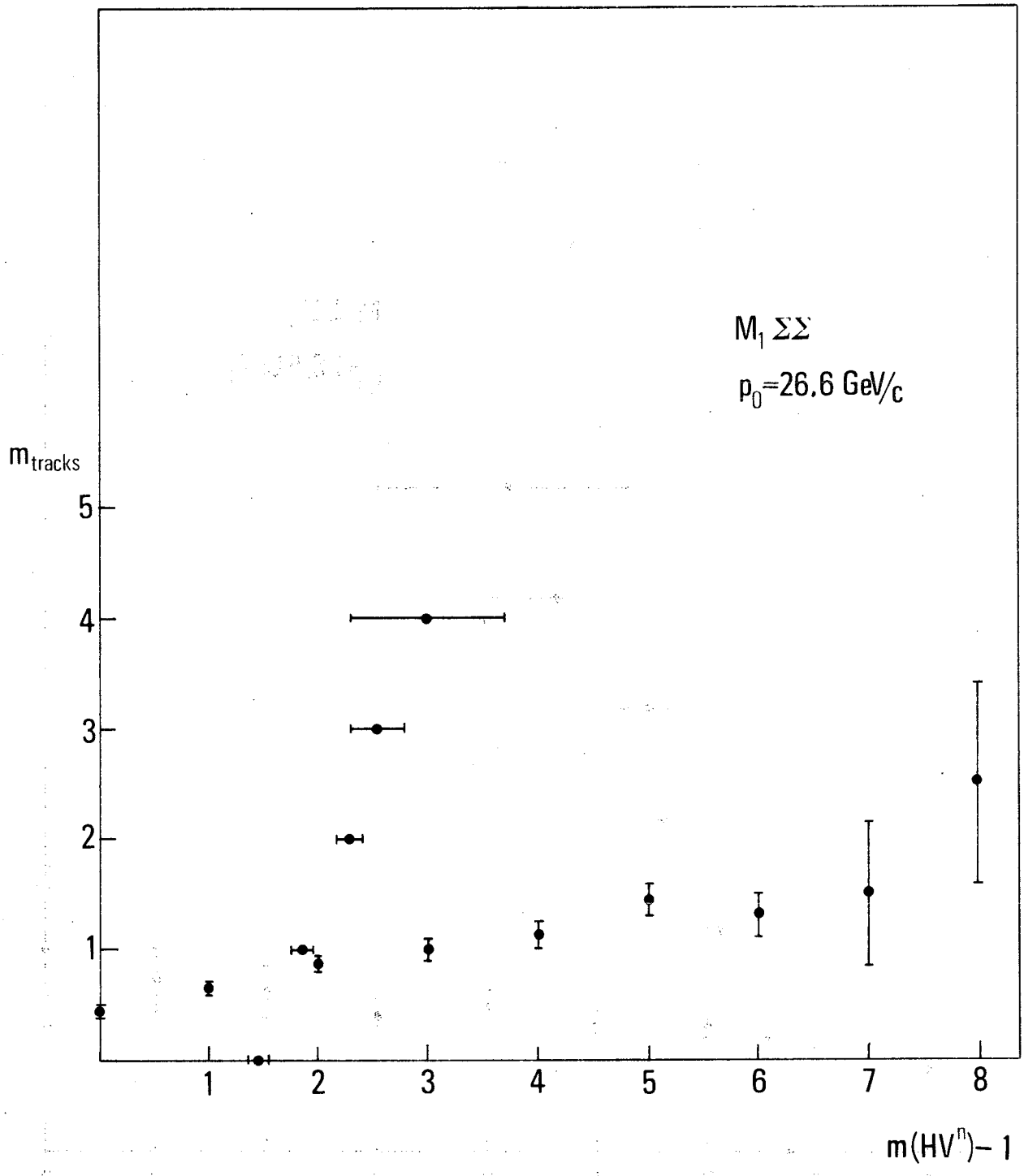

Fig. 8 Regression lines similar to those of the previous figure, except that we have used the neutral trigger and in the computation of $\langle m(HV^n)\rangle$ the HV responsible for the trigger have been subtracted in each event: $s^{\frac{1}{2}}$ = 53.2 GeV; $[M_1\Sigma\Sigma]$.

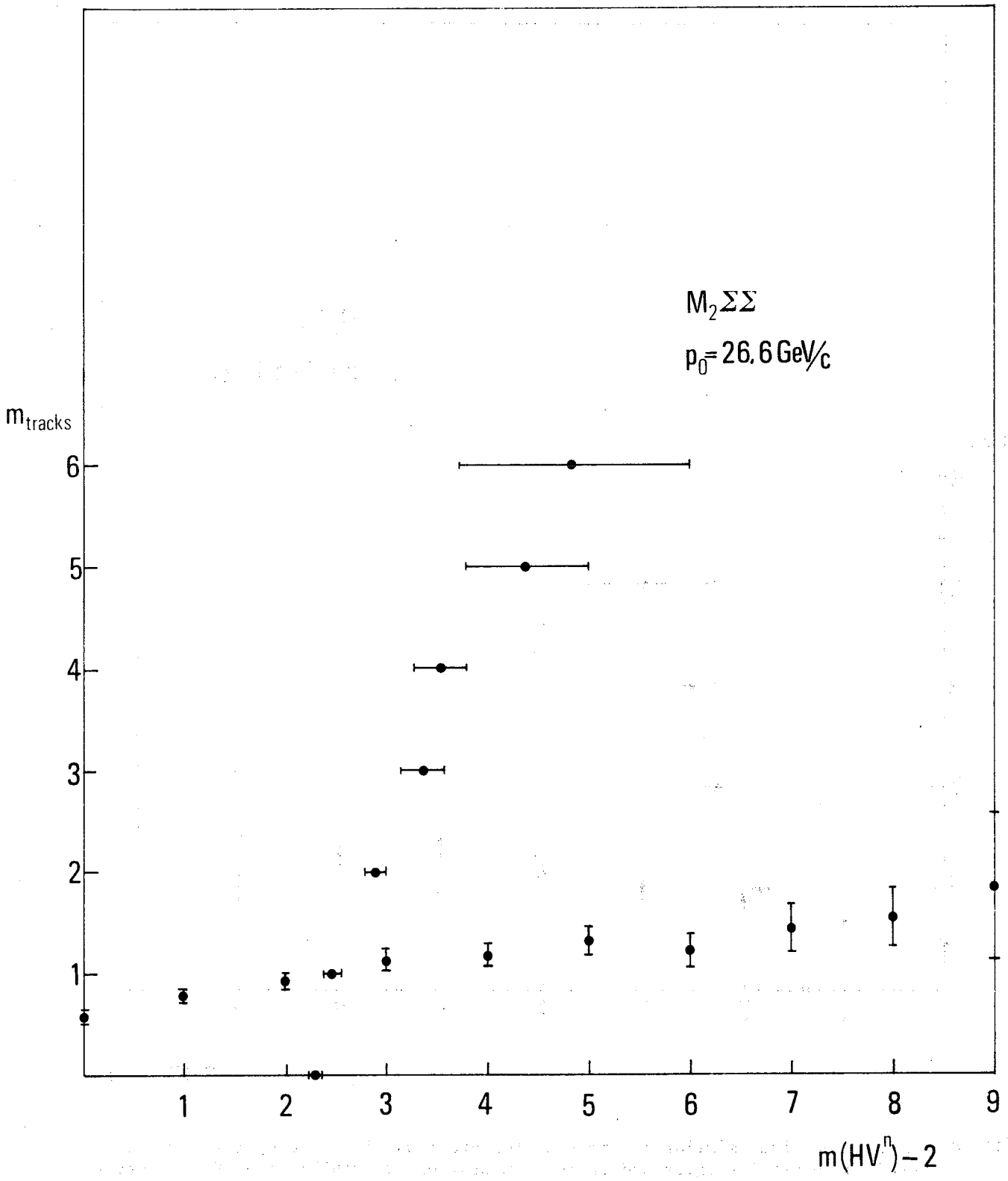

Fig. 9 Regression lines similar to those of the preceding figure, except that the trigger is $[M_2\Sigma\Sigma]$.

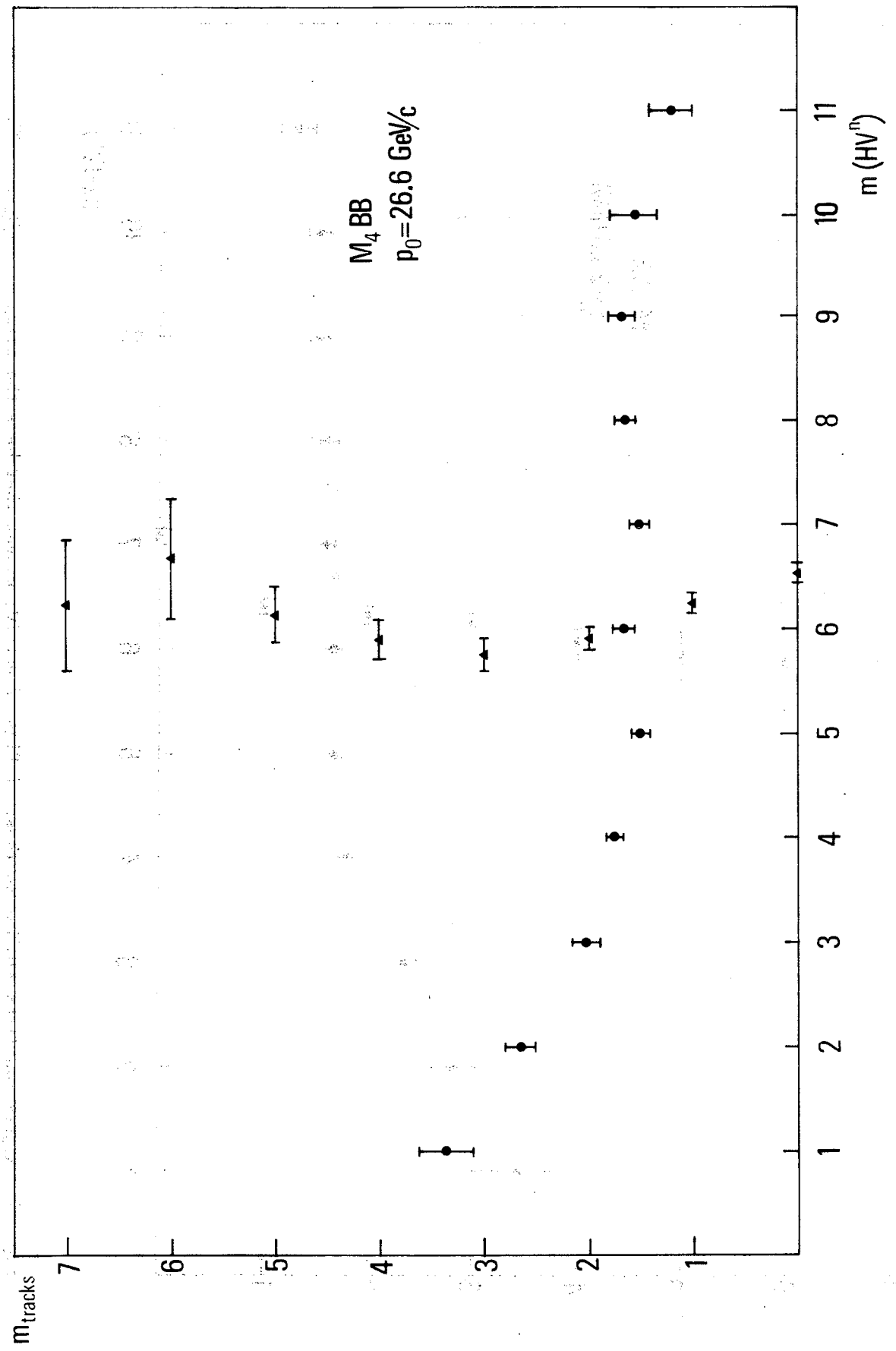

Fig. 10 Regression lines similar to those of Fig. 7, except that the trigger is [M_4BB].

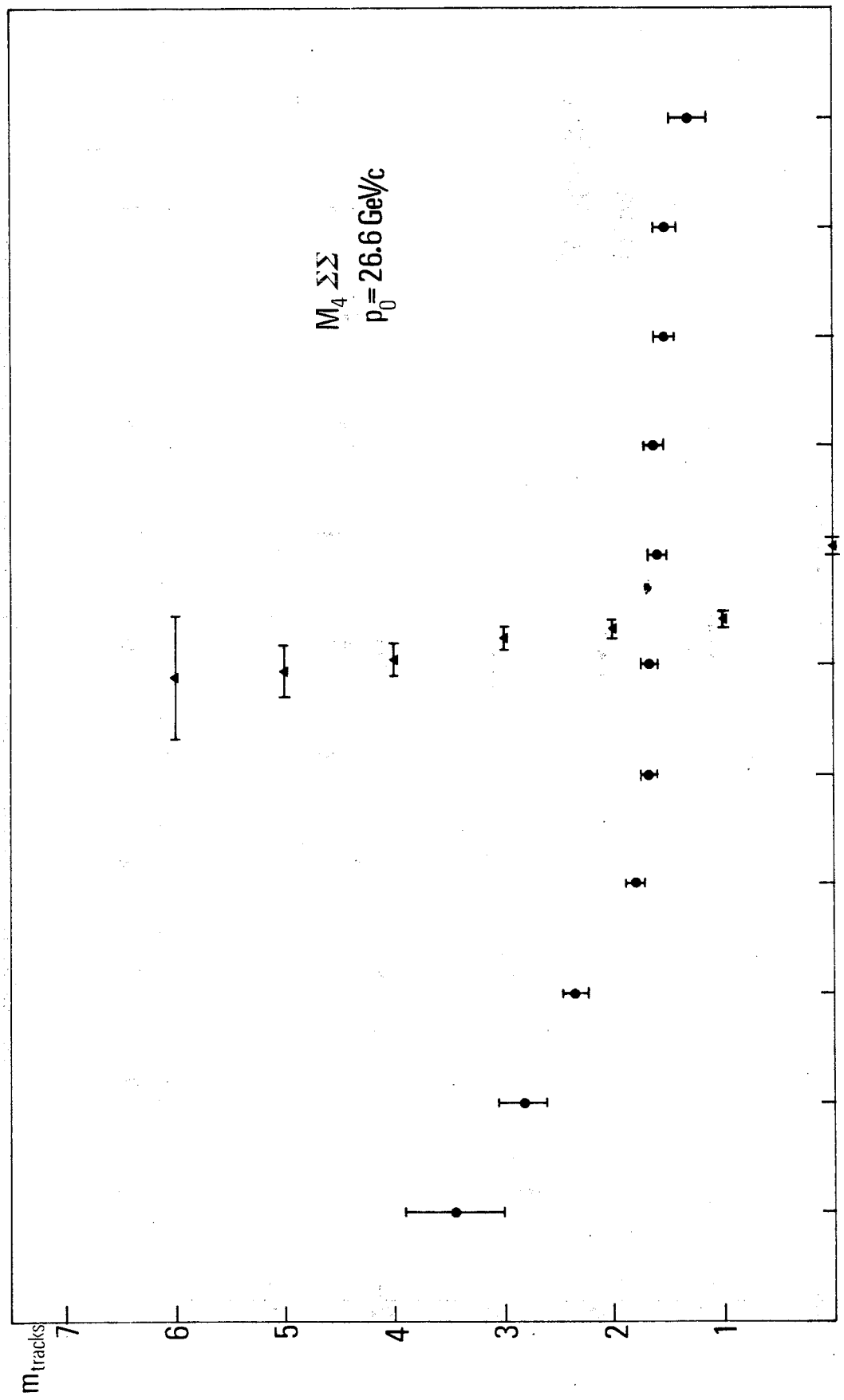

Fig. 11 Regression lines similar to those of Figs. 7 and 10, except that here the trigger is $[M_4 \Sigma\Sigma]$. The points of this figure agree within the statistical errors with those of Fig. 10.

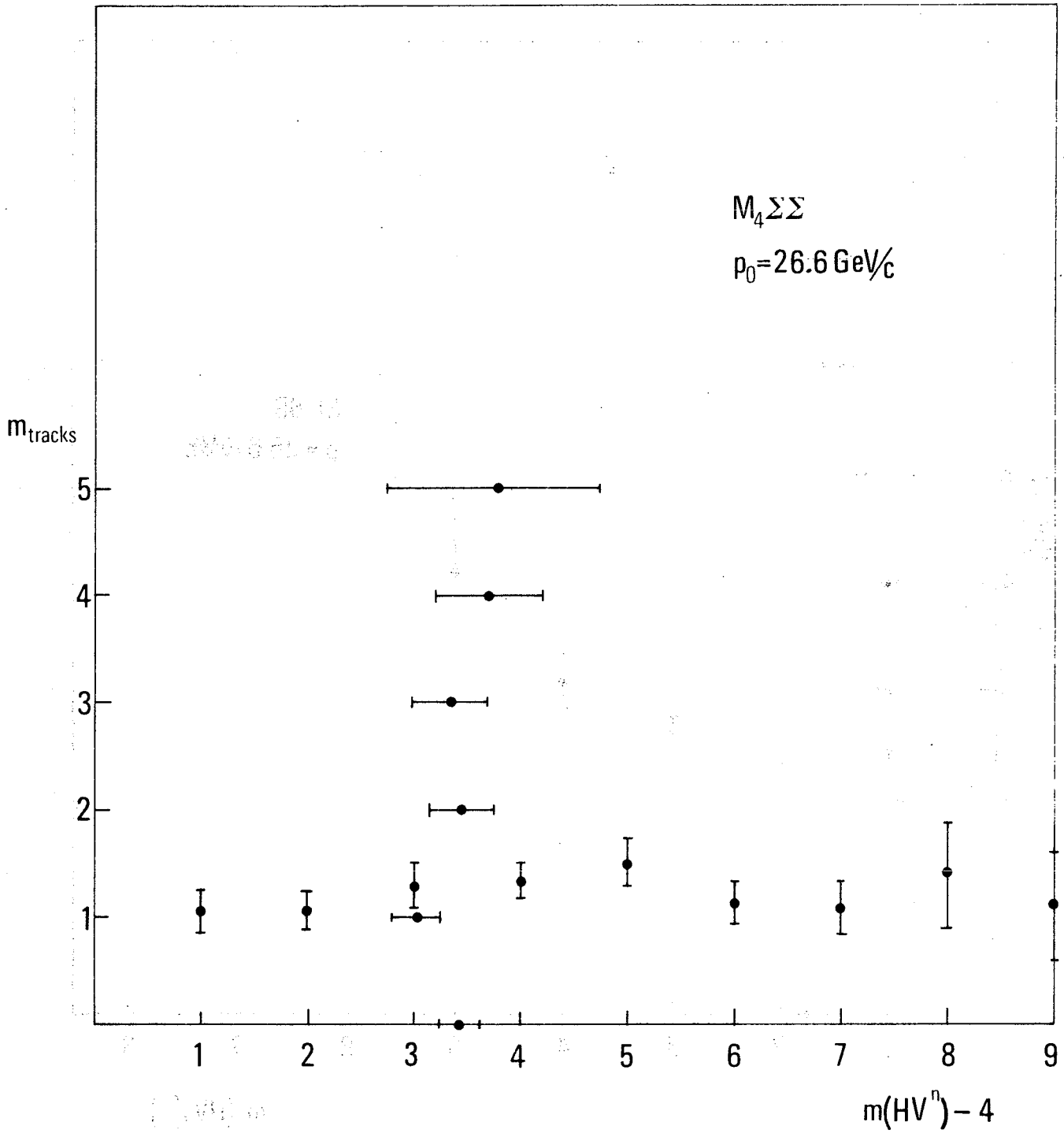

Fig. 12 Regression lines similar to those of Figs. 8 and 9, except that here the trigger is $[M_4\Sigma\Sigma]$.

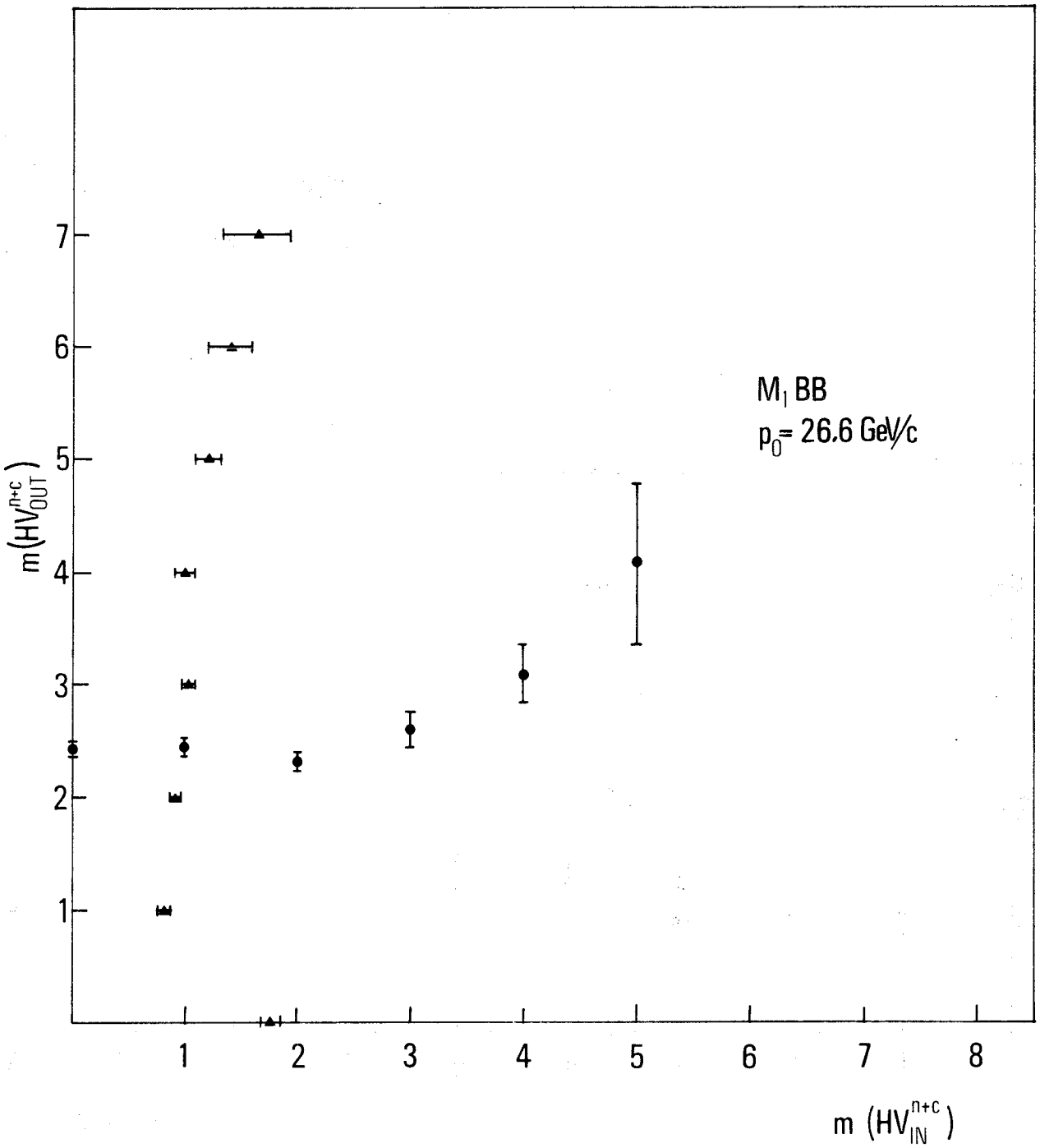

Fig. 13 Regression lines relative to the variables x = $m(HV_{IN})$ and y = $m(HV_{OUT})$: $s^{\frac{1}{2}}$ = 53.2 GeV; $[M_1BB]$

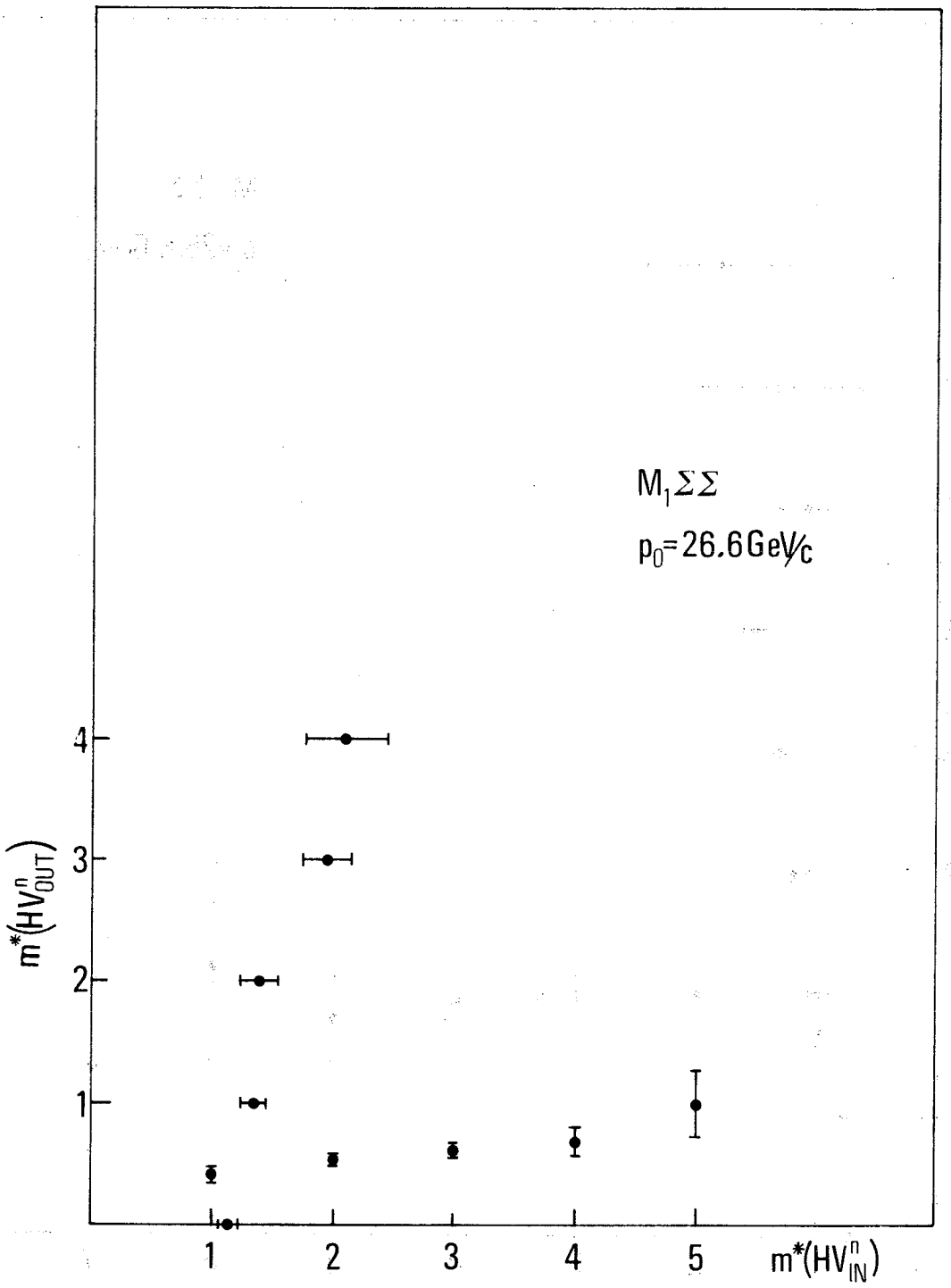

Fig. 14 Regression lines similar to those of the preceding figure, except that we have used here the neutral trigger and we have subtracted in each event the HV responsible for the trigger: $s^{\frac{1}{2}}$ = 53.2 GeV; $[M_1\Sigma\Sigma]$.

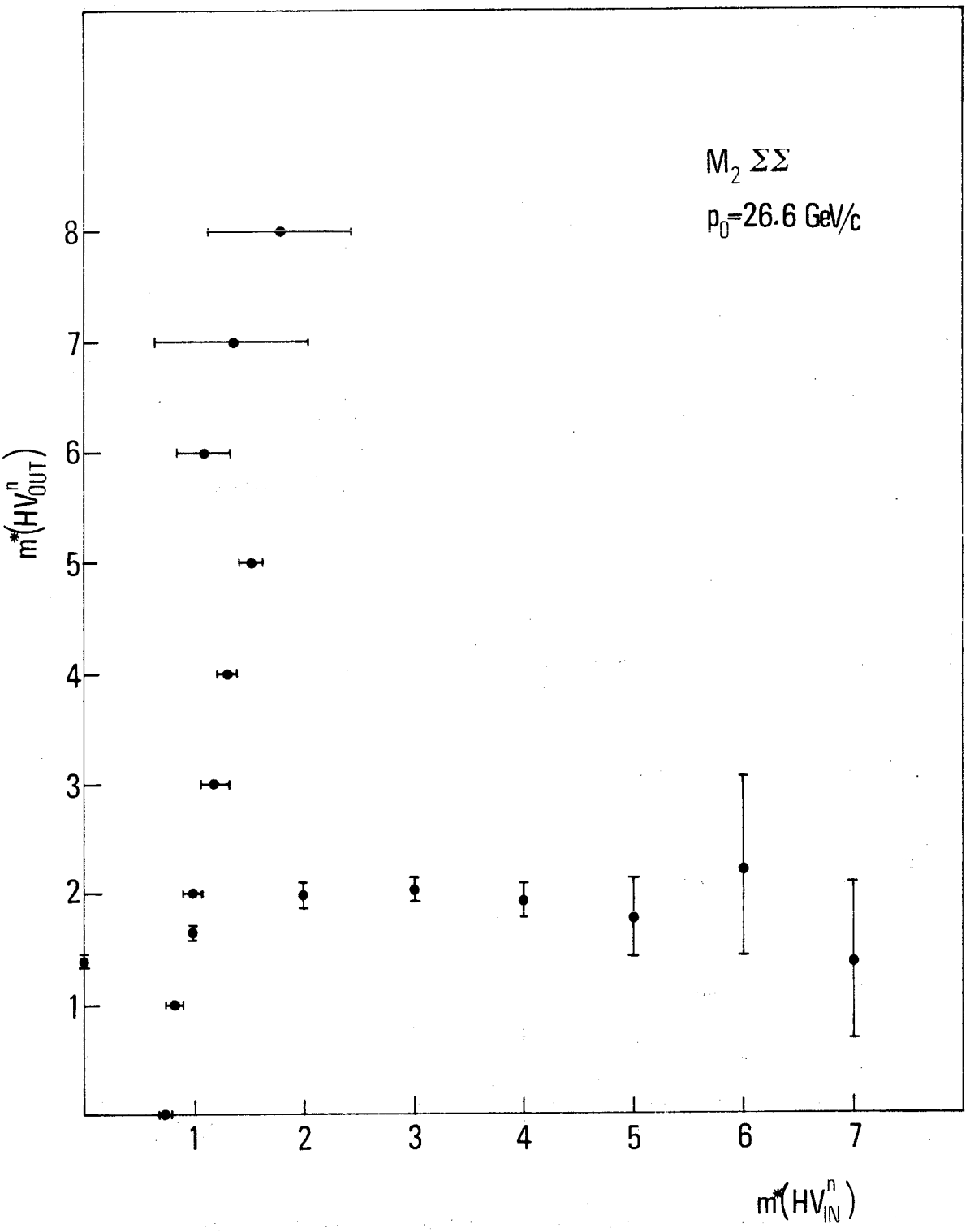

Fig. 15 Regression lines similar to those of the previous figure, except that the trigger is $[M_2\Sigma\Sigma]$.

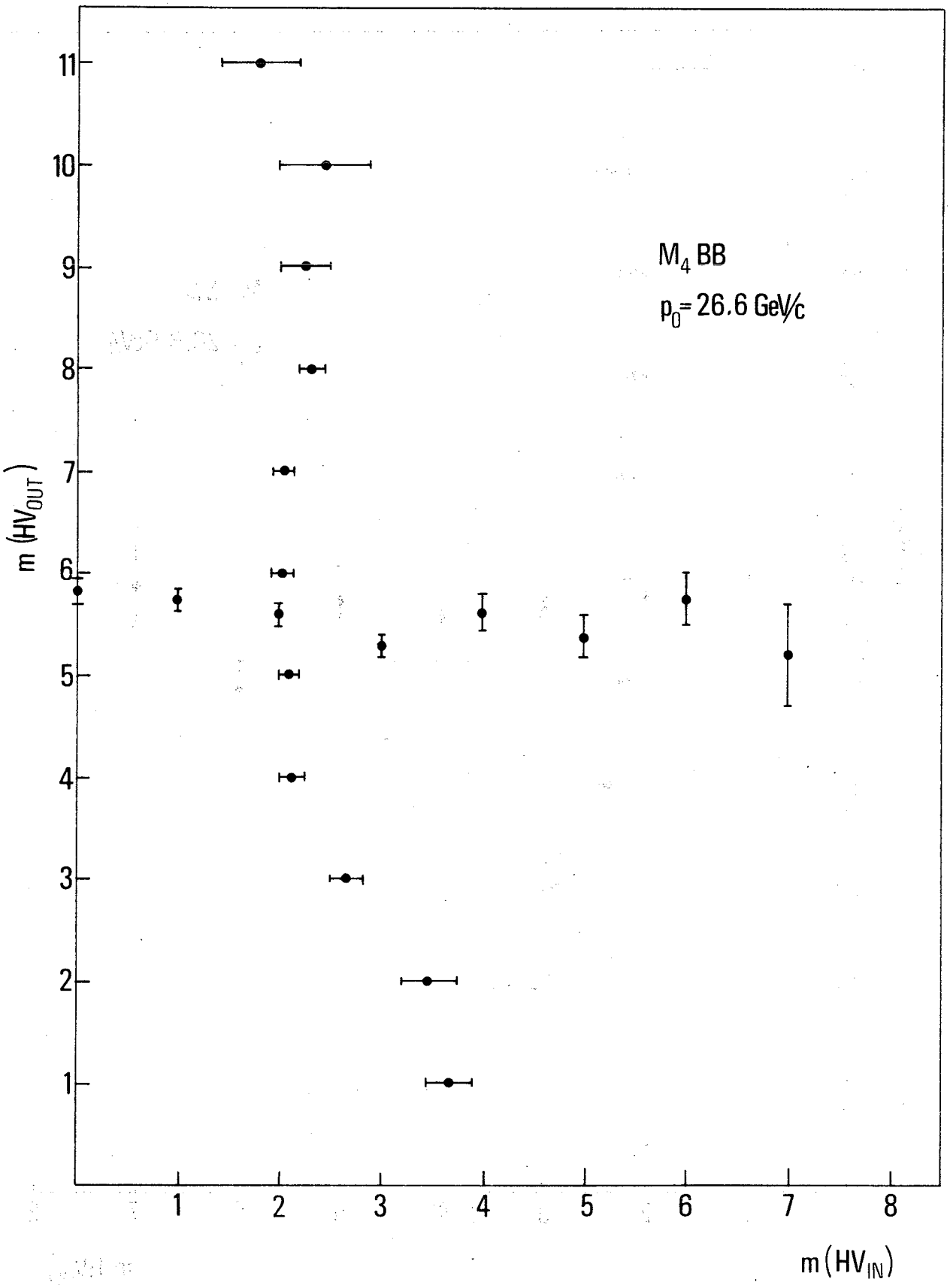

Fig. 16 Regression lines relative to the variables x = m(HV_{IN}) and y = m(HV_{OUT}): s^2 = 53.2 GeV; [M_4BB].

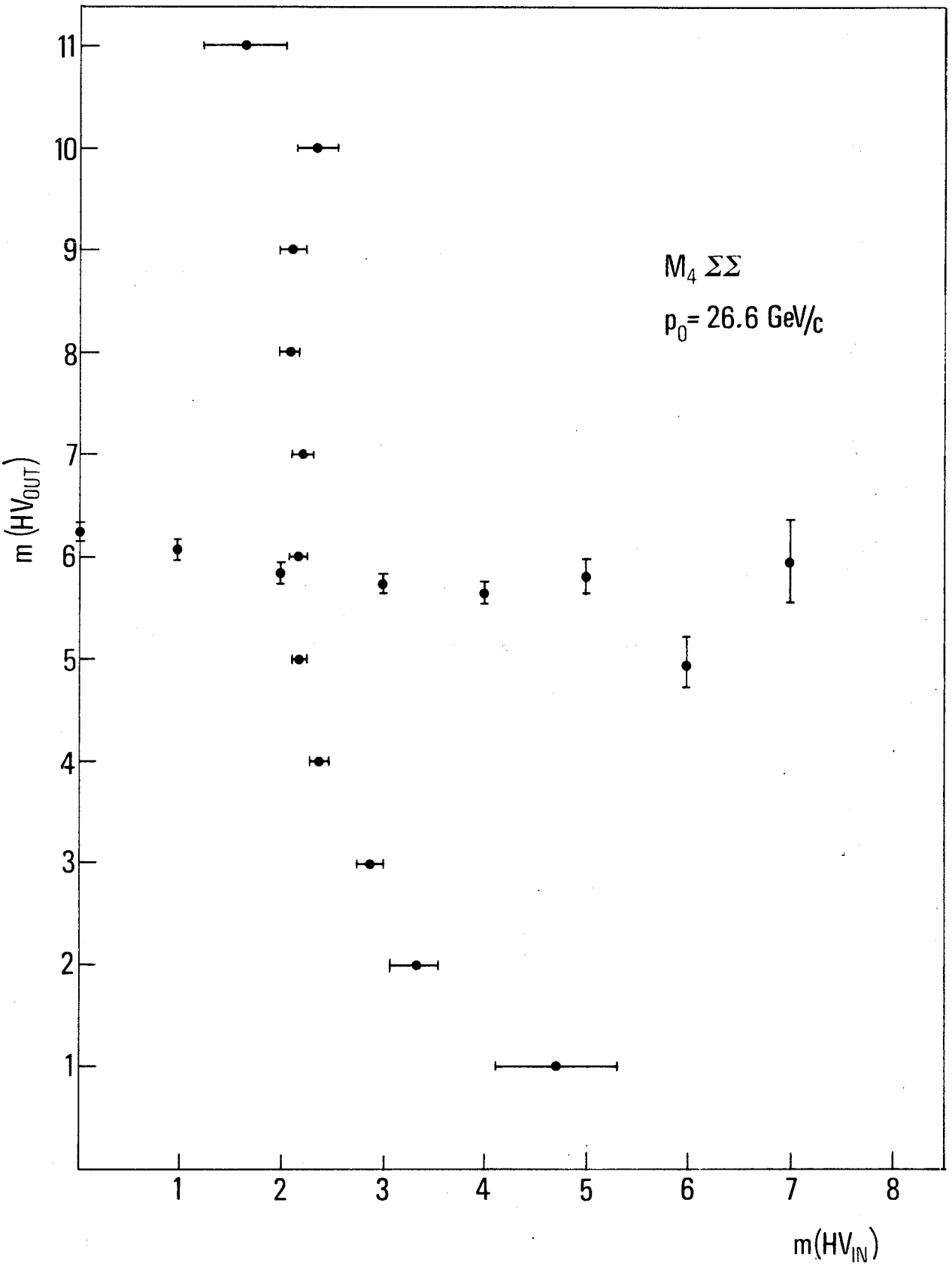

Fig. 17 Regression lines similar to those of the preceding figure, except that the trigger is $[M_4\Sigma\Sigma]$.

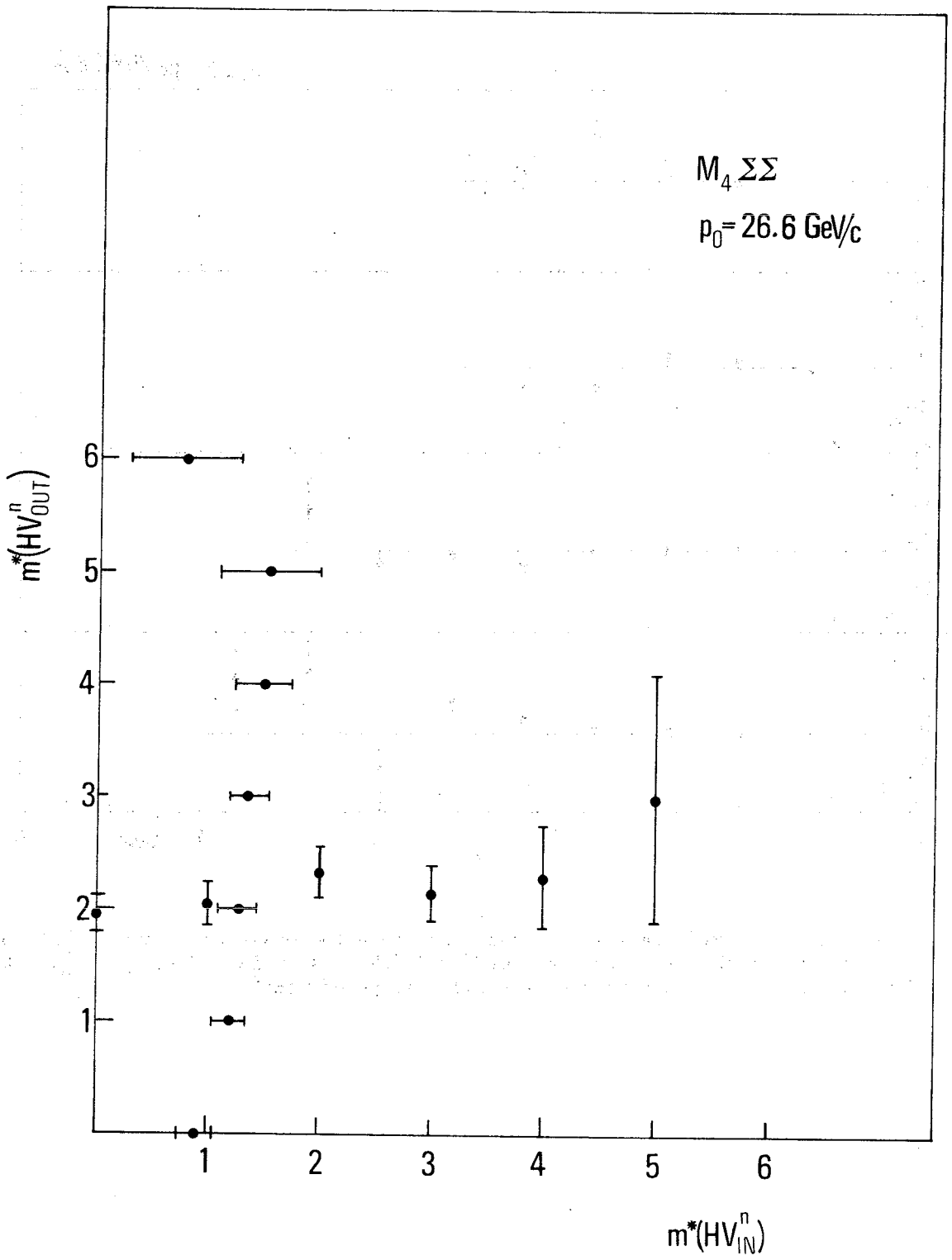

Fig. 18 Regression lines similar to those of the previous figure, except that only HV^n are considered and those for the trigger have been subtracted in each event.

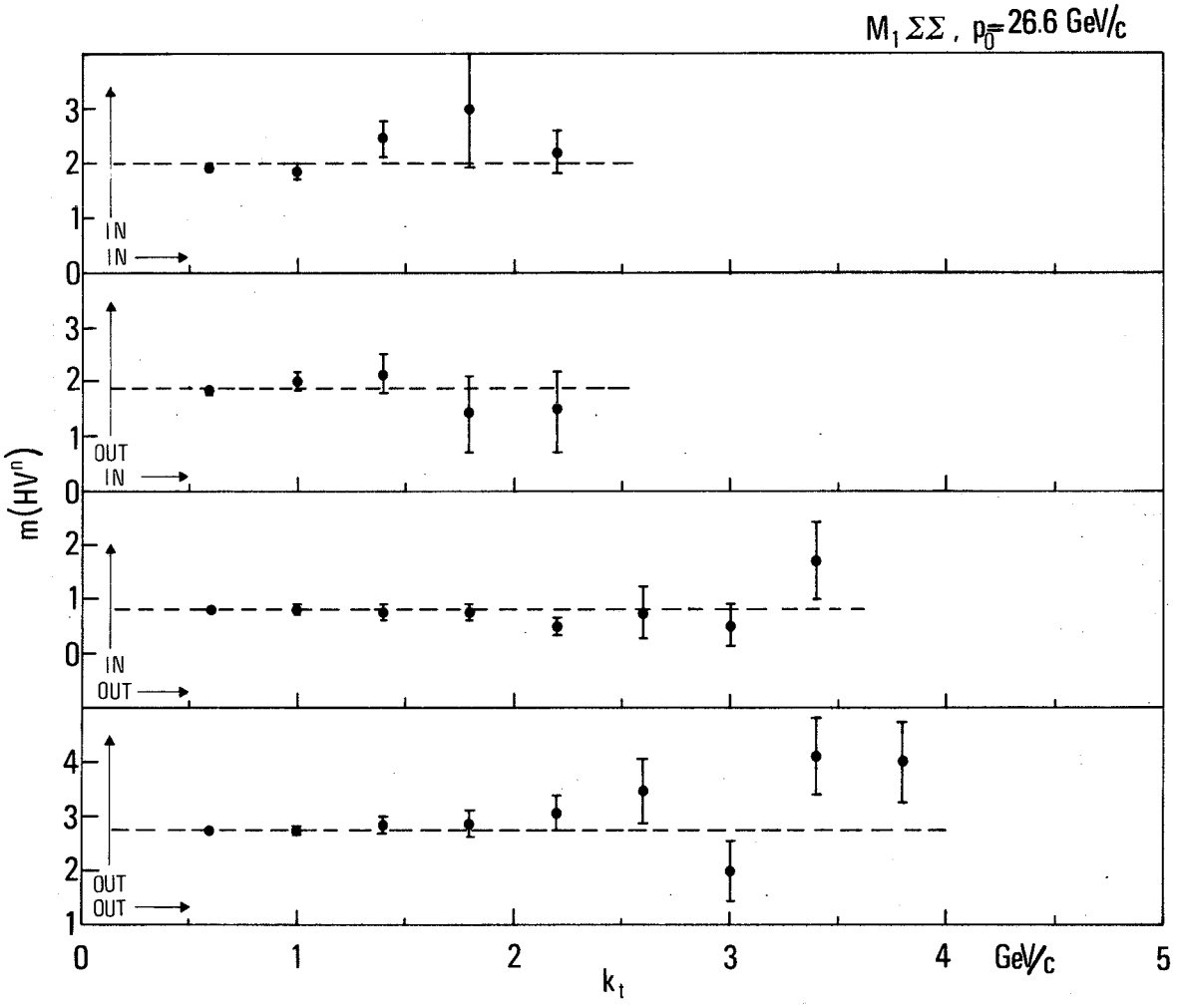

Fig. 19 Mean value of m(HV^n) versus the transverse momentum, observed in any one of the HV^n separately for the two detectors "OUT" and "IN". $s^{\frac{1}{2}}$ = 53.2 GeV; $[M_1 \Sigma\Sigma]$. The broken line corresponds to the over-all average of m(HV^n).

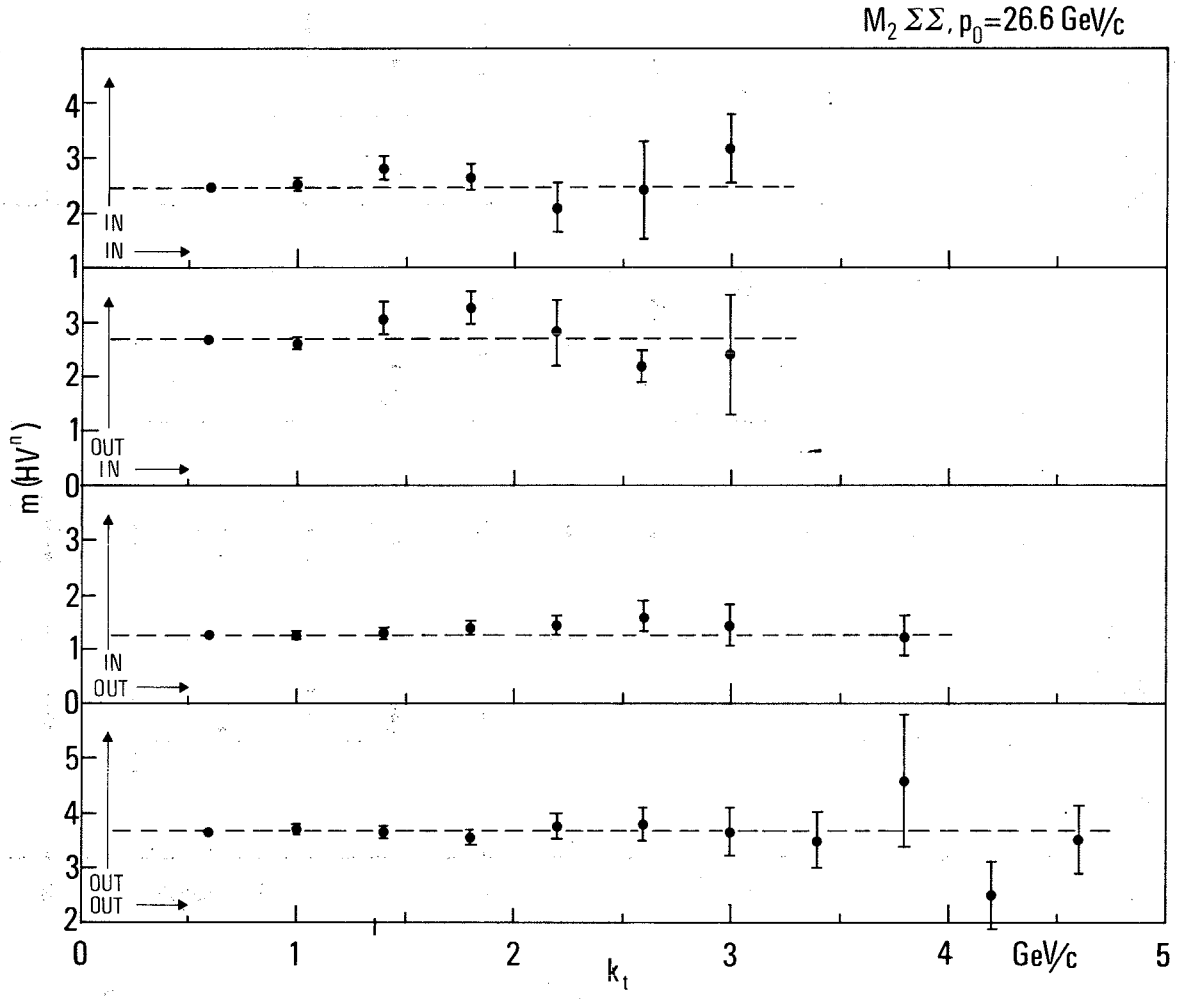

Fig. 20 Similar to the preceding figure, but for the trigger mode $[M_2\Sigma\Sigma]$.

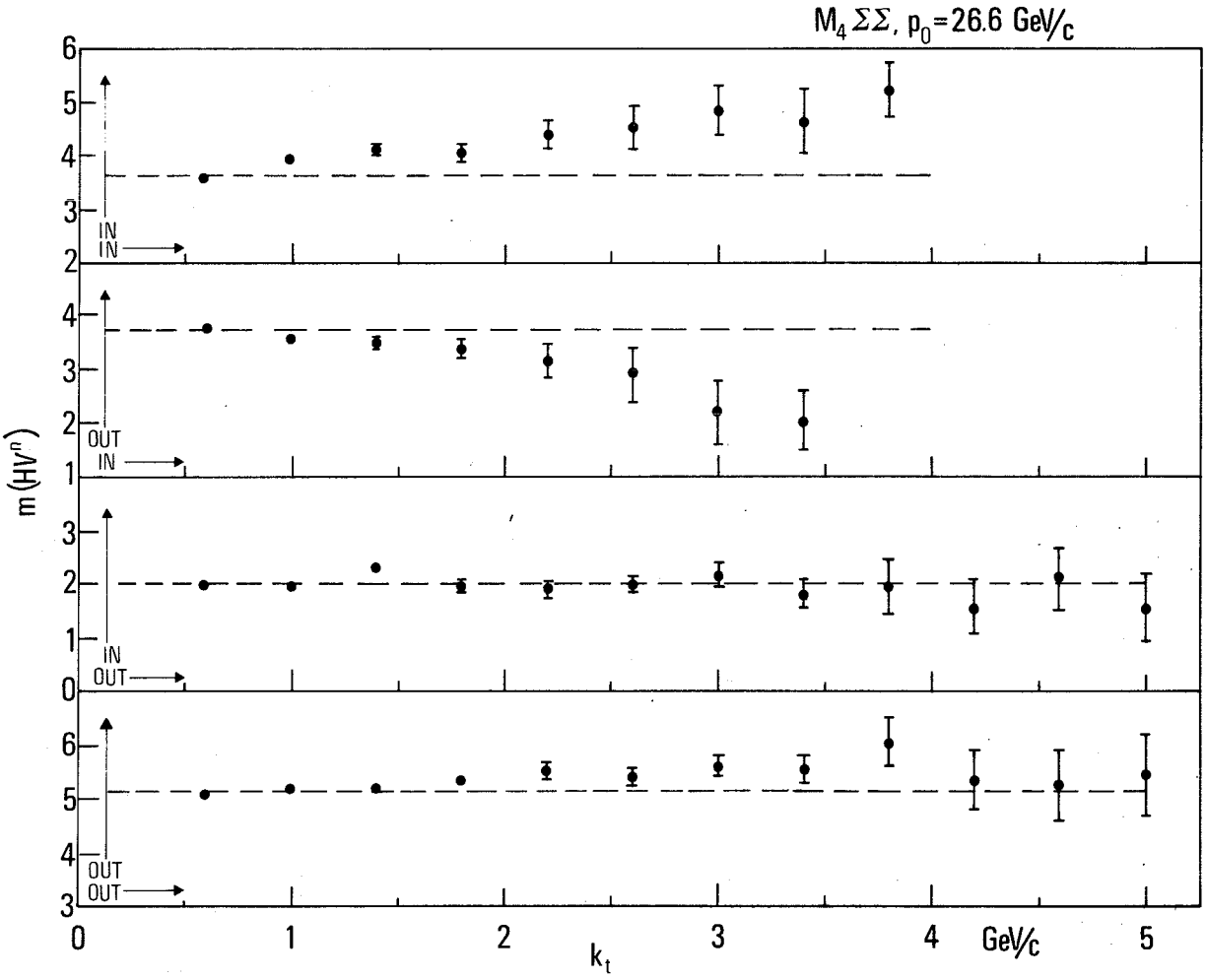

Fig. 21 Similar to Figs. 19 and 20, but for the trigger mode $[M_4 \Sigma\Sigma]$.

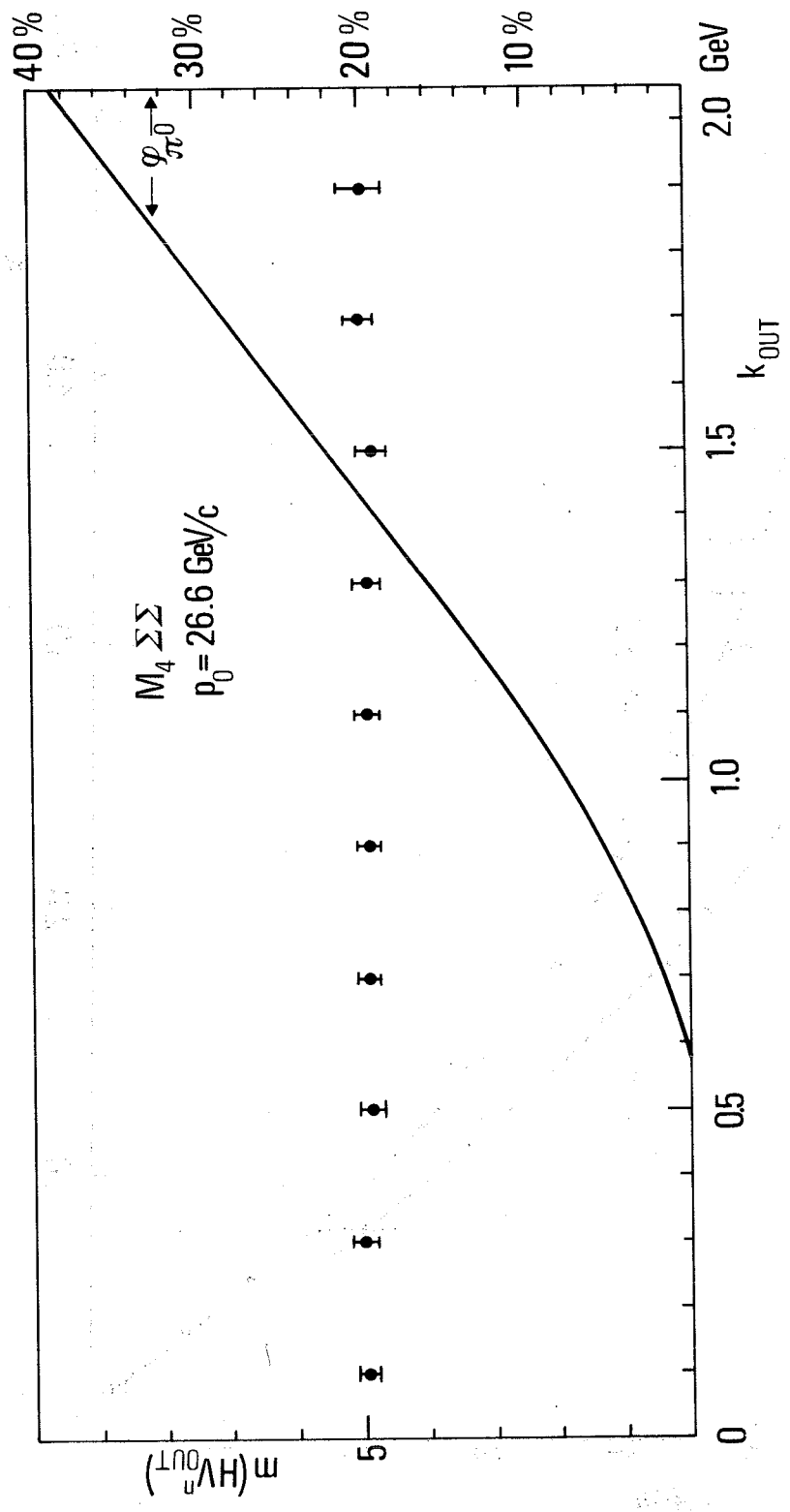

Fig. 22 Mean value of $m(HV^n_{OUT})$ versus k_{OUT}, i.e. photon energy observed in the "OUT" detector. The curve ϕ_{π^0} indicates the probability that the energy k -- observed in a single lead-glass HV plus the LBs behind it -- is due to two gamma-rays originating from the same π^0. s^2 = 53.2 GeV; $[M_4\Sigma\Sigma]$.

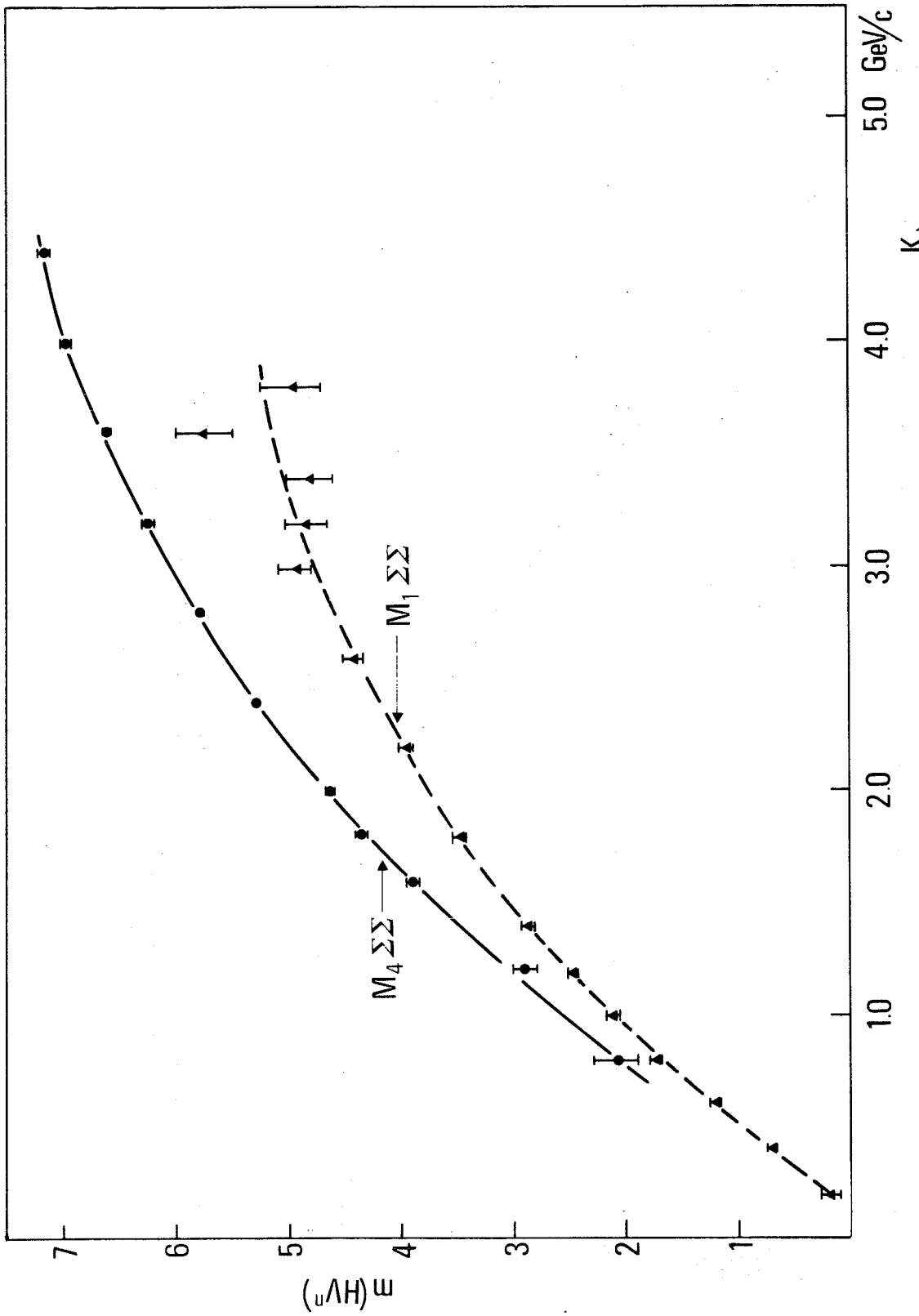

Fig. 23 Mean value of $m(HV^n)$ versus total transverse momentum K_t observed in any one of the HV^n: $s^{\frac{1}{2}} = 53.2$ GeV; $[M_1 \Sigma\Sigma]$ and $[M_4 \Sigma\Sigma]$.

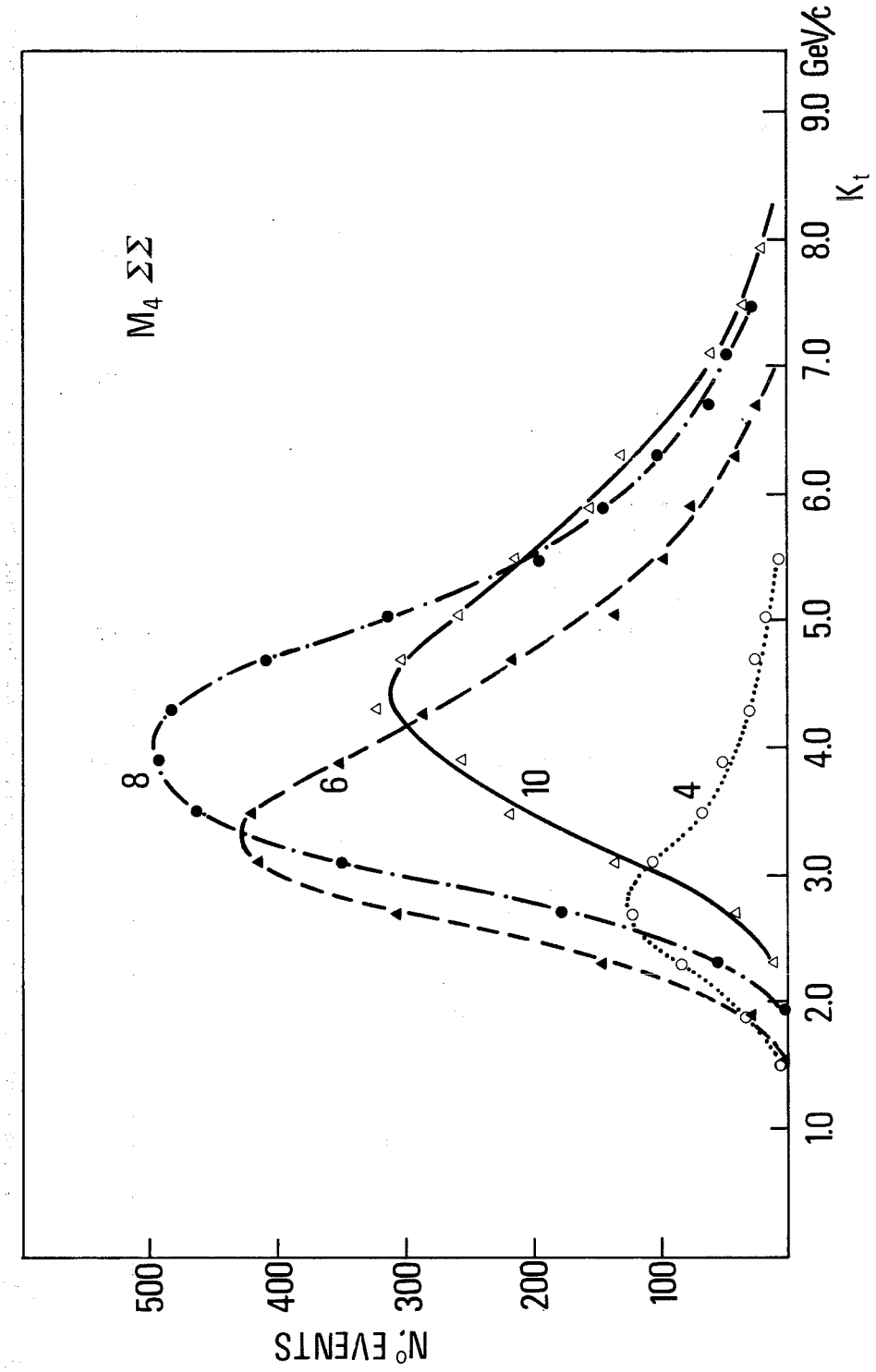

Fig. 24 Distribution of K_t observed in all HV + LB for a few values of the multiplicity: m(HV^m) = 4, 6, 8, 10; $\sqrt{s}$ = 53.2 GeV; E_{cf} = 30 MeV; $[M_4\Sigma\Sigma]$.

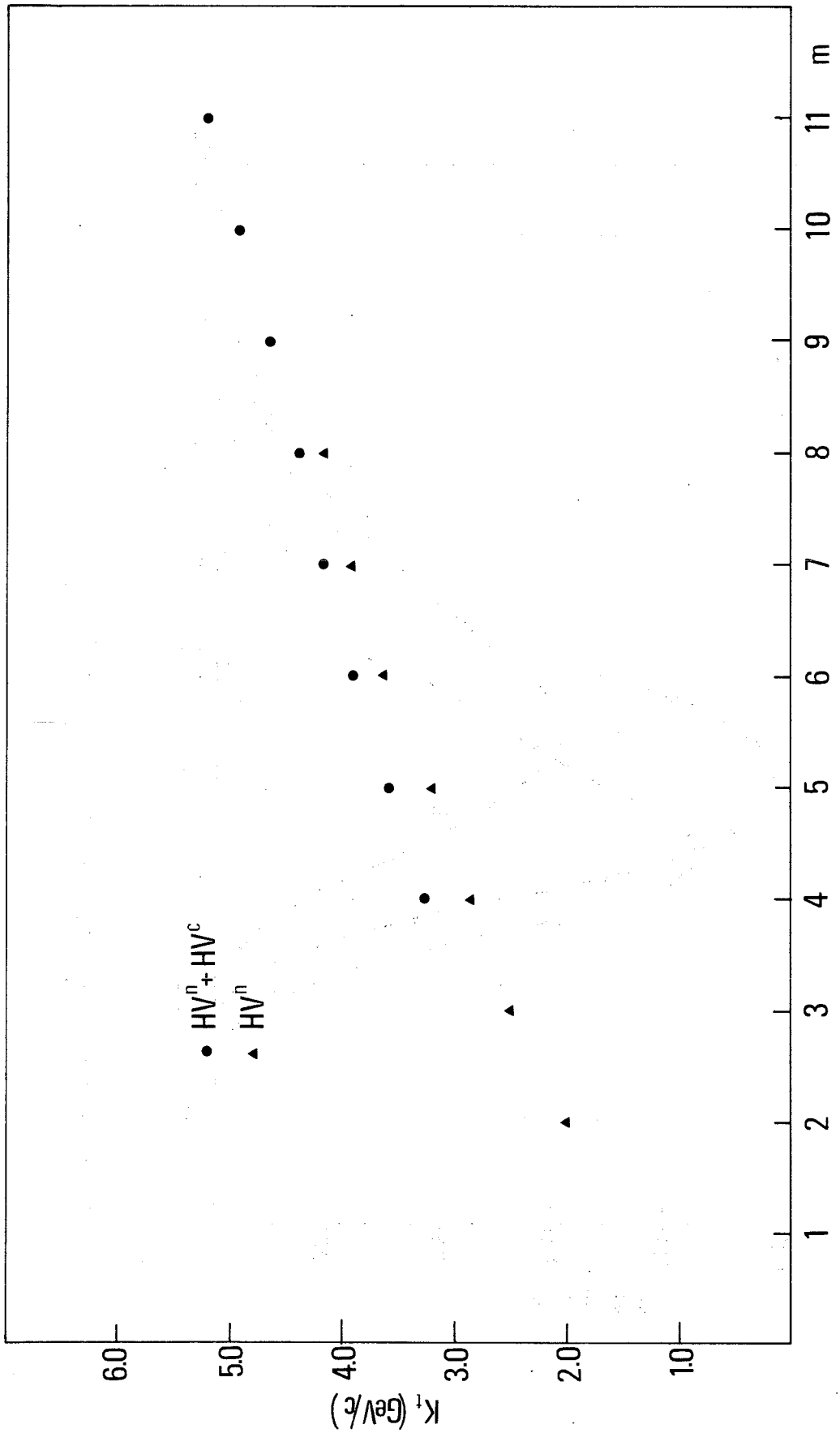

Fig. 25 Dependence of total transverse momentum K_t observed in all HV + LB versus multiplicity m(HV).
Dots $HV = HV^n + HV^c$, triangles only HV^n: $s^{\frac{1}{2}} = 53.2$ Gev/c; $[M_4 \Sigma\Sigma]$.

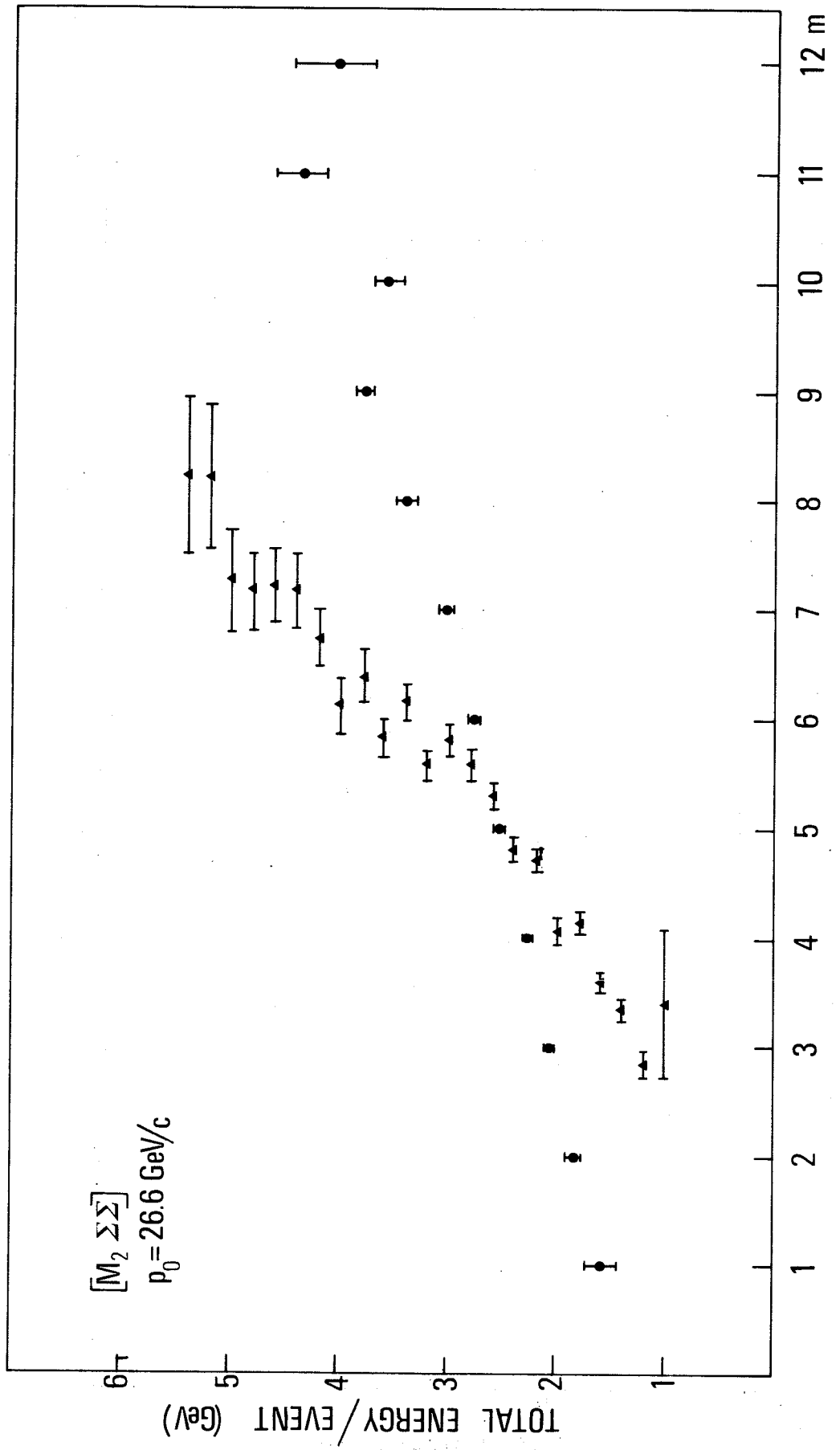

Fig. 26 Total energy per event observed in HV (neutral + charged) versus multiplicity of $HV^n + HV^c$: $s^{\frac{1}{2}} = 53.2$ GeV; $[M_2\Sigma\Sigma]$.

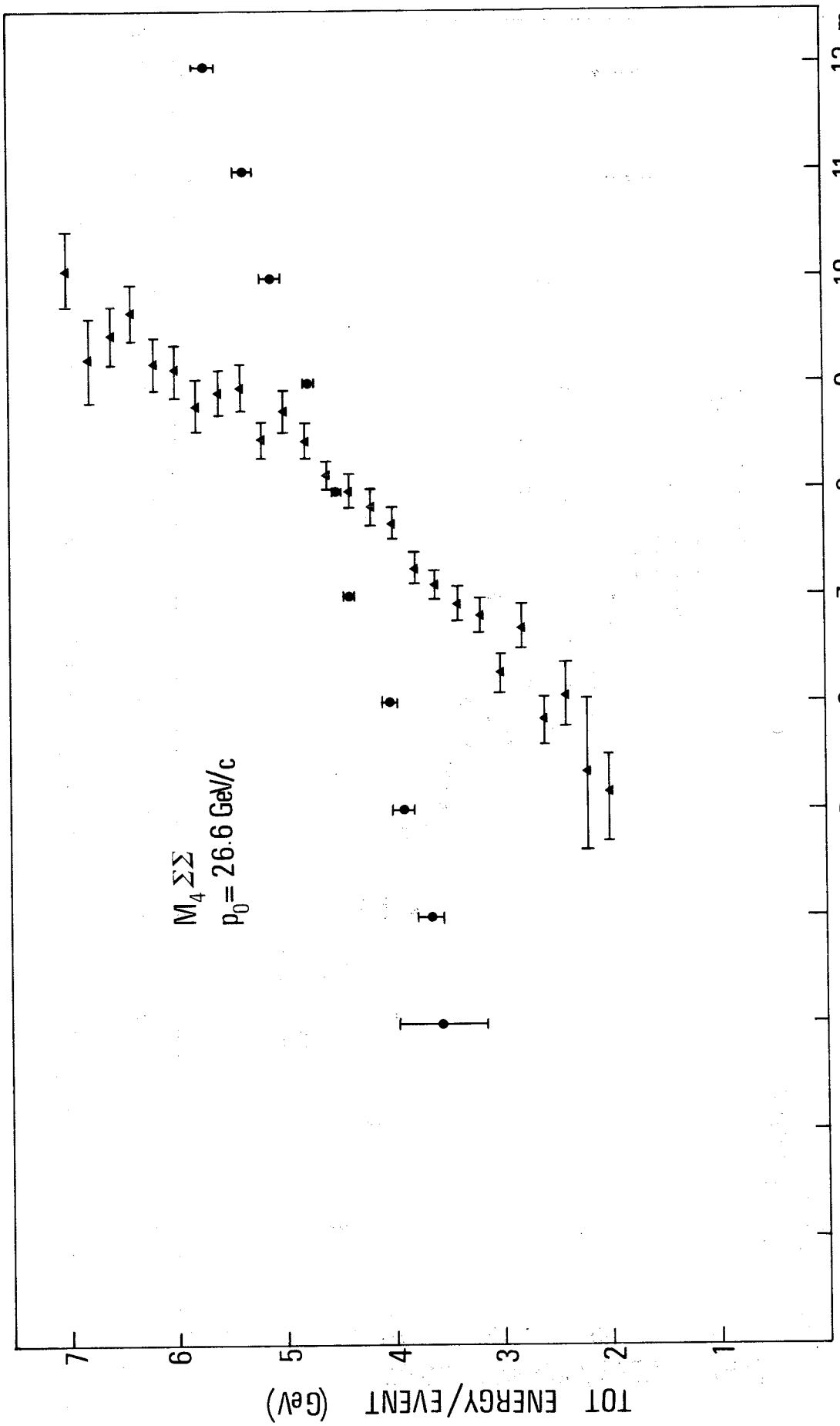

Fig. 27 Similar to the previous figure, but for $[M_4\Sigma\Sigma]$.

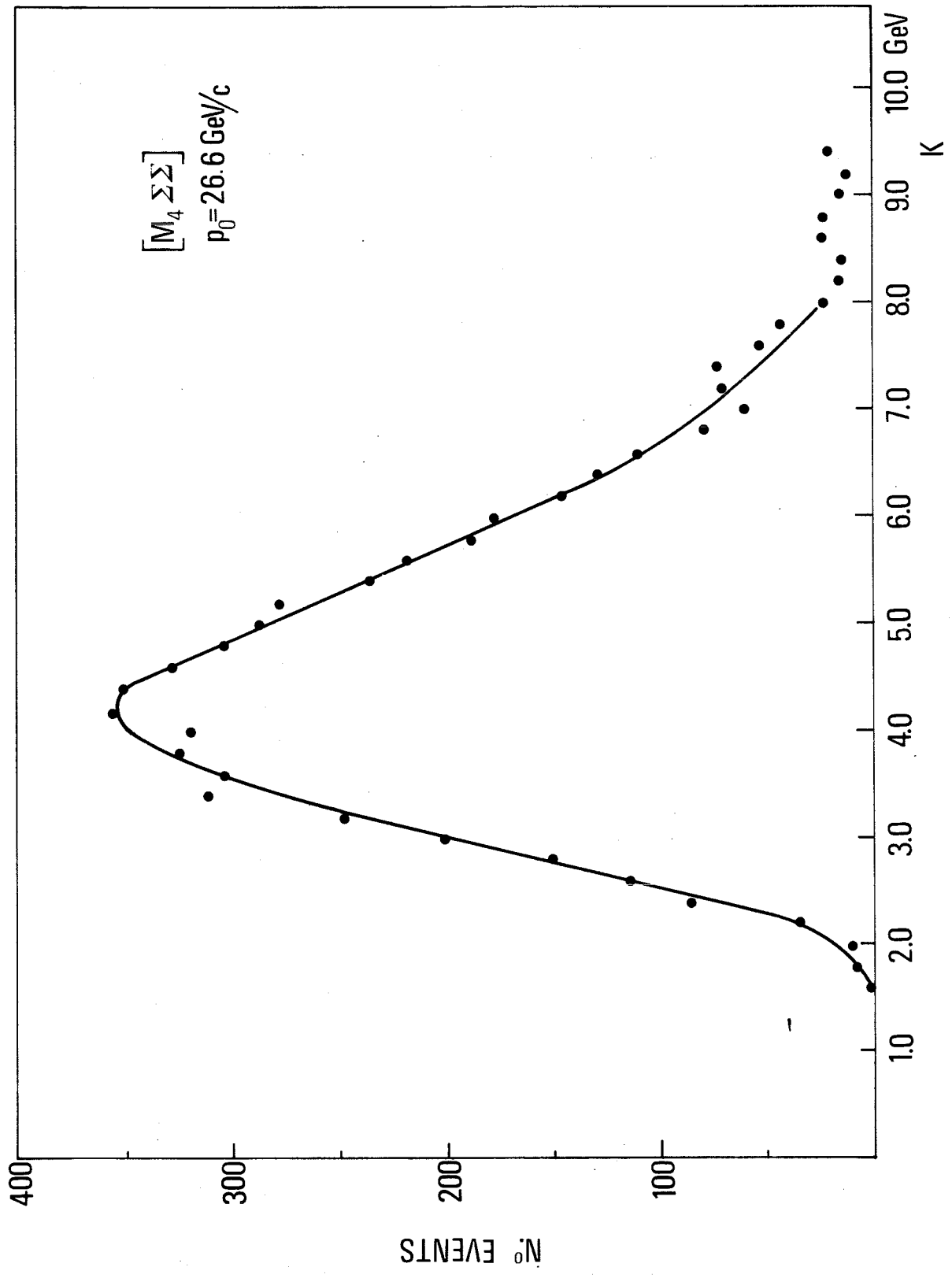

Fig. 28 Distribution of total energy observed in $HV^n + HV^c$. $s^{\frac{1}{2}} = 53.2$ GeV; $[M_4\Sigma\Sigma]$. The increase from zero to the maximum observed from 1.5 to 4 GeV is due to the threshold of the trigger.

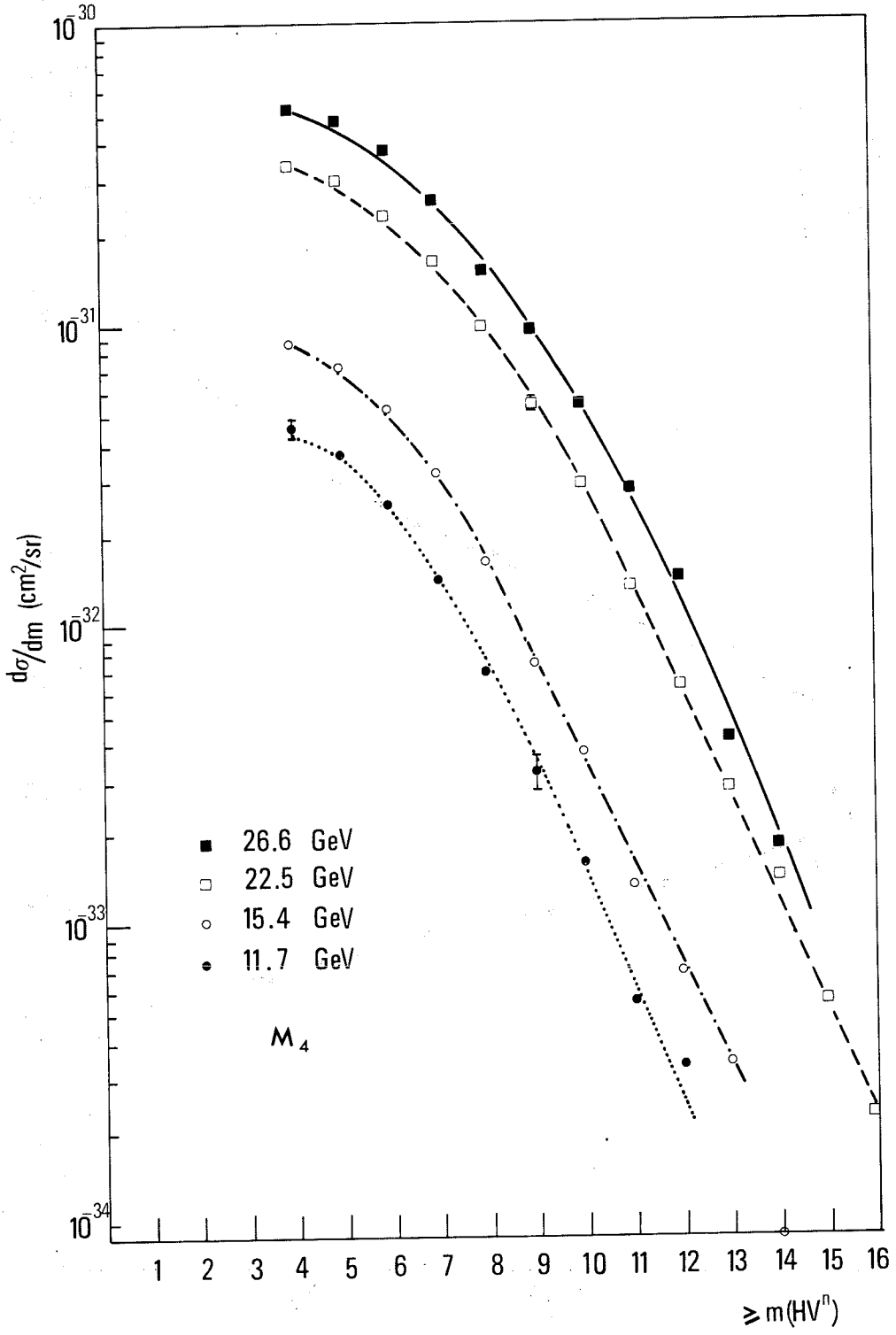

Fig. 29 Integral distribution of the multiplicity of the fired HV^n for four colliding beam energies with trigger $[M_4 \Sigma\Sigma]$.

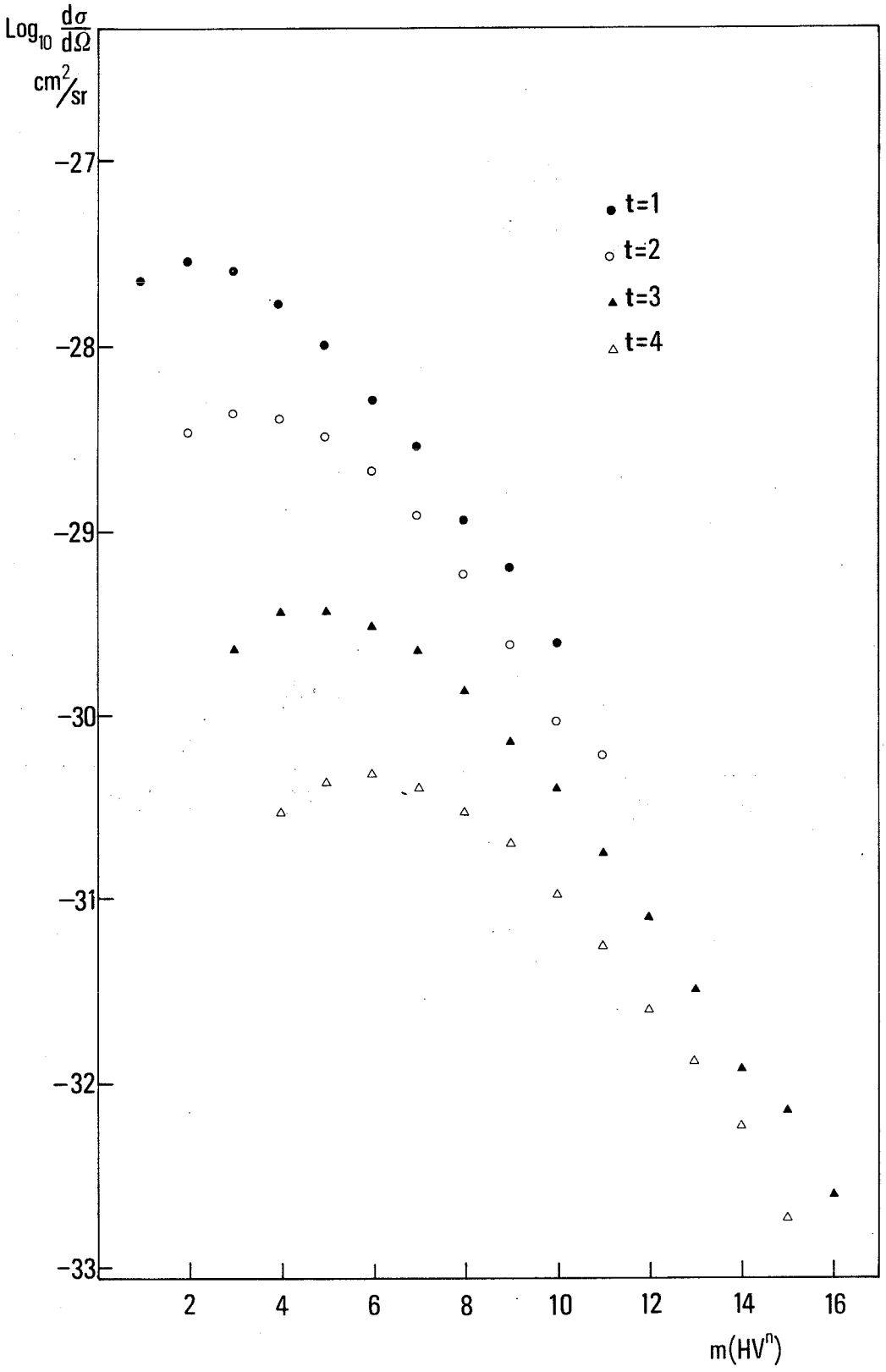

Fig. 30 Distribution of the multiplicity of the fired HV^n for various trigger modes at a c.m. energy $s^{\frac{1}{2}} = 53.2$ GeV.

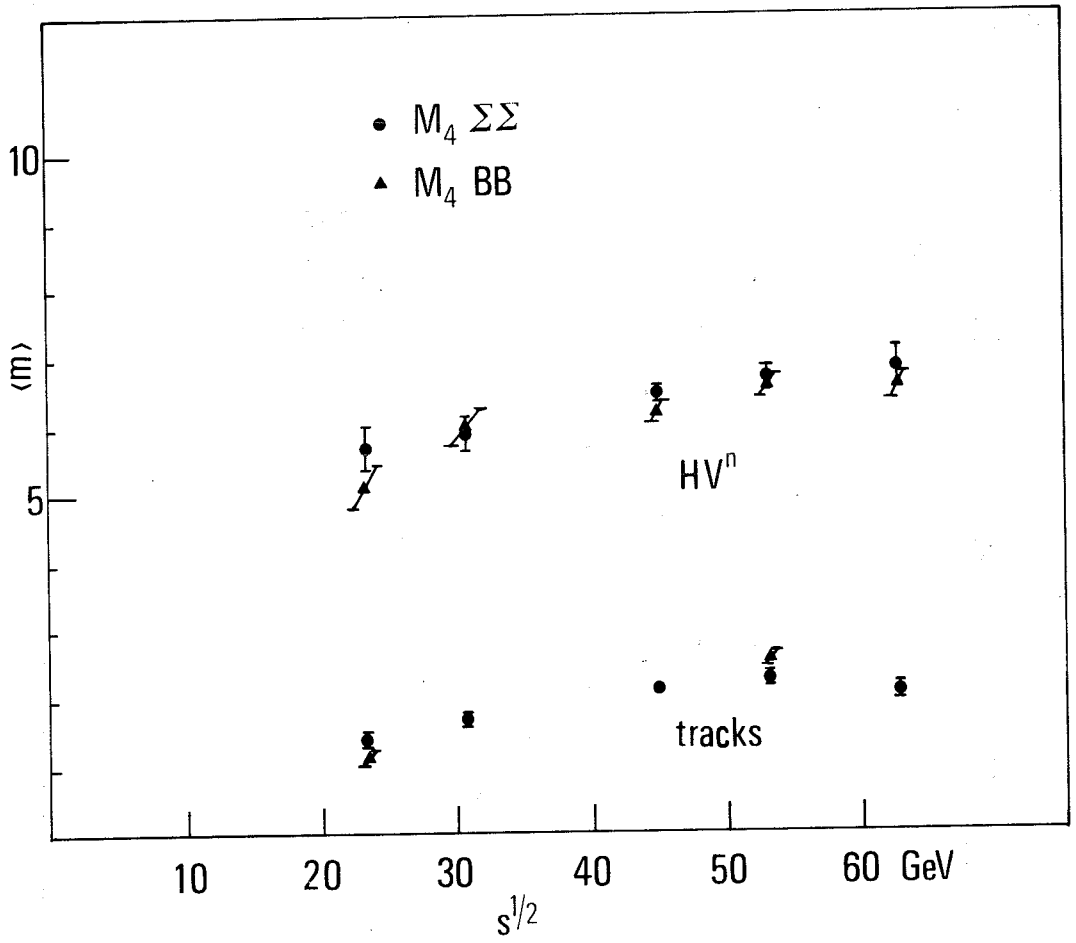

Fig. 31 Average multiplicity of the fired HV^n and of the reconstructed tracks plotted as a function of c.m. energy.

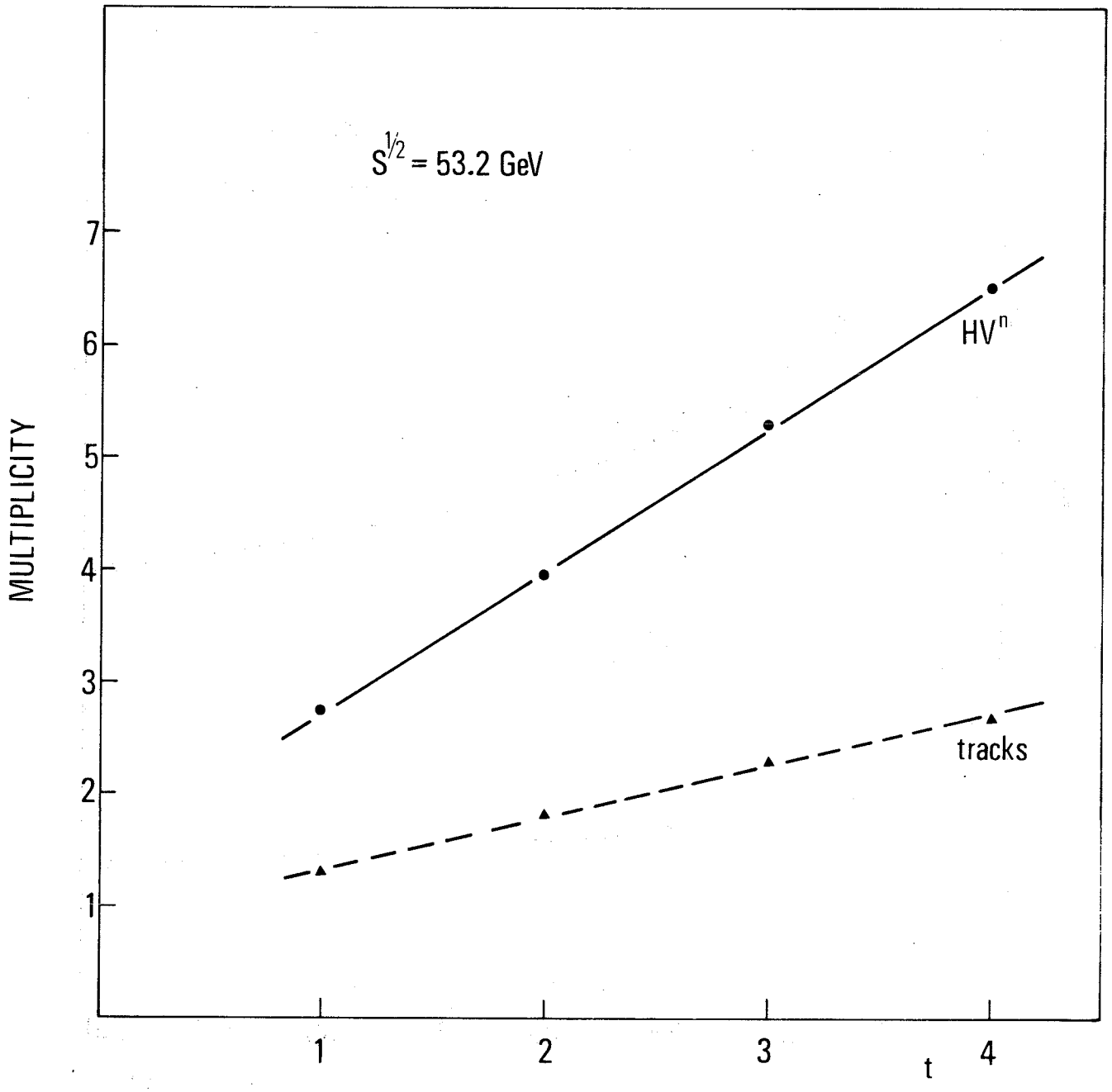

Fig. 32 Average multiplicity of the fired HV^n and of the reconstructed tracks versus trigger mode t ($s^{\frac{1}{2}}$ = 53.2 GeV).

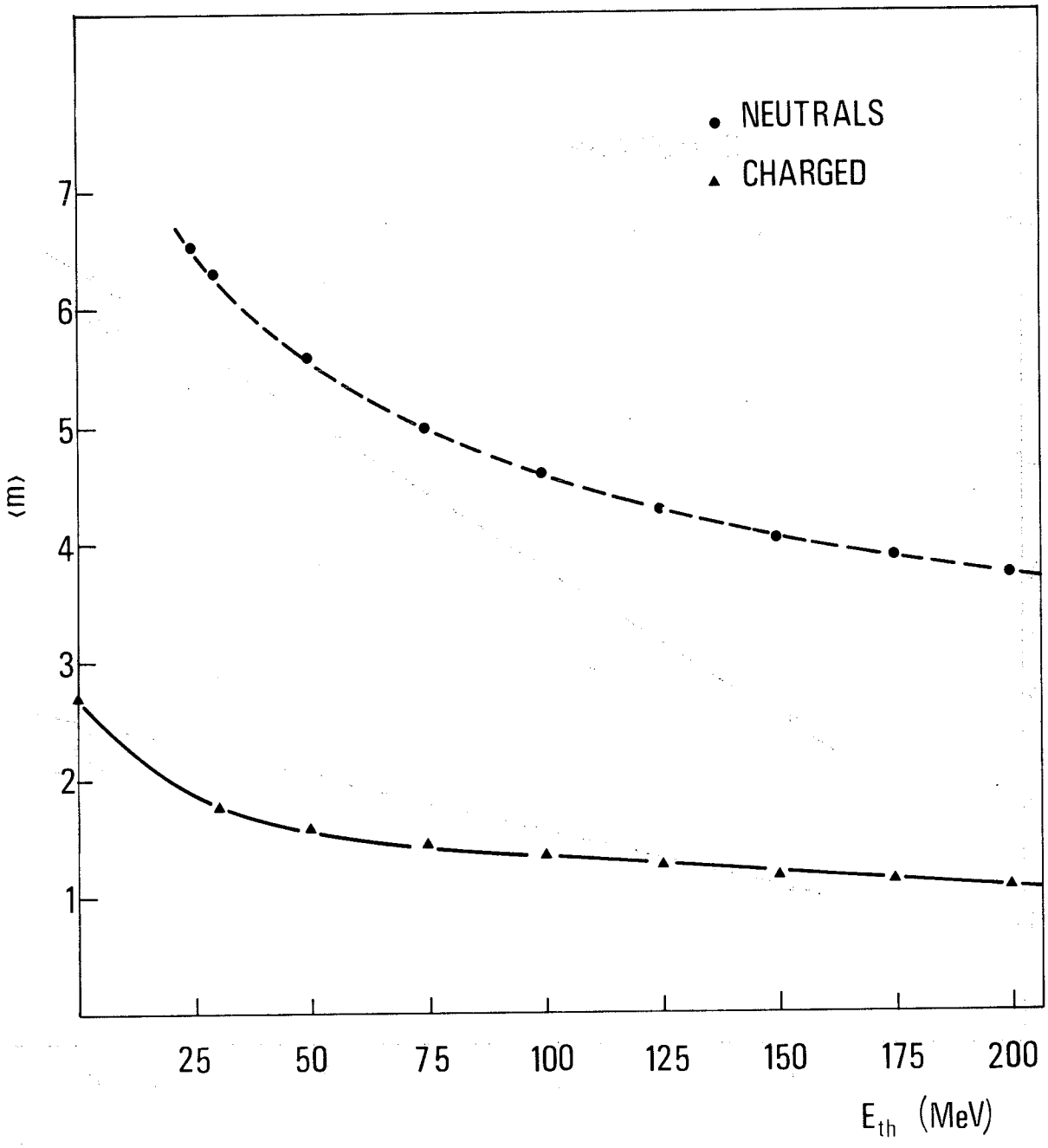

Fig. 33 Average multiplicity of the HV^n and HV^c versus cut-off energy for $t = 4$ and $s^{\frac{1}{2}} = 53.2$ GeV.

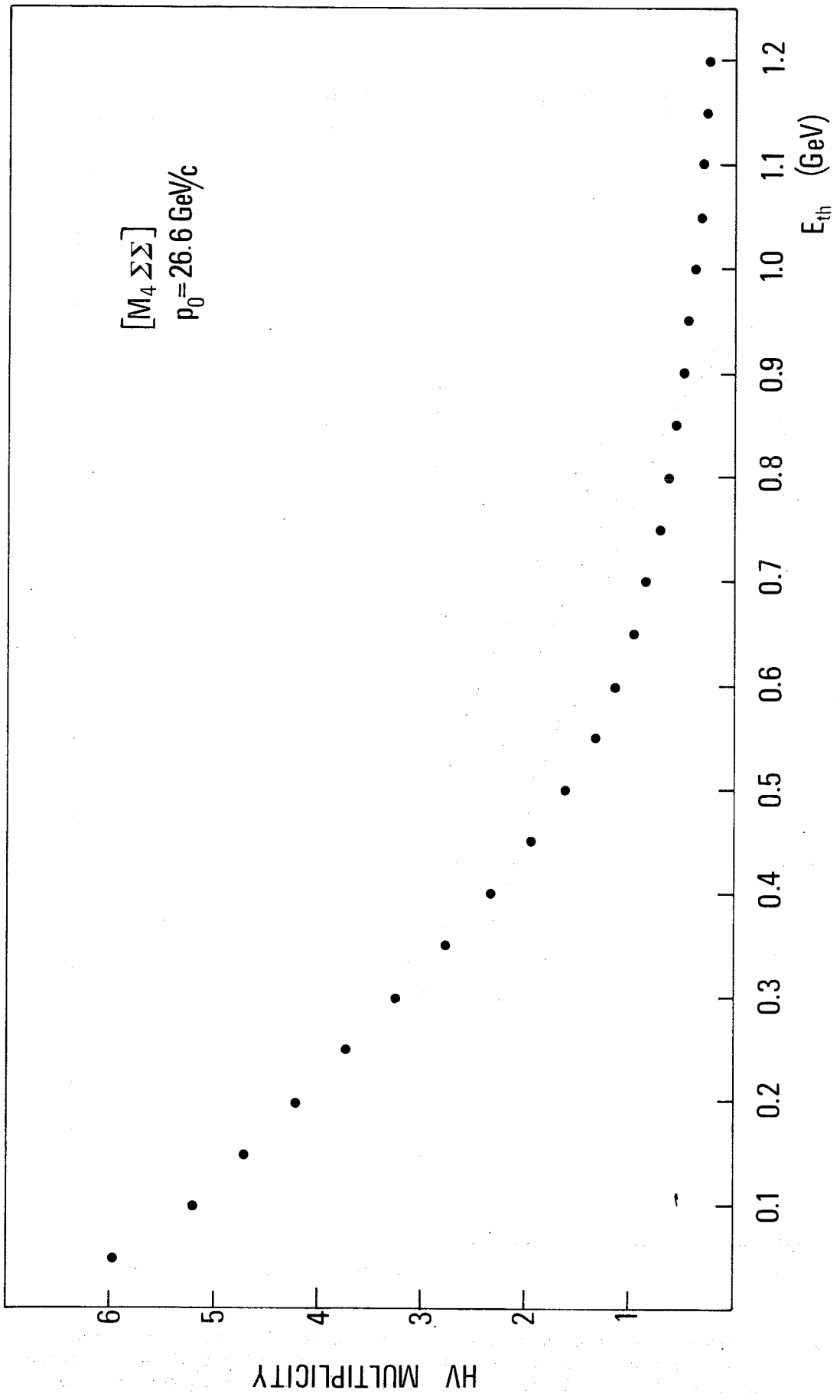

Fig. 34 Average multiplicity of $HV = HV^n + HV^c$ versus cut-off energy for t = 4 and $s^{\frac{1}{2}} = 53.2$ GeV.

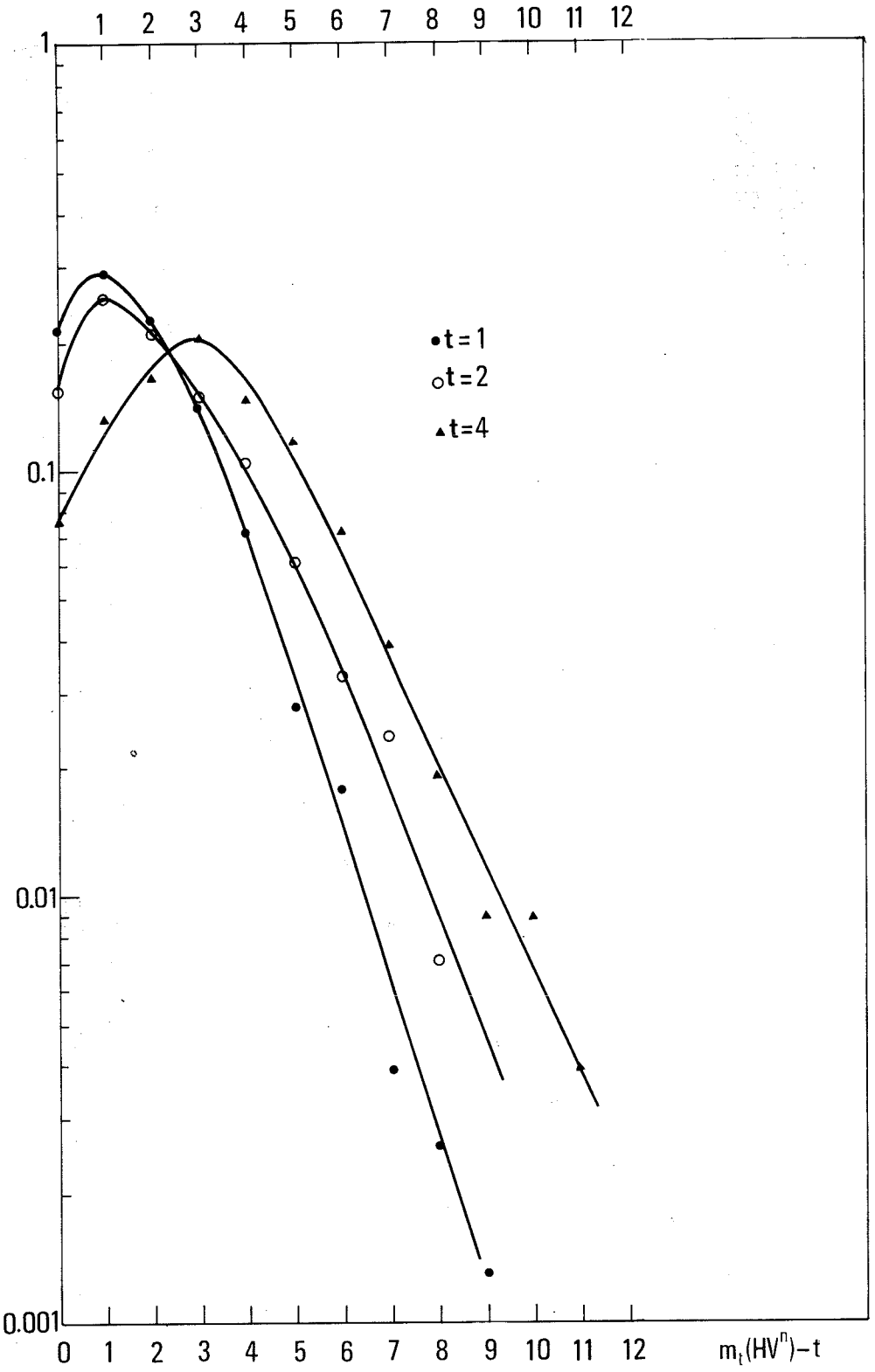

Fig. 35 Distribution of the multiplicity of the fired HV_1^n obtained in the various neutral trigger modes at a c.m. energy $s^{\frac{1}{2}}$ = 53.2 GeV. Notice that the variable plotted in abscissa is $[m_t(HV^n) - t]$ and that each curve is normalized to an integrated counting rate equal to 1.

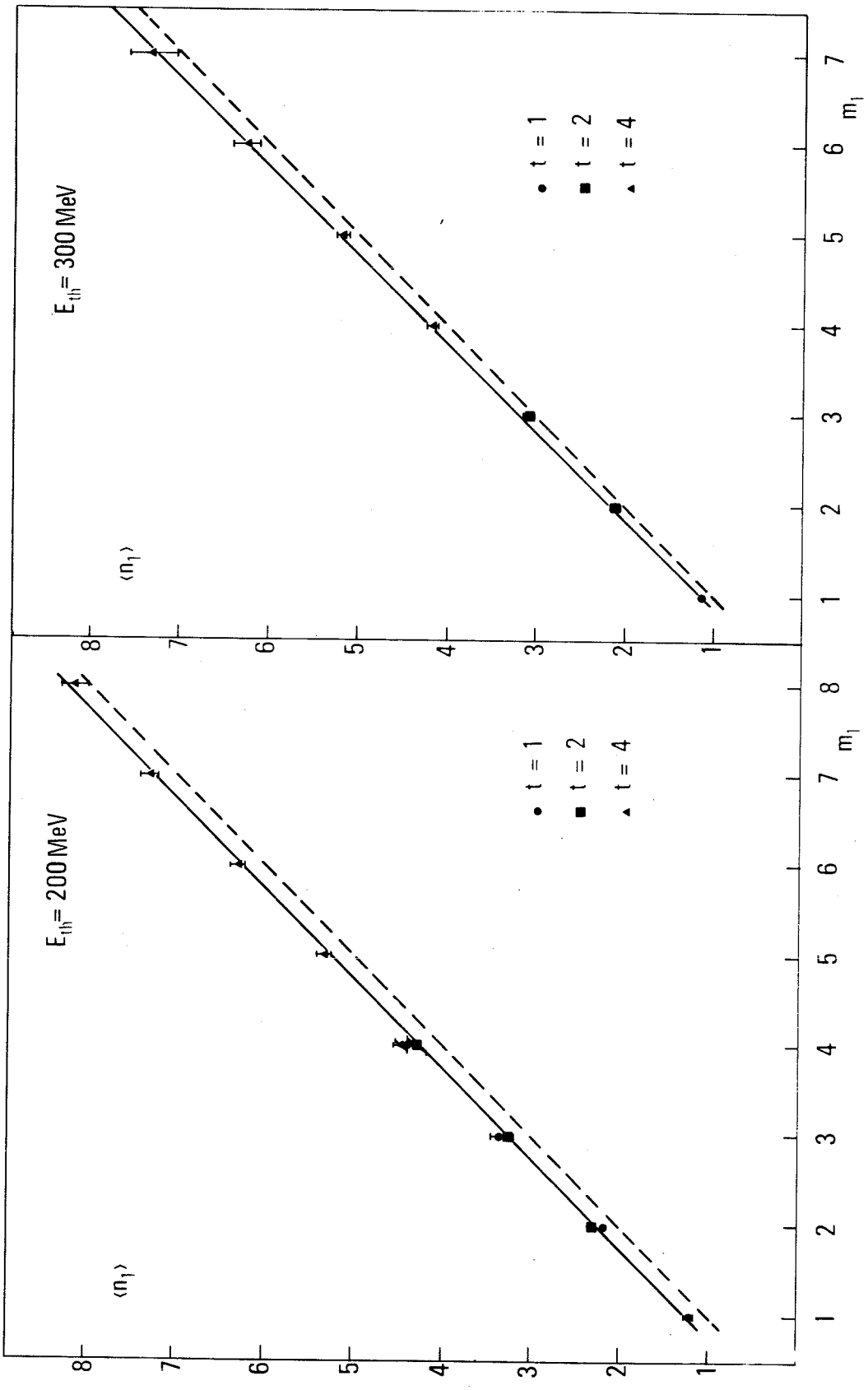

Fig. 36 Average value $\langle n_1 \rangle$ of the number of photons per event that have deposited an energy $E \geq E_{th}$ in the HV counters as a function of m_1, computed by considering only events with $n_1 > m_1$. The results obtained with three trigger modes M_t are plotted together for two values of E_{th}.

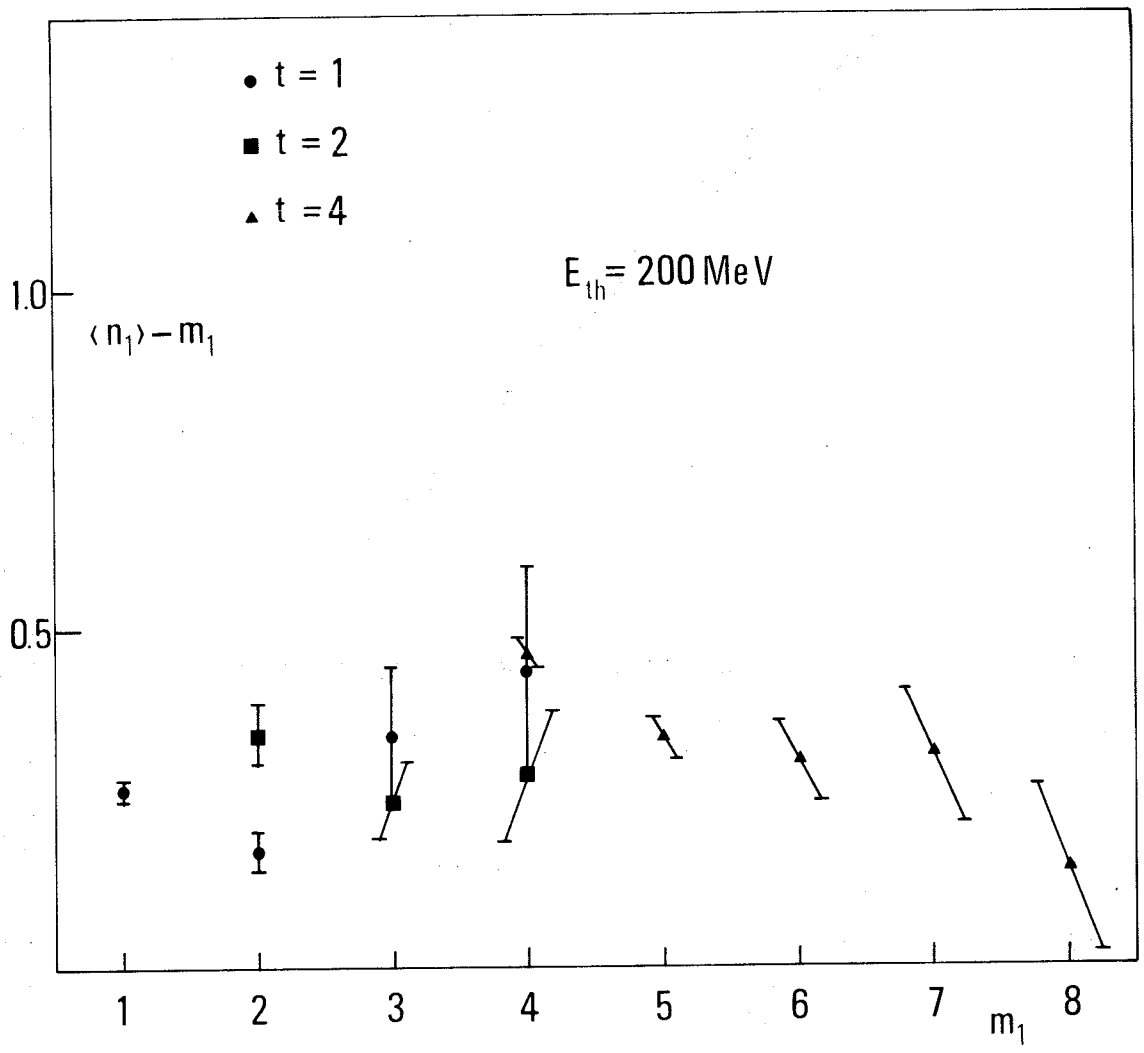

Fig. 37a Plot of the difference between the experimental points and the broken lines of Fig. 36 versus m_1.

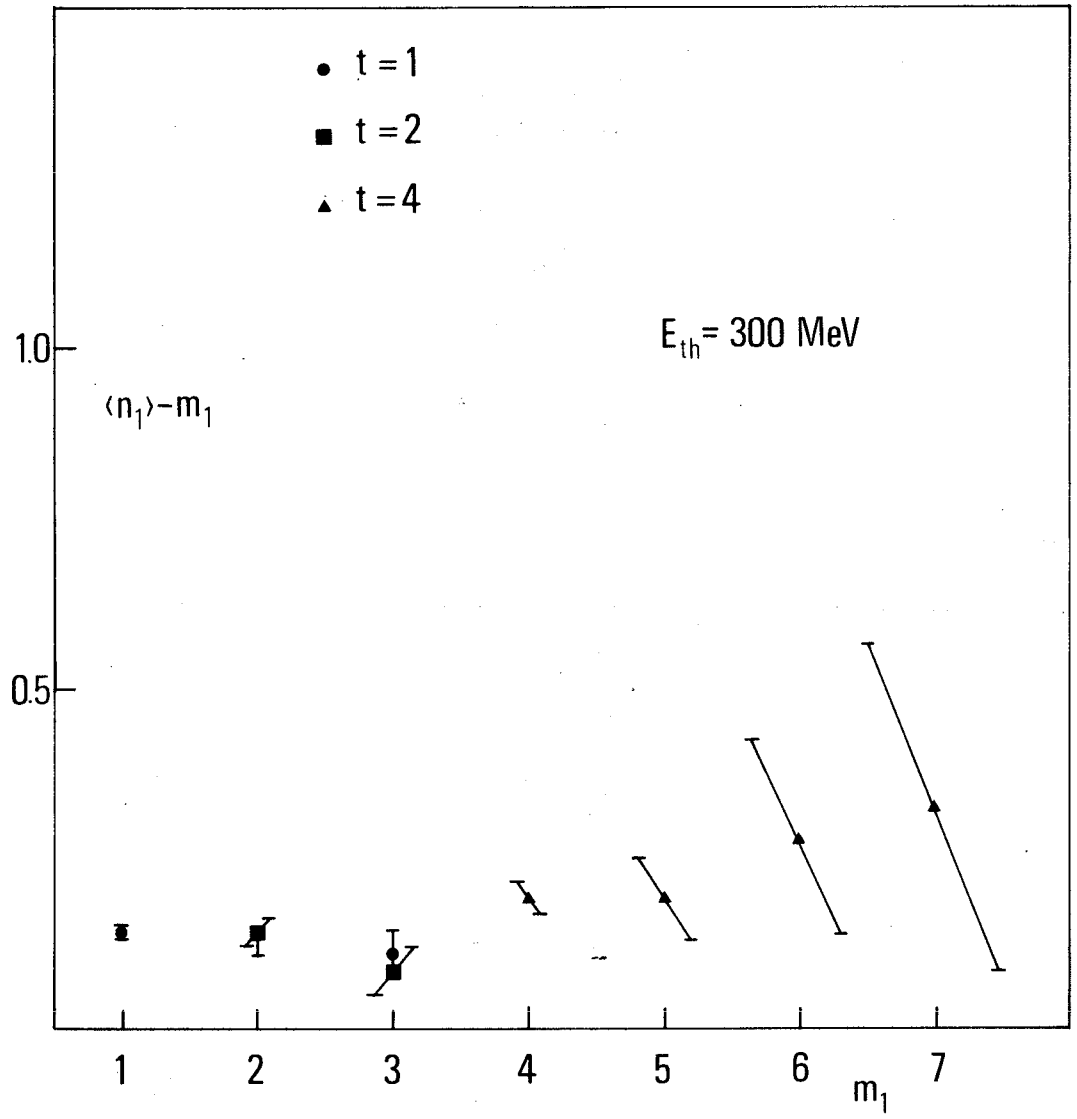

Fig. 37b Plot of the difference between the experimental points and the broken lines of Fig. 36 versus m_1.

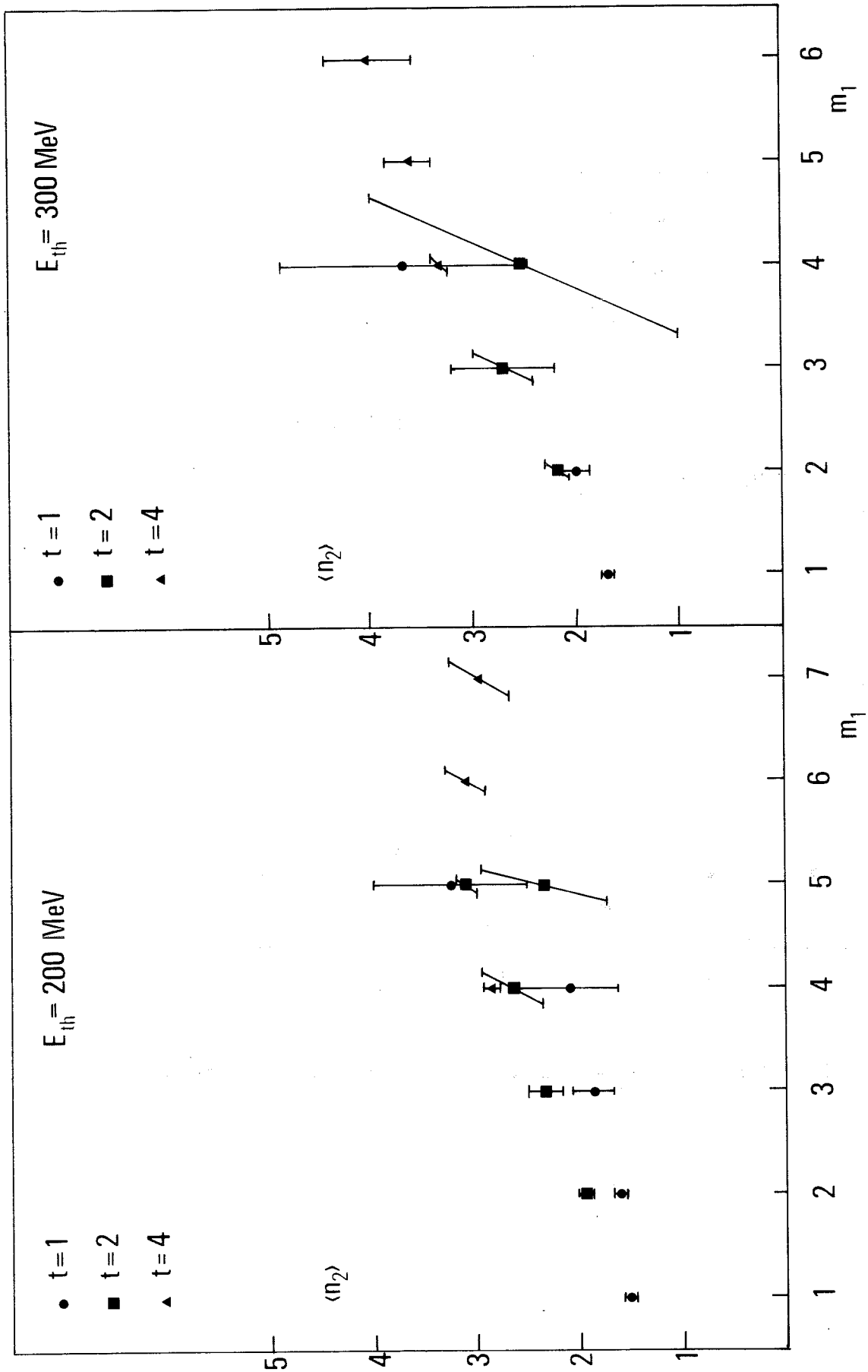

Fig. 38 Average value $\langle n_2 \rangle$ of the number of photons per event that have deposited an energy $E_{cf} = 30$ MeV $\geq E \geq E_{th}$ in the HV counters, as a function of m_1. The results obtained with three trigger modes are plotted together for two values of E_{th}.

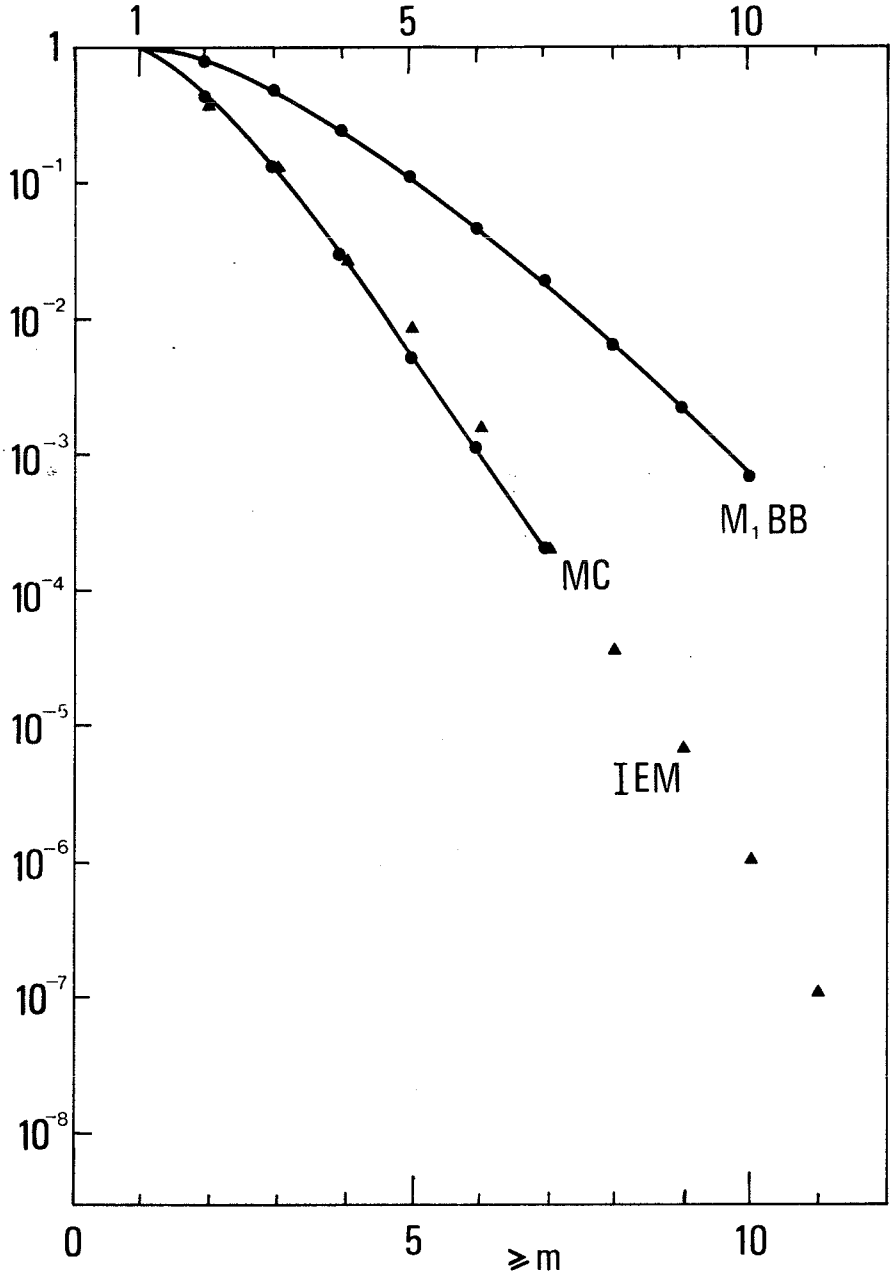

Fig. 39 Comparison of the integral multiplicity distribution observed at $\sqrt{s}$ = 53.2 GeV with the trigger mode $[M_1BB]$ with the results of the Monte Carlo computation and the independent emission model.

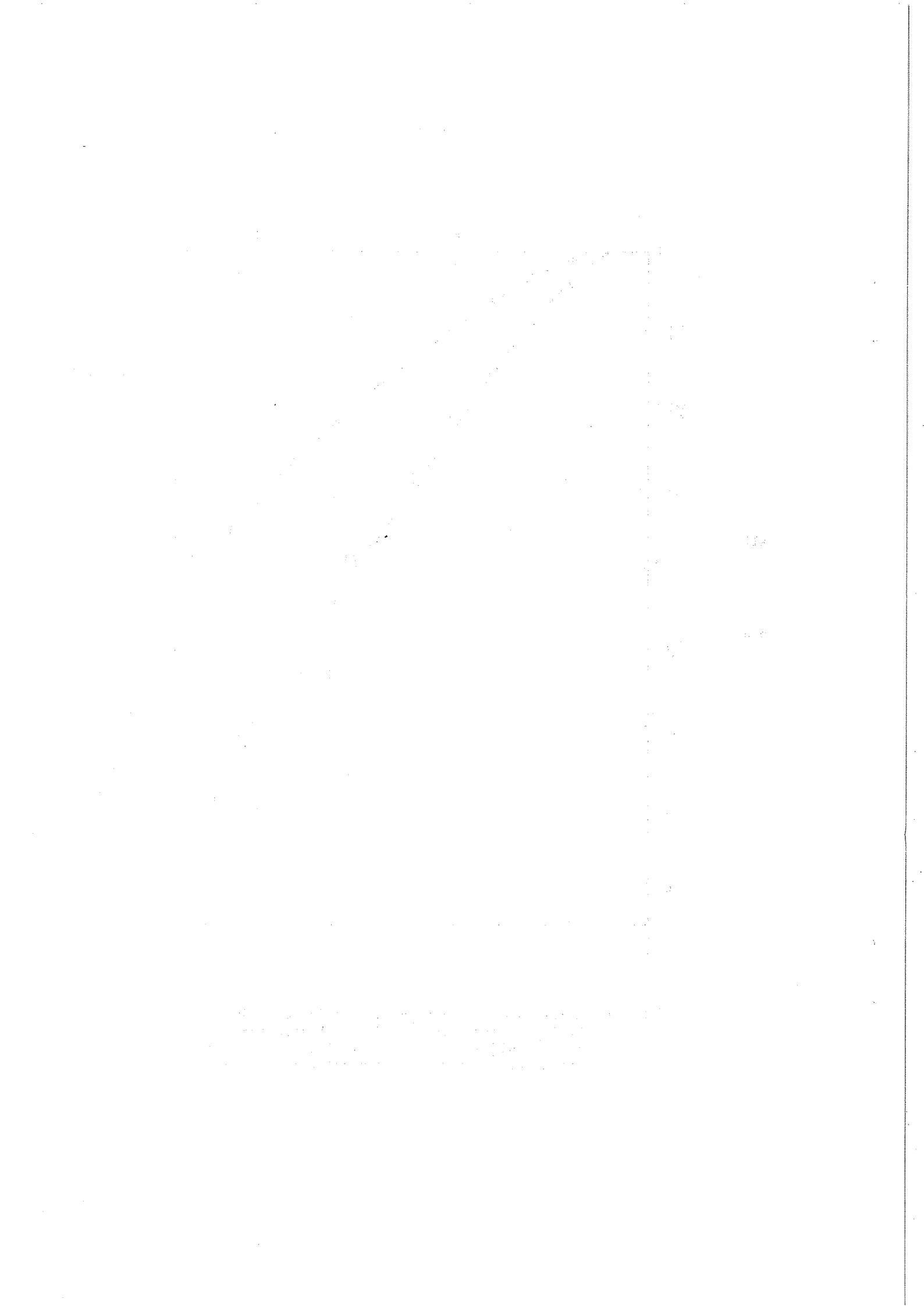

APPENDIX A

THE MAIN CORRECTIONS

The main corrections are listed in Table A.1.

The corrected values of the counting rates HV^c and HV^n are obtained from the observed values by the two relationships

$$HV^c_{corr} = HV^c_{obs} \times \exp\left(\sum c_i\right) \tag{A.1a}$$

$$HV^n_{corr} = HV^n_{obs} \times \exp\left(\sum n_i\right) \tag{A.1b}$$

valid for $c_i \ll 1$ and $n_i \ll 1$. Since we have

$$HV^c_{obs} \simeq \frac{1}{5} HV^n \ , \tag{A.2}$$

in almost all cases we can write

$$n_i \simeq -\frac{1}{5} c_i \ . \tag{A.3}$$

The first correction c_1 should be introduced for taking into account that the efficiency of the spark chambers is smaller than 1. The estimate of c_1 ($\sim$ 10%) is based on the analysis of the spark distribution along the reconstructed tracks.

The correction c_2, due to spurious tracks originating inside the interaction region is obtained (as explained in Section B.3 of Appendix B) by extrapolating, within the interaction region, the number of spurious tracks that are observed to originate outside the interaction region.

The correction c_3 originates from the fact that some of the charged HV are due to a charged particle moving almost in the same direction as the neutral secondary that triggers the HV counter. A good estimate of this correction would involve the knowledge of possible short-range orders between neutral and charged secondaries. If the secondaries were completely uncorrelated, n_3 would amount to +1% for the "HV out" and 0.5% for the "HV in".

The correction c_4 originates from the fact that, by assuming sharp edges of the interaction region, one throws away a certain number of good tracks originating in the halo of the interaction region.

Finally the correction n_5 is due to the conversion of the gamma-rays in the walls of the vacuum chamber and counter A. The other materials placed between the first spark chamber and the HV counters are irrelevant for the computation of this correction because, by requiring at least 8 sparks per reconstructed track, at least one spark should be observed in the first spark chamber. For this reason, $n_5 \simeq 2\%$ for the "OUT" detector as well as for the "IN" detector, in which a layer of lead 0.17 cm thick was placed in front of the Z counters.

The corrections n_1, n_2, n_4 and c_5 are obtained from the relationship (2.3).

Table A.1

Main corrections to the counting rates $HV^c(c_i)$ and $HV^n(n_i)$

Efficiency of spark chambers	$c_1 = +10\%$	$n_1 \simeq -2\%$
Spurious tracks originating from the interaction region	$c_2 = -5\%$	$n_2 = +1\%$
Angular resolution between neutral and charged secondaries		$n_3 = \begin{matrix} +1\% \text{ OUT} \\ +0.5\% \text{ IN} \end{matrix}$
Good tracks originating in the halo of the interaction region	$c_4 = +5\%$	$n_4 = -1\%$
Conversion of gamma-rays in material in front of the HV	$c_5 = -10\%$	$n_5 = +2\%$
	$\sum c_i \simeq 0$	$\sum_i n_i = +0.01$

APPENDIX B

EVALUATION OF THE BACKGROUND

Our main concern has always been with the background of the counters, in particular the lead-glass Čerenkov counters, as well as with the data provided by the spark chambers[20].

The background of the counters is mainly due to the superposition of two types of events: (i) events produced by the interaction of a proton with the residual gas or the vacuum chamber walls; (ii) accidentals of various types.

Both types of events affect the collected data in two different ways:

a) They affect the trigger in the sense that the adopted trigger conditions are fulfilled only because a pp interaction -- not adequate for the adopted trigger mode -- is in accidental coincidence with one, or more, secondary of other origin [either (i) or (ii)].

b) They affect the multiplicity of events triggered by pp interactions that fulfil the conditions imposed by the adopted trigger mode.

Therefore four classes of HV background should be examined which will be denoted with self-explaining notations as 1a, 1b, 2a and 2b, below.

The classes 1a and 1b are discussed in Section B.1, the classes 2a and 2b in Section B.2.

Section B.3 is devoted to the discussion of some problems connected with the reconstruction of the tracks from the sparks, recorded by means of the spark chambers. The most important are: (i) the problem of the efficiency of reconstruction, i.e. the problem of how many tracks "are lost" in the analysis because of the limited efficiency of the spark chambers; (ii) the spurious tracks, i.e. the tracks reconstructed erroneously by the computer because of reconstruction ambiguities. In the course of the discussion of these two problems, we will also give some useful information on the spark-chamber background.

B.1 EVENTS PRODUCED BY PROTON COLLISION AGAINST THE RESIDUAL GAS OR THE VACUUM CHAMBER WALLS (CLASSES 1a AND 1b)

The background due to this type of event can be estimated from the results of ISR runs made with a single beam.

The main difficulty that one encounters in the subtraction of single-beam data from those observed in two-beam runs derives from the normalization of the one-beam data. We have tried to overcome this difficulty by assuming that the frequency of the one-beam events is proportional to the corresponding beam current.

Thus we found the results summarized in Table B.1, from which we can conclude that the data obtained with the trigger modes involving the BB coincidences are not affected appreciably by this type of background.

The situation is different for the trigger modes involving ΣΣ. In spite of this, we did not correct the ΣΣ data for this type of background. We have compared, however, the corresponding results with those obtained from the BB data, so that the difference can provide an estimate of the background of ΣΣ data. In all cases we found that the difference was small.

The interactions of protons with gas and vacuum chamber walls that affect the multiplicity of the events, i.e. class 1b, are still less important.

B.2 ACCIDENTALS OF VARIOUS TYPES (CLASSES 2a AND 2b)

The most important accidentals affecting the trigger (i.e. class 2a) are the following:

$$[M_3 \cdot \Sigma\Sigma] \cdot 2\tau \cdot S'$$
$$[M_2 \cdot \Sigma\Sigma] \cdot 2\tau \cdot D'$$
$$[M_1 \cdot \Sigma\Sigma] \cdot 2\tau \cdot T'$$
$$[\Sigma\Sigma] \cdot 2\tau \cdot Q' \ ,$$

where τ (= 50 nsec) is the resolution time of the trigger and S', D', T' and Q' are total single, double, threefold and fourfold counting rates of the HV fired by events produced in all possible ways. The frequencies of these four categories of events have been estimated from time-of-flight measurements between any M_t and ΣΣ. The upper limit of the sum of the four terms written above in the case of M_4 (M_2) is of the order of 8% (2%) depending on beam stability. With BB this type of accidental remains the same, whereas other kinds, like $[\Sigma\Sigma_{acc}] \cdot M_4$, are reduced by two orders of magnitude, passing from ΣΣ to BB trigger modes.

The accidentals of class 2b can be estimated from the analysis of the so-called "pedestal events" obtained by triggering at random. The gate during which the pulses of all Čerenkov counters were accepted is 200 nsec. The multiplicity distributions of the HV fired in pedestal events, taken at $s^{\frac{1}{2}} = 53.2$ GeV, are given as example in Table B.2 for a few values of k_{cf}. We see that the multiplicity of the HV (charged + neutrals) fired with $k_{cf} = 30$ MeV is very small. Only in a particularly bad run we found 0.3 particles/event, which is very small with respect to the observed average multiplicities not only of HV^n but also of HV^c.

Other background data obtained from pedestal events that may be of interest are: (i) the frequency of events with pulse height $\geq$ 50 MeV and 200 MeV registered in the "LB out" counters amounts to 0.3% and 0.1%, respectively, whereas for the "LB in" the same type of events have a frequency equal to about half that of the "LB out"; (ii) The average number of sparks distributed at random is 9.5 for pedestal events and the events with more than 20 sparks are 13%.

B.3 TRACK RECONSTRUCTION

Two main problems are faced in the reconstruction of individual tracks from spark chamber data, i.e. the efficiency of reconstruction and the percentage of spurious tracks. These may have different origins, among which the two most important are: (i) tracks due to a single beam; (ii) tracks reconstructed erroneously by the computer because of ambiguities of reconstruction.

The number of spurious tracks depends largely on the number of wire planes used in the track reconstruction (these are all together 4x, 4y and 2η planes at 15°).

In the reconstruction of the individual tracks at the beginning, we required the presence of sparks in at least 7 planes, i.e.

$$\geq 3x \text{ plane sparks}$$
$$\geq 3y \text{ plane sparks}$$
$$\geq 1\eta \text{ plane sparks} .$$

Let us indicate by (x_0,y_0) the coordinates of the origin of a track in the (x,y) plane (z = 0) and define a fiducial "volume" of dimensions

$$-15 \text{ cm} \leq x_0 \leq +15 \text{ cm}, \quad -2.5 \text{ cm} \leq y_0 \leq 2.5 \text{ cm} . \qquad (B.1)$$

With the $[M_4\Sigma\Sigma]$ trigger, the number of tracks originating outside the fiducial volume in one-beam runs is about equal to that produced inside. From this result, we estimate that the number of one-beam tracks originating inside the fiducial volume in the two-beam runs amounts to about 20%. This 20% is computed as follows. One starts from the map of the crossing points with the plane z = 0 of the reconstructed tracks (called "origins") obtained with one-beam runs, and one computes the ratio r of the number of origins outside to the number of origins inside a fiducial "strip" $-15 \leq x \leq +15$ cm.

On a similar map, obtained from two-beam runs, one counts the number N_{ext} of origins lying outside the same fiducial strip and one assumes

$$\frac{N_{int}}{N_{ext}} = \frac{1 - r}{r} ,$$

where N_{int} is the (unknown) number of internal origins due to one-beam interactions.

The spurious tracks of type (ii) represent a rather large contribution as one recognizes from the following example: in the case $s^{\frac{1}{2}} = 53.2$ GeV and M_4, the ratio of the number of tracks originating outside the interaction region defined above, to the number of tracks originating inside the interaction region, amounts to 38% when at least 7 sparks (i.e. $\geq 3x$, $\geq 3y$ and $\geq 1\eta$ plane) are required; but it is reduced to 18% when both η planes are imposed. Finally their number becomes 6% if sparks are required in all 10 x, y and η planes (Table B.3). On the contrary, passing from 7 to 8 sparks, neither the number of HV^c nor the number of tracks originating inside the interaction region undergo an appreciable change.

The situation is illustrated in Figs. B.1, B.2 and B.3, which show the distributions of the intersection points with the equatorial vertical plane (z,y_0) of the reconstructed tracks: Fig. B.1 refers to a one-beam run, Figs. B.2 and B.3 to a two-beam run analysed by reconstructing the tracks with sparks in at least 7 planes (Fig. B.2) and all 10 planes (Fig. B.3).

Thus we arrived at the conclusion that in selecting between all possible ways of pairing the (x,y) and (y,z) reconstructed projections

$$x = x_0 + \alpha z, \quad y = y_0 + \beta z \ , \tag{B.2}$$

the requirement of 7 sparks is not sufficient for eliminating the great majority of ambiguous cases.

Therefore, in the final analysis presented here, for reconstructing a track, we required at least 8 sparks by the following procedure: of all tracks that had been reconstructed with at least 7 sparks, we kept only those that had an 8th spark within 2 mm.

By imposing these more restrictive requirements, also the number of events with at least 1 track originating outside the interaction region is considerably reduced (last column of Table B.3). This means that, by requiring a greater number of sparks, the spurious tracks of type (B.2) not only diminish in number but, at the same time, they turn out to be assembled in a very scanty number of events which can be interpreted as due to beam-gas or beam-walls interactions.

On the contrary, the number of tracks originating inside the interaction region is reduced by only a very small amount when 8 instead of 7 sparks per reconstructed track are imposed: their multiplicity distribution (Fig. B.4) does not change appreciably passing from 7 to 8 sparks.

Further interesting information can be obtained from the data of Tables B.4 and B.5.

The results of this analysis are in agreement with the assumption that the "two-beam" tracks originating outside the interaction region are mainly due to

"spurious tracks" due to accidental alignment of sparks (more frequent when an event is crowded because of many tracks and/or background sparks) which are paired incorrectly with either a true or a spurious track in the other projection.

For all these reasons, in the final analysis, we have required, as said above, 8 sparks per reconstructed track. Under these conditions we found the useful relation

$$\left\langle \frac{\text{Tracks}}{\text{Events}} \right\rangle \propto \left\langle \frac{\text{Sparks}}{\text{Events}} \right\rangle \ .$$

The number of reconstructed tracks n_{tr} is in general smaller than the number of charged particles n_{ch} that cross the spark chambers. The difference

$$\Delta_{tr} = n_{ch} - n_{tr} \qquad \text{(B.3)}$$

is due to various causes, the most important of which are:

a) The efficiency η of the single planes of the spark chambers is smaller than 1 ($\eta \simeq 0.90$);

b) The reconstructed projections in the (x,z) and (y,z) planes are paired incorrectly by the computer with the result that one (or both) of the coordinates (x_0,y_0) of the origin of the reconstructed track falls outside the interaction region and the track is rejected. The incorrect pairing of the projections only exceptionally produces the opposite effect, i.e. the (erroneous) interpretation of a "true track" originating outside the interaction region as a track originating inside the interaction region.

Therefore, both points (a) and (b) produce a positive value of the correction (B.3) to be applied to n_{tr}. One may even be brought to suspect that such a correction increases with the multiplicity n_{ch} of the events more than in proportion to n_{ch}.

In short, one can say that the correction Δ_{tr} originates from the fact that, for various reasons, a certain fraction of the so-called HV^n are in reality HV^c, but the corresponding tracks have not been reconstructed or have been reconstructed incorrectly.

From these remarks it appears that the two following questions require an answer:

- Which is the value of Δ_{tr} that, applied to the observed value of n_{tr}, allows a reasonable determination of n_{ch}?
- How many of the HV^n are in reality HV^c?

In order to answer the second question, one has to distinguish two subcases according to whether an HV^c has been classified among the HV^n because (i) the corresponding track originates outside the interaction region and (ii) the corresponding track has not been reconstructed at all.

An approximate estimate of the correction (i) is obtained by adopting the reasonable assumption that the fraction of the HV^c that originates outside the interaction region is equal to the fraction of reconstructed tracks that originate outside the interaction region:

$$\frac{(HV^c)_{\text{OUT i.r.}}}{HV^c} = \frac{\text{Tracks} \geq 8 \text{ sparks OUT i.r.}}{\text{Tracks} \geq 8 \text{ sparks}} \qquad (B.4)$$

where the right-hand side is directly observed. Thus from the second column of Table B.3, we see, for example, that for $s^{\frac{1}{2}} = 53.2$ GeV and M_4, the value of the ratio (B.4) amounts to 0.18. But we know that $HV^c/HV^n \sim 1/5$, and therefore the correction of type (i) that should be applied to the number of HV^n, amounts to a decrease of the uncorrected value of HV^n of no more than

$$\frac{(HV^c)_{\text{OUT i.r.}}}{HV^c} \times \frac{HV^c}{HV^n} = 0.18 \times 0.2 = 3.6\% \ . \qquad (B.5)$$

A similar estimate of correction (ii) shows that this also is not very large.

We prefer, however to proceed to look for an answer to the first question. This is done in the following by two different methods that both provide upper limits.

(1). The first estimate of n_{ch} is based on the observed value of the average number of Z counters fired per event. This type of information is collected for two cases, as examples, in the first part of Table B.6.

The values of $\bar{m}_Z$ (total) shown in the 5th column of Table B.6 cannot, however, be directly compared with the observed value of $\bar{m}_{tr}$ (8th column), because of various causes:

a) The moderate spatial resolution of the Z counters due to their area (each of the d = 20 Z counters has an area of 50×6.5 cm^2. They lay in two planes placed 34.2 cm from the centre of the interaction region);

b) The solid angle Ω_Z covered (on each side of the interaction region) by 10 Z counters is appreciably different from the solid angles Ω_{ch} covered (on each side of the i.r.) by the spark chambers:

$$\Omega_Z = 1.676, \quad \Omega_{ch} = 0.780, \quad \Omega_{ch}/\Omega_Z = 0.465 \ . \qquad (B.6)$$

c) A layer of lead 0.17 cm thick ($\sim 0.3\ X_0$) was placed in front of the Z counters of the "IN" detector.

A crude estimate of the correction (a) can be obtained under the assumption that the charged particles are emitted isotropically and without correlation. In our case, such an assumption should give a fairly good estimate of the correct value, because it is used only within the angular region Ω_Z which is not very large and centred around 90° with respect to the common direction of the two initial protons in the frame of their c.m. Under this assumption one can apply Eqs. (B.18) and (B.19) of Ref. 1, i.e.

$$n_{ch} = -d \ln \left(1 - \frac{\bar{m}_Z}{d}\right) \tag{B.7a}$$

$$\sqrt{\overline{(\delta n_{ch})^2}} = \sqrt{\frac{\bar{m}_Z}{1 - (\bar{m}_Z/d)}} \ . \tag{B.7b}$$

The values obtained by such a procedure should now be multiplied by the ratio Ω_{ch}/Ω_Z shown by Eq. (B.6). The final results of these two operations are shown in the last column of Table B.6. They are slightly larger than $\bar{m}_{tr}$. Furthermore, $\bar{n}_{ch}$ goes down from 2.86 to 2.49 if correction (c) is applied to the Z counters of the "IN" detector*).

(2). A second procedure is based on the total number of sparks per event (Table B.3). Let us discuss the case $s^{\frac{1}{2}} = 53.2$ GeV for the "OUT" detector. We will try to clarify the relationships between:

a) the number of charged particles n_c crossing the detector;

b) the number of reconstructed tracks m_r;

c) the number of charged HV: HV^c.

The total number of sparks per event that would be produced if the efficiency of each plane of the spark chambers was $\eta = 1$ (and not $\eta = 0.90$) would be (Table B.3)

$$\frac{44.5}{0.90} = 49 \ .$$

We should now subtract the number of sparks distributed at random in the pedestal events in the spark chambers of the outside detector, i.e. $\frac{1}{2} \times 9.5 = 4.7$. Thus we obtain

$$49 - 5 = \text{sparks/event} \ ,$$

*) $\bar{m}_Z(\text{IN}) = 0.70 \times 2.1 = 1.47$, $\bar{m}_Z(\text{OUT} + \text{IN}) = 3.2 + 1.5 = 4.7$

$\bar{n}_{ch} = -20 \ln \left(1 - \frac{4.7}{20}\right) = -20 \ln 0.765 = 5.36.$

from which the maximum number of tracks that can be reconstructed is

$$\frac{44 \text{ sparks}}{10 \text{ planes}} = 4.4 \text{ tracks} . \tag{B.8}$$

These tracks originate in part outside, in part inside, the interaction region in the ratio

$$\frac{2.4 \times 0.38}{2.4 \times (1 - 0.38)} = \frac{0.9}{1.5} .$$

Therefore, the maximum number of tracks originating inside the interaction region should not be greater than

$$4.4 \times (1 - 0.38) = 4.4 \times 0.62 = 2.7 . \tag{B.9}$$

This value is very close to that obtained from the multiplicity of the fired Z counters (column 9 of Table B.6).

This number should not be used, however, for evaluating the number of HV^c, since in the definition of the latter we have considered only tracks originating inside the interaction region. This means that an HV with a pulse height greater than k_{cf}, with a reconstructed track originating outside the interaction region, has been classified as HV^n. Therefore, an upper limit for the number of HV^c that have been erroneously classified as HV^n is obtained by multiplying the observed HV^c by the ratio of Eq. (B.8) to 1.5. Thus we obtain

$$(HV^c)_{corr} = (HV^c)_{obs} \frac{4.4}{1.5} = (HV^c)_{obs} \times 2.9 . \tag{B.10}$$

The factor 2.9 is certainly largely overestimated, because it does not take into account two facts: (a) there are tracks crossing the spark chambers that do not cross the HV counters; (b) an appreciable fraction of the charged particles crossing the HV do not give pulses above k_{cf} = 30 MeV.

But even so, the corresponding correction on the number of HV^n is not dramatic.

Since the total number of

$$HV = HV^c + HV^n$$

fired with a pulse height $\geq k_{cf}$ does not depend on this correction, we can write

$$(HV^c)K + (HV^n)x = HV , \tag{B.11}$$

where, according to Eq. (B.10), one has K = 2.9. From Eq. (B.11) it follows that

$$x = 1 - \frac{(HV^c)_{obs}}{(HV^n)_{obs}} \times (K - 1) = 1 - \frac{1}{5} 1.9 = 1 - 0.38 = 0.62 . \tag{B.12}$$

We can conclude that the correction originating from the inefficiency of the procedure of track reconstruction amounts to a decrease of the observed HV^n, which is certainly smaller than $\sim$ 30%.

Table B.1

Background estimates at $s^{\frac{1}{2}}$ = 53.2 GeV

	$M_1\Sigma\Sigma$	M_1BB	$M_4\Sigma\Sigma$	M_4BB
1. p + gas and p + walls				
1a) affecting the trigger	1%	-	< 10%	< 1%
1b) affecting the multiplicity of the events	much less than 1a			
2. Accidentals				
2a) affecting the trigger	< 2%		< 8%	
2b) affecting the multiplicity of the events	-		< 0.3 particles/event	

Table B.2 *)

Multiplicity distribution of HV fired in pedestal events at $s^{\frac{1}{2}} = 53.2$ GeV

k_{cf}	30 MeV	70 MeV	150 MeV	30 MeV	70 MeV	150 MeV	30 MeV	70 MeV	150 MeV
m	OUT	OUT	OUT	IN	IN	IN	OUT + IN	OUT + IN	OUT + IN
0	0.9845	0.9917	0.9953	0.9901	0.9944	0.9979	0.9783	0.9876	0.9936
1	1.10×10^{-2}	0.601×10^{-2}	3.88×10^{-3}	6.59×10^{-3}	4.85×10^{-3}	1.94×10^{-3}	1.377×10^{-2}	8.73×10^{-3}	5.43×10^{-3}
2	3.30×10^{-3}	2.13×10^{-3}	7.76×10^{-4}	2.33×10^{-3}	5.82×10^{-4}	-	3.88×10^{-3}	2.72×10^{-3}	7.76×10^{-4}
3	9.70×10^{-4}	-		5.82×10^{-4}	-	1.94×10^{-4}	2.52×10^{-3}	5.82×10^{-4}	-
4	-	-		1.94×10^{-4}	-		1.16×10^{-3}	-	-
5	-	1.94×10^{-4}		-	1.94×10^{-4}		-	1.94×10^{-4}	1.94×10^{-4}
6	1.94×10^{-4}			-			1.94×10^{-4}	-	
7				1.94×10^{-4}				1.94×10^{-4}	
8									
9									
10							1.94×10^{-4}		
Total	1.0000	1.0000		1.0000	1.0000	1.0000	1.0000	1.0000	1.0000
$\langle m \rangle$	0.025	0.014	0.01	0.02	0.01	0.01	0.04	0.02	0.01
σ	0.30	0.26	0.24	0.29	0.25	0.23	0.54	0.49	0.46

*) Data obtained from the runs: 2384, 2385, 2386, 2388 and 2398, corresponding to a total of 5,157 events. The frequency 1.94×10^{-4} corresponds to 1 event.

Table B.3

Spurious tracks originating from reconstruction ambiguities at $s^{\frac{1}{2}}$ = 53.2 GeV with trigger M_4

Required number of sparks	No. tracks $y_0 \geq 2.5$ cm / No. tracks	No. events with at least 1 track $y_0 \geq 2.5$ cm / No. events
≥ 7 ($\geq 3x$, $\geq 3y$, $\geq 1\eta$)	0.38 *)	0.52
≥ 8 **) ($\geq 3x$, $\geq 3y$, 2η)	0.18	1.8×10^{-2}
10	0.06	2.7×10^{-3}

*) This percentage is appreciably lower in runs with $s^{\frac{1}{2}} < 53.2$ GeV and/or trigger M_2 (M_1), since in these cases the number of sparks per event is smaller and the procedure of pairing the two reconstructed projections is considerably simplified (see last column of Table B.4).

**) Notice that this requirement is slightly different from the requirement of "at least 8 sparks" as explained in the text and that was finally adopted. We checked that these two requirement schemes give practically the same result.

Table B.4

Number of sparks used for the reconstruction of tracks when at least 7 sparks/track are imposed

$s^{\frac{1}{2}}$ (GeV)	Trigger mode	Sparks / Events (OUT)	Tracks / Events (OUT)	Sparks / Tracks (OUT)	Track $y_0 \geq 2.5$ cm / Tracks
53.2	M_4	44.5	2.4	18.5	0.38
30.8	M_4	29.6	1.3	22.8	0.27
53.2	M_1	27.9	1.1	25.4	0.27

Table B.5

Dependence of the number of tracks reconstructed upon the number of sparks required per track

$s^{\frac{1}{2}}$ (GeV)	Trigger mode	Tracks with $\geq$ 8 sparks / Tracks with $\geq$ 7 sparks	Tracks with 10 sparks / Tracks with $\geq$ 7 sparks
53.2	M_4	0.64	0.18
30.8	M_4	0.78	0.30
53.2	M_1	0.74	0.23

Table B.6

The average values of the Z counters compared with the number of tracks per event

$s^{\frac{1}{2}}$ (GeV)	Trigger mode	$\bar{m}_Z$ OUT	$\bar{m}_Z$ IN	$\bar{m}_Z$ Total	$\bar{m}_{tr}$ OUT	$\bar{m}_{tr}$ IN	$\bar{m}_{tr}$ Total	$\bar{n}_{ch}$ computed	σ **)
53.2	M_4	3.2	2.1	5.3	1.50 (1.1)	0.67 (0.46)	2.17 (1.56) *)	2.86 ± 0.04	(1.25)
53.2	M_1	1.56	0.95	2.5	0.73 (0.58)	0.33 (0.27)	1.06 (0.85)	1.24 ± 0.02	(0.79)

*) The values in brackets are obtained by imposing that the tracks originate within the interaction region.

**) σ = variance.

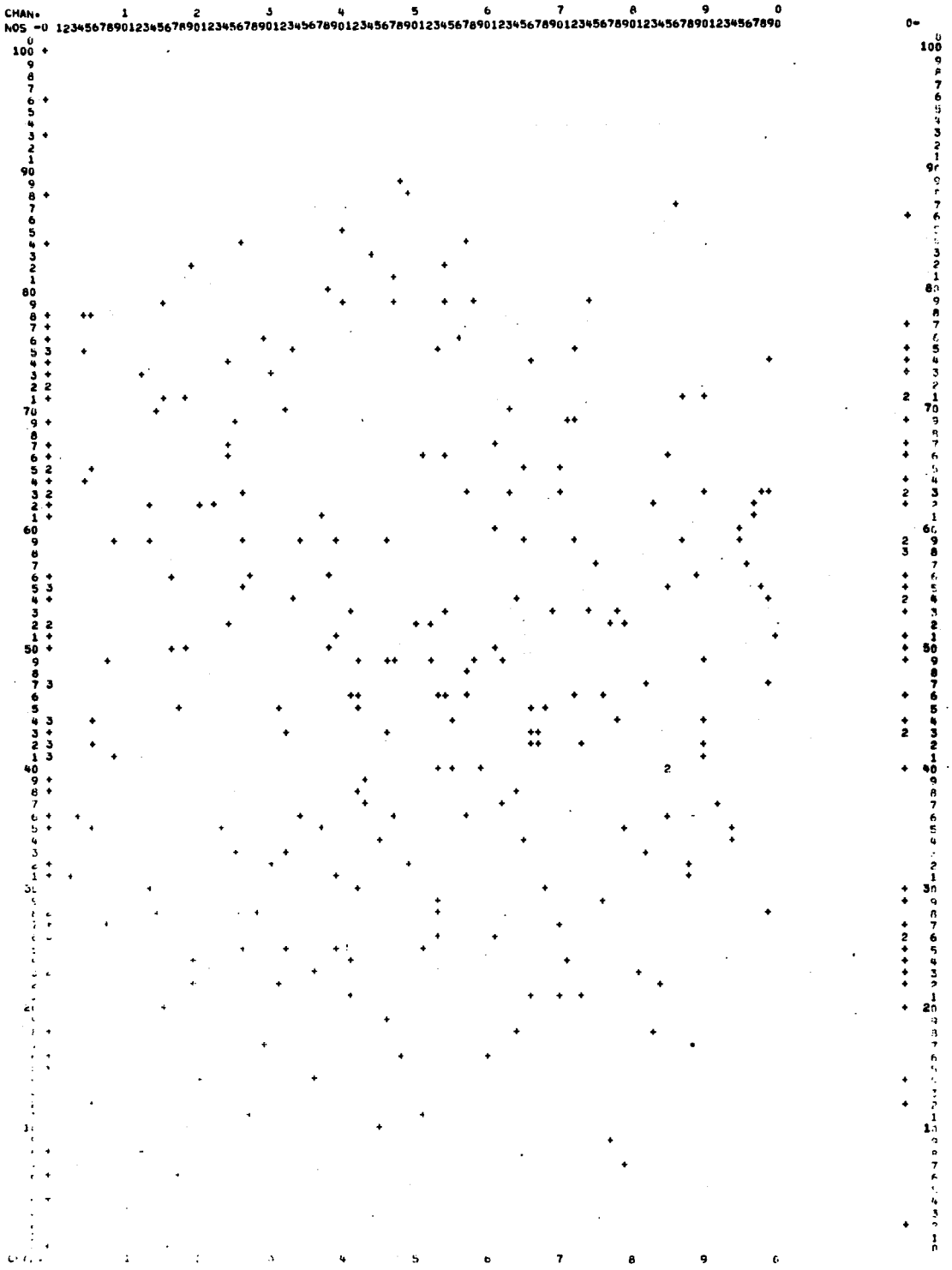

Fig. B.1 Distribution of the intersection points with the equatorial horizontal plane of the tracks reconstructed from the data of a run with a single beam: the reconstruction of these tracks was made from sparks in 7 planes as explained in the text.

Fig. B.2 The same as Fig. B.1 for the case of a two-beam run.

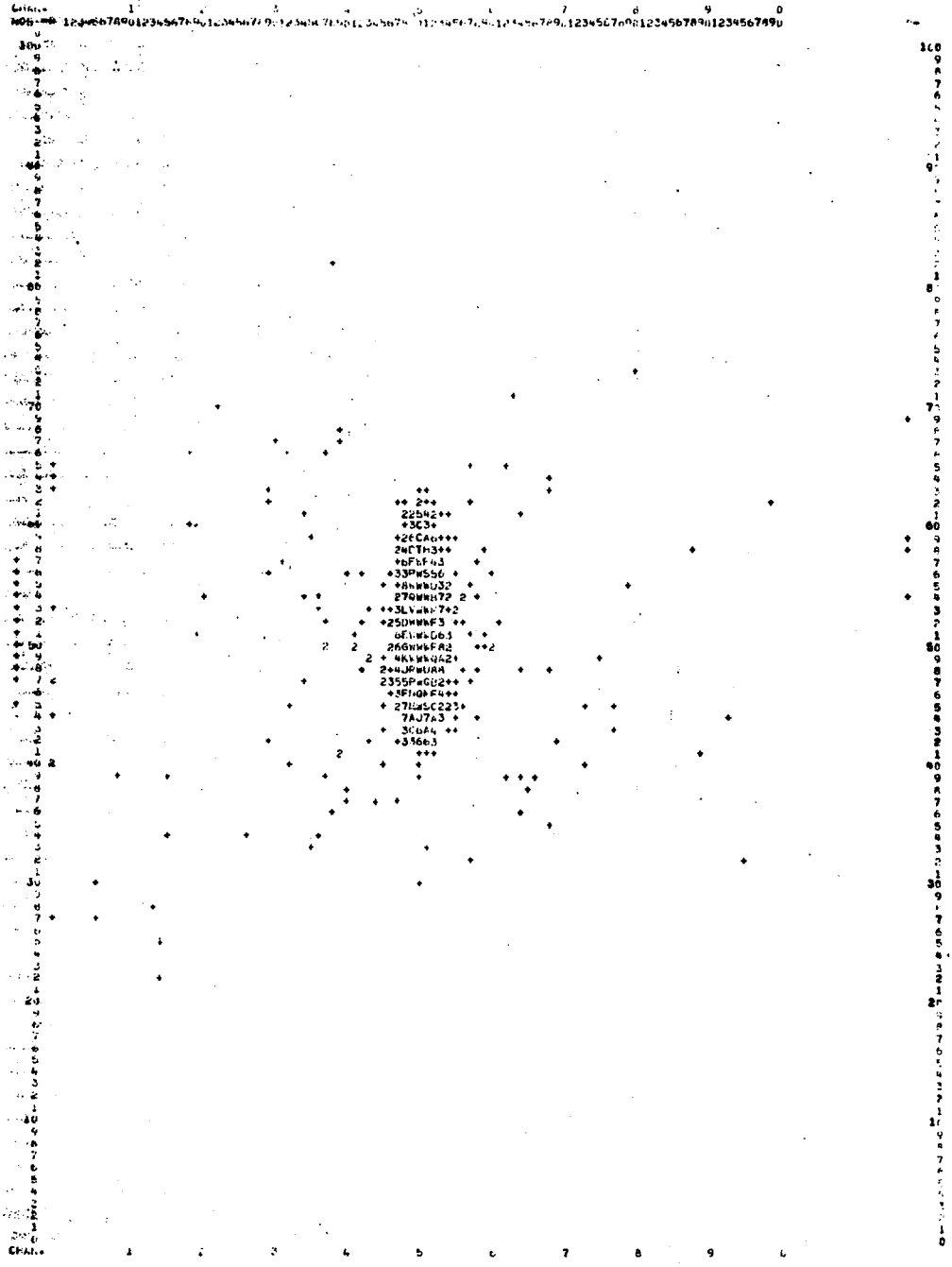

Fig. B.3 The same as Fig. B.2, but the tracks were reconstructed requiring sparks in all 10 planes.

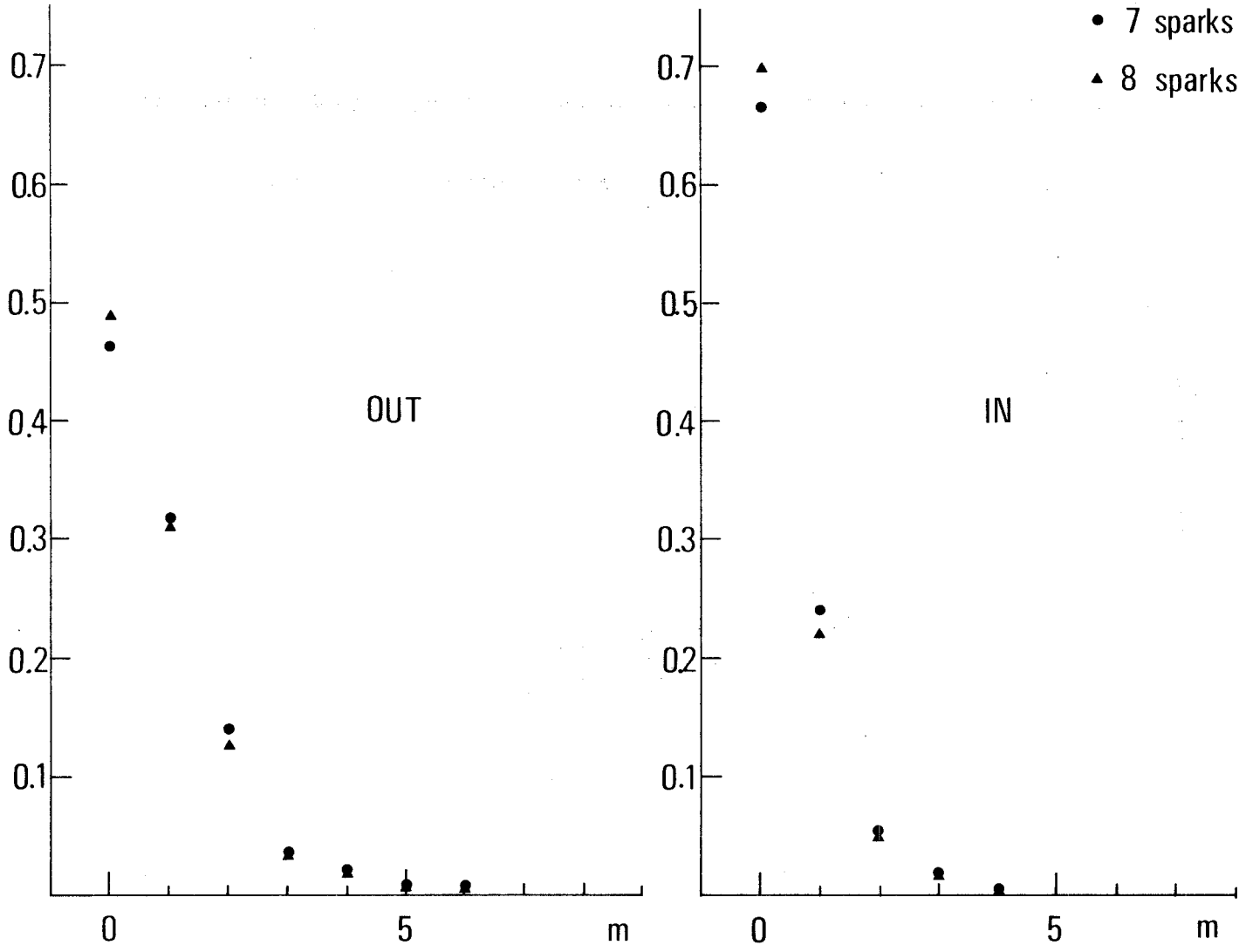

Fig. B.4 Multiplicity distribution of tracks reconstructed by requiring 7 and 8 sparks per track. Only tracks originating in the interaction region are taken into account.

APPENDIX C

POSSIBLE CONTRIBUTION OF SPURIOUS GAMMA-RAYS

A contribution to the multiplicity of the HV^n could arise from spurious gamma-rays, i.e. gamma-rays originating from the decay of π^0 produced in the walls of the vacuum chamber (or other objects in the surroundings) by charged secondary particles or by the primary nucleon scattered in the pp collision.

A distinction should be made from the beginning according to whether the spurious gammas are produced: (a) in the walls of the vacuum chamber and other materials by secondary particles moving from the i.r. towards the detector; (b) in the walls of the vacuum chamber by charged particles moving within the solid angle not covered by the counters; (c) in other objects placed in the surroundings.

a) A rough overestimate of this effect is obtained by assuming that the inelastic cross-section of charged secondaries against nuclei of the various materials is given by

$$\sigma_{coll} = 62.8 \times A^{2/3} \text{ mb} , \qquad (C.1)$$

that one π^0 is produced in each inelastic collision, and that one of its decay gamma-rays always crosses the detector. Thus we find that the number of HV counters fired by this type of spurious gamma-ray generated in all materials between the i.r. and the HV counters amounts to less than 4% of the charged secondaries that cross the detector. Considering that this value is overestimated by a factor greater than 4, we can conclude that the corresponding correction certainly does not exceed 1%.

b) The spurious gamma-rays originating in the part of the walls of the vacuum chamber in the solid angle not covered by the detector can be expressed in the form

$$\langle n_\gamma \rangle = c\, g(x) , \qquad (C.2)$$

where

$$c = \bar{n}_{ch} \sum_i \frac{\rho_i N_A}{A_i} d\bar{\sigma}_{inel}(A) \qquad (C.3)$$

is a constant and

$$g(x) = \frac{\Omega(x)}{4\pi} \frac{1}{\sin \alpha(x)} \qquad (C.4)$$

a geometric factor. In expression (C.3) N_A is Avogadro's number, $\bar{n}_{ch}$ the average number of charged particles crossing the walls at an angle α, and d the thickness of the walls (steel) of the vacuum chamber. In expression (C.4) $\Omega(x)$ is the solid angle under which one of the two detectors is seen from a point downstream at the distance x from the i.r. It should be averaged with respect to x.

The expression (C.2) is obtained assuming that one π^0 is produced in each inelastic collision and that the corresponding gamma-rays are emitted isotropically in the laboratory frame. Both assumptions are in error in the sense of giving a value of C too large. Taking[21]

$$\sigma_{inel}(A) = A^{0.15}\, \sigma_{inel}(p)$$

$$\sigma_{inel}(p) = 36 \text{ mb}$$

$$\bar{n}_{ch} = 6, \quad d = 1 \text{ mm} ,$$

one finds

$$c \simeq 2 \times 10^{-3} .$$

The geometrical factor g(x) is different for the HV and the LB counters. Its mean value, with respect to x, is of the order of 0.2 for the HV and 0.5 for the LB counters. Therefore one can conclude that the expression (C.2), averaged with respect to the distance x, is of the order 10^{-3} for the LB and about 2 times smaller for the HV counter. This means that the contribution of the second class of spurious gamma-rays is also negligibly small.

c) The spurious gamma-rays produced in the surrounding objects could be evaluated by considerations similar to those sketched under (b). We prefer, however, to notice that the most important objects are the side walls of the spark chambers and the concrete blocks placed on the two sides of the lead-glass counters in order to protect them from radiation moving parallel to the x-axis. We believe, however, that the spurious gammas produced in these materials should be relatively rare because of the two following reasons:

i) From the inspection of the distribution of the sparks in the spark chambers we do not see a large density of sparks in the vicinity of the side walls of the chamber. The sparks, in general, appear to be concentrated in the central region of spark chambers.

ii) From the inspection of the number of times that each single HV (and LB) is fired we do not observe any appreciable increase of counting rates in the lead-glass counters close to the concrete block with respect to those in the central region ($\theta = 90°$).

APPENDIX D

MONTE CARLO CALCULATION

D.1 ASSUMPTIONS

(1) Four-momentum conservation is not imposed on the emitted π^0, but it is assumed to be assured by final nucleons. Total energy E_{tot} of all π^0 produced is computed; the event is rejected if E_{tot} is larger than $s^{\frac{1}{2}}$.

(2) The emission of n π^0 is assumed to be independent of the emission of charged pions.

(3) The observed single-particle inclusive spectrum[22]

$$\frac{dN}{dp_t} = B^2 p_t \, e^{-Bp_t}, \quad B = 5.7 \ (GeV/c)^{-1} \tag{D.1}$$

is assumed to hold for any value of multiplicity and in the whole angular range. This hypothesis will be called "uncorrelated emission".

(4) The inclusive angular distribution[23] observed for charged pions is assumed to hold for any value of n_0,

$$\frac{dN}{d\Omega} = \frac{a_1}{a_2 + \sin^2 \theta}, \qquad a_1 = 0.106 \ sr^{-1}, \quad a_2 = (6.3 \pm 4.0) \times 10^{-3} \tag{D.2}$$

(5) The multiplicity distribution is assumed to be Poissonian in the variable n_0 with average value[24]

$$\langle n_0 \rangle = \frac{1}{2} \left[\langle n_{\pi^+} \rangle + \langle n_{\pi^-} \rangle \right], \tag{D.3}$$

which can be put in the form[24]

$$\begin{aligned} \langle n_0 \rangle &= A_0 + B_0 \ln s + \frac{C_0}{s^{\frac{1}{2}}} \\ A_0 &= \frac{1}{2} \left[A_{\pi^+} + A_{\pi^-} \right] = -2.15 \\ B_0 &= \frac{1}{2} \left[B_{\pi^+} + B_{\pi^-} \right] = 0.855 \\ C_0 &= \frac{1}{2} \left[C_{\pi^+} + C_{\pi^-} \right] = 1.85 \ . \end{aligned} \tag{D.4}$$

D.2 STEPS OF COMPUTATION

D.2.1 Computation of gamma-rays from π^0 decay

(1) The angle θ^* of emission of a π^0 in the c.m. of the pp collision is extracted according to the distribution (D.2).

(2) The transverse momentum $p_t^* = p^* \sin \theta^*$ is extracted according to the distribution (D.1).

(3) The momentum of the π^0

$$p^* = \frac{p_t^*}{\sin \theta^*} \tag{D.5}$$

is computed from the results of points (1) and (2). If $p^* > p^*_{max}$ the event is rejected.

(4) The azimuthal angle ϕ^* is extracted according to a uniform distribution.

(5) The Lorentz transformation from the c.m. to the laboratory frame is made without introducing any approximation.

(6) The decay of the π^0 is computed in its c.m. according to a uniform distribution in solid angle.

(7) The Lorentz transformation from the rest frame of the π^0 to the laboratory frame is computed.

(8) The final results, i.e. k_1, k_2, θ_1, θ_2, ϕ_1, ϕ_2, defining the energy and direction of the two gamma-rays in the laboratory frame are stored on magnetic tape for a total number of π^0 equal to 200,000.

D.2.2 Construction of multipion events

(9) The number n_0 of π^0 produced in an event is extracted according to the Poisson law.

(10) From the pool of π^0 recorded on the magnetic tape as explained under point (8), n_0 "neutral pions" are extracted at random.

(11) The total energy of the n_0 π^0

$$E_{tot\pi^0} = \sum_{1}^{n_0} (k_1 + k_2) \tag{D.6}$$

is computed. If $E_{tot} \geq s^{\frac{1}{2}}$, the event is rejected.

(12) The point of generation of the event within the interaction region is extracted according to a triangular distribution of 30 cm base.

(13) One verifies if at least one of the 2 gamma-rays enters the detector with an energy $\geq$ 10 MeV. If not, the event is recorded as an "unfavourable event".

D.2.3 Instrumental features

(14) The HV crossed by each one of the gamma-rays entering the detector is determined and the conversion efficiency into electrons is assumed to be 90% as obtained from the total gamma-ray cross-section[25]. This means that in 10% of the cases the gamma-ray is not detected by the HV's and therefore is lost for the subsequent computations.

(15) The mean value of the energy deposited by the shower is computed by means of the following empirical relation, obtained from best fit of an *ad hoc* Monte Carlo computation[7]

$$\langle E_{HV} \rangle = \sqrt{k_{MeV}} \frac{\varepsilon_c}{L_{rad}} , \qquad (D.7)$$

where ε_c = 13.4 MeV is the critical energy of the lead glass and L_{rad} the corresponding radiation length (L_{rad} = 2.5 cm). The proportionality factor of dimensions (energy)$^{-\frac{1}{2}}$, not explicitly shown in Eq. (D.7), turns out to be numerically equal to 1.

(16) The fluctuations of E_{HV} around the value (D.7) are computed as follows:

a) the average number of electrons crossing the glass is computed by means of the relation

$$\langle n_e \rangle = \frac{E_{HV}}{\varepsilon_c} \frac{1}{t_{HV}} , \qquad (D.8)$$

where the first factor represents the track length of the shower in the lead glass and t_{HV} is the thickness crossed by the axis of the shower inside the HV, measured in radiation lengths;

b) a Poissonian distribution for the number of electrons n_e (treated as a continuous variable) is assumed and used for extracting n_e;

c) the "actual energy" deposited in the HV is computed by the relation

$$E_{HV} = n_e \varepsilon_c t_{HV} , \qquad (D.9)$$

similar to relation (D.8).

(17) When $E_{HV} \neq 0$, one computes the "transit factor" T_f due to the absorption of the light in that part of the lead glass that lies between the point of impact of the shower and the photocathode of the photomultiplier; the amplitude of the HV pulse A_{HV} is connected to the energy E_{HV} by the relation[26]

$$A_{HV} = \frac{E_{HV}}{T_f} , \qquad (D.10)$$

where

$T_f = 1 + \beta_i \ (d - 17.5) \times 10^{-2}$

d = distance from the phototube of the impact point, in cm

$\beta_1 = 2.7$ ("OUT" detector)

$\beta_2 = 1.5$ ("IN" detector).

(18) The events with a number m of fired HV equal to or greater than the trigger mode adopted (for example M_1 or M_4) each with an amplitude equal to or greater than the chosen threshold ($E_{th} \simeq 150$ MeV nominal) are selected and analysed by means of the same programmes used for the events observed experimentally.

D.3 RESULTS OF THE MONTE CARLO COMPUTATION

All computations have been made at $s^{\frac{1}{2}} = 53.2$ GeV, so that Eqs. (D.3) and (D.4) give

$$\langle n_{\pi^0} \rangle = 4.95 \ . \qquad \text{(D.11)}$$

They have been repeated for a few values of E_{cf} and E_{th} and either by neglecting or taking into account the fact that sometimes the shower initiated by a photon in one HV counter gives also in the near-by HV counter a pulse $\geq E_{cf}$. The main features of the various models are summarized in Table D.1. The main results are summarized in Table D.2.

The lower value given by model B with respect to model A for $\langle n_{\pi^0} \rangle_{\geq 1\gamma}$ arises from the fact that by introducing a trigger with a higher threshold one selects events of higher multiplicity.

The ratio

$$\frac{\langle m_{HV} n \rangle A'}{\langle m_{HV} n \rangle A} = 1.08 \pm 0.02$$

means that the effect of showers trespassing from one HV counter to the others, averaged over the angular distribution and spectrum observed for the single π^0, amounts to 8% in very good agreement with the result of other rather careful evaluations[7].

From the numbers of π^0 giving at least 1 gamma-ray and just 2 gamma-rays within the detector in the case of model A, we deduce:

a) the average number of π^0 producing just 1 gamma-ray within the solid angle of the detector is

$$\langle n_{\pi^0} \rangle_{1\gamma} = \langle n_{\pi^0} \rangle_{\geq 1\gamma} - \langle n_{\pi^0} \rangle_{2\gamma} = 1.63 - 0.39 = 1.24 \ , \qquad \text{(D.12)}$$

b) the average number of gamma-rays within the solid angle of the detector per neutral pion detectable is

$$\frac{\langle n_\gamma \rangle}{\langle n_{\pi^0} \rangle_\Omega} = 2 \times \frac{\langle n_{\pi^0} \rangle_{2\gamma}}{\langle n_{\pi^0} \rangle_{\geq 1\gamma}} + 1 \times \frac{\langle n_{\pi^0} \rangle_{1\gamma}}{\langle n_{\pi^0} \rangle_{\geq 1\gamma}} =$$

$$= 2 \times \frac{0.39}{1.63} + 1 \times \frac{1.24}{1.63} = 2 \times 0.24 + 1 \times 0.76 = 1.24 \ . \qquad \text{(D.13)}$$

It may be useful to notice that the first line of Eq. (D.13) can be written in the form

$$\frac{\langle n_\gamma \rangle}{\langle n_{\pi^0} \rangle_\Omega} = 1 + \frac{\langle n_{\pi^0} \rangle_{2\gamma}}{\langle n_{\pi^0} \rangle_{>1\gamma}} = 1 + 0.24 \ . \qquad \text{(D.14)}$$

Only a part of these gamma-rays are actually detected because: (i) the cut-off energy used in the analysis of the Čerenkov is set at $E_{cf} = 30$ MeV; (ii) sometimes 2 gamma-rays cross the same Čerenkov counter.

The actual number of HV^n fired by gamma-rays is provided by the Monte Carlo: for the computation A′ one obtains:

$$\langle m_{HV^n} \rangle_{A'} = 1.61 \pm 0.01 \ . \qquad \text{(D.15)}$$

Dividing this figure by $\langle n_{\pi^0} \rangle_{\geq 1\gamma}$ we obtain

$$\frac{\langle m_{HV^n} \rangle}{\langle n_{\pi^0} \rangle_{\geq 1\gamma}} = \frac{1.61 \pm 0.01}{1.63 \pm 0.01} = 0.99 \pm 0.01 \ . \qquad \text{(D.16)}$$

This figure should be independent (or almost independent) of the assumption of full uncorrelation of the emitted pions, since it is determined by the spectrum of the single π^0 and the geometry of the detector. Therefore we can assume that in the CCR detector the number of fired HV^n practically coincides with the corresponding number of π^0 at least as long as n_γ is not too far from $\langle n_{\pi^0} \rangle$.

Other results are:

i) The gamma-ray solid angles of the HV counters in the c.m. of the pp collision (Table D.3).

ii) The multiplicity distribution of the fired HV (m_{HV}) and of the π^0 (n_{π^0}) with ≥ 1 gamma in the detector (Table D.4).

iii) The dependence of m_{HV} on the value adopted for E_{cf} (Table D.5).

Table D.1

Main features of the various Monte Carlo computations

Model	E_{cf} (MeV)	E_{th} (MeV)	Showers trespassing from one HV to the next one	Trigger mode
A	30	150	no	M_1
A′	30	150	yes	M_1
B	10	10		

Table D.2

Main results of Monte Carlo computations

Model	3,810 events		9,956 events	
	$\langle n_{\pi^0} \rangle_{\geq 1\gamma}$	$\langle n_{\pi^0} \rangle_{2\gamma}$	$\langle m_{HV} n \rangle$	σ
A	1.63 ± 0.01	0.39 ± 0.09	1.49 ± 0.01	0.71
A′	1.63 ± 0.01	0.39 ± 0.09	1.61 ± 0.01	0.71
	22,420 events			
B	1.36 ± 0.004	0.17 ± 0.0026		

Table D.3

Gamma-ray solid angles of the HV counters in the c.m. of the pp collision from the centre of the interaction region

HV	1	3	5	7	Ω^*_{tot}
	2	4	6	8	
	15	13	11	9	
	16	14	12	10	
Ω^*_{OUT}	0.0655	0.0835	0.1020	0.1143	1.4612
Ω^*_{IN}	0.03795	0.0500	0.06150	0.06885	0.8732
					2.3344
Ω_{lab} †)	0.050	0.063	0.081	0.089	

†) Computed from the geometry

Table D.4

Multiplicity distributions of fired HV and π^0 detected per event

m_{HV}	N/N_{tot}	n_{π^0}	N/N_{tot}
0	-	0	0.640
1	0.552	1	0.332
2	0.320	2	0.026
3	9.773×10^{-2}	3	0.0013
4	2.501×10^{-2}		
5	3.817×10^{-3}		
6	1.004×10^{-3}		
7	2.009×10^{-4}		
	N_{tot} = 9,956 events		N_{tot} = 3,810 events

Table D.5

Dependence on E_{cf} of the mean number of fired HV

E_{cf} (MeV)	$\langle m_{HV} \rangle$
10	1.652
30	1.487
60	1.301
150	1.059
200	0.546
250	0.299

APPENDIX E

INDEPENDENT EMISSION MODEL (IEM)

The IEM presented in this Appendix, although based on the same general assumptions, has advantages and disadvantages with respect to the Monte Carlo computation given in Appendix D. Some of the instrumental features of our experimental set-up that are easily taken into account in the Monte Carlo computation are not incorporated in the IEM because it would become unnecessarily complicated. The IEM, however, provides its results in the form of an analytic expression much more transparent, from the physical point of view, than tables of numbers or histograms.

The assumption of no correlations between the particles emitted in a high-energy collision of hadrons is expressed by the adoption of the following form for the inclusive cross-section for emission of at least n identical particles (pions)[27]

$$\frac{1}{\sigma_{inel}} \frac{d^n\sigma_{in}}{d\xi_1, \ldots, d\xi_n} = \prod_1^n{}_i \rho(p_i) , \tag{E.1}$$

where

$$d\xi_i = \frac{d^3p_i}{E_i}$$

and

$$\rho(p_i) = \frac{1}{\sigma_{inel}} \frac{d^1\sigma_{in}}{d\xi_i} \tag{E.2}$$

is the single-particle distribution function for a pion of momentum p_i.

The exclusive cross-section of n particles

$$\frac{1}{\sigma_{inel}} \frac{d^n\sigma_{ex}}{d\xi_i, \ldots, d\xi_n} = e^{-\langle n\rangle} \prod_1^n{}_i \rho(p_i) \tag{E.3}$$

and the probability that m particles are produced in a phase-space volume Ω

$$\psi_m(\Omega) = \psi_m^P(\langle m\rangle_\Omega) = \frac{\langle m\rangle_\Omega^m}{m!} e^{-\langle m\rangle_\Omega} \tag{E.4}$$

are easily derived from Eq. (E.1)[27,28].

We recall that

$$\langle n \rangle = \int \rho(p_i)\, d\xi_i \tag{E.5}$$

is the average number of π^0 mesons emitted per inelastic collision in the available phase space, and

$$\langle m \rangle_\Omega = \int_\Omega \rho(p_i)\, d\xi_i \tag{E.6}$$

is the average number of π^0 mesons emitted in the phase-space volume Ω per inelastic collision. The same expression (E.4) is easily obtained by assuming that the cross-section σ_n per production of n pions in the whole phase space follows the Poisson law:

$$\frac{\sigma_n}{\sigma_{inel}} = \psi_n^P(\langle n \rangle) \ . \tag{E.7}$$

For the distribution function when there are at least t particles in Ω -- i.e. with our trigger mode M_t -- we obtain[28]

$$\rho_{\geq t}(p) = \rho(p)\ \psi_{\geq t-1}(\Omega) \ , \tag{E.8a}$$

where

$$\psi_{\geq t-1}(\Omega) = \sum_{t-1}^{\infty} {}_n \frac{\langle m \rangle_\Omega}{n!}\, e^{-\langle m \rangle_\Omega} \ . \tag{E.8b}$$

Equations (E.8) predict a series of parallel momentum (and energy) distributions for different t which seems to be generally observed (Fig. 29).

E.1 THE $\pi^0 \to 2\gamma$ DECAY

Equations (E.4) and (E.8) give the qualitative aspects of uncorrelated pion production but, for a quantitative comparison, at least the $\pi^0 \to 2\gamma$ kinematics must be included.

We introduce the probability functions $\Gamma_0(p_i)$, $\Gamma_1(p_i)$, $\Gamma_2(p_i)$, which are the probabilities that a π^0 of momentum p_i deposits 0, 1 or 2 gammas in Ω. These can be obtained by integrating the decay probability over appropriate phase-space regions of the photon momenta.

In the IEM we obtain the following gamma-ray multiplicity distribution

$$\psi_m = \sum_{m_0}^{m} {}_j\ \psi_{2j-m}^P(\bar{n}_1)\ \psi_{m-j}^P(\bar{n}_2) \ , \tag{E.9}$$

where

$$m_0 = \begin{cases} \frac{m}{2} & \text{if m is even} \\ \frac{m+1}{2} & \text{if m is odd} \end{cases}$$

and

$$\bar{n}_1 = \int \Gamma_1(p)\ \rho(p)\ dp \qquad \text{(E.10a)}$$

$$\bar{n}_2 = \int \Gamma_2(p)\ \rho(p)\ dp \qquad \text{(E.10b)}$$

are the average numbers of π^0 which deposit 1 and 2 gammas in Ω, respectively.

The derivation of Eq. (E.9) proceeds in the following way. The probability of producing n pions is expressed as an integral over all phase space of the exclusive cross-section $(1/\sigma_{inel})\ (d^n\sigma_{ex}/d\xi, \ldots, d\xi_n)$. The probability functions Γ_0, Γ_1 and Γ_2 are then introduced into the integral by multiplying the integrand by

$$\prod_{i=1}^{n} \left[\Gamma_0(p_i) + \Gamma_1(p_i) + \Gamma_2(p_i)\right]$$

which is unity by definition of the Γ's. The contribution of m pions to the production of N gammas in Ω can then be identified and Eq. (E.9) can be obtained by summation over m.

Integrating the single-particle distribution obtained by Winter[8] by using the Monte Carlo computation (Appendix D), we obtain

$$\bar{n}_1 = \frac{1.24}{4.95} = 0.25, \quad \bar{n}_2 = \frac{0.39}{4.95} = 0.079\ . \qquad \text{(E.11)}$$

In these calculations, we have ignored the effect of the threshold of our trigger which records events only if there is at least 1 gamma in Ω with $E \geq E_{th} \simeq 160$ MeV. This effect will now be estimated. The phase space available for the trigger is denoted by Ω_t. If we denote by $\psi_{N_1 N_0}$ the multiplicity distribution when there is at least N_0 gammas in the Ω_t, then

$$\psi_N - \psi_{N_1 N_0} = \sum_{j=0}^{N_0-1} \psi_{N,j}(\Omega,\Omega_t)\ , \qquad \text{(E.12)}$$

where $\psi_{N,j}(\Omega,\Omega_t)$ is the multiplicity distribution when there are exactly j particles in Ω_t. For $N_0 = 1$, noting that $\psi_{N,0}(\Omega,\Omega_t)$ is simply the distribution for the phase volume $\Omega - \Omega_t$, and assuming $\bar{n}_2$ to represent uncorrelated gammas, we may write

$$\psi_{N,1} = (1 - x^N)\ \psi_N\ , \qquad \text{(E.13)}$$

where $x = \bar{N}(\Omega,\Omega_t)/\bar{N}(\Omega)$ is the ratio of $\bar{n}_1$ for $\Omega - \Omega_t$ and $\bar{n}_1$ for Ω. The Monte Carlo yields a value of 0.9 for x, and the effect on the multiplicity distribution is to reduce the small N part of ψ_N but as N gets large, $\psi_{N,1}$ and ψ_N become equal. Equation (E.13) using Eq. (E.11) is plotted in Fig. 39.

APPENDIX F

ESTIMATE OF THE CORRECTIONS TO THE INCLUSIVE GAMMA-RAY PRODUCTION CROSS-SECTION

In Eq. (4.4) the cross-section for production of gamma-rays is expressed in terms of the ratio of measured numbers

$$\left[\frac{M_1 \Sigma\Sigma(90°)}{\Sigma\Sigma}\right], \tag{F.1}$$

where for simplicity of notation we have dropped the lower limit on the energy of the detected photons. In the same Eq. (4.4) we have introduced a factor 1/F for taking into account the bias introduced in our data by requiring that in each event besides t (= 1) photons there should be at least one charged particle crossing each of the two downstream counters $\Sigma_1(B_1)$, $\Sigma_2(B_2)$. In this appendix we shall derive the exact expression of F and show that its value differs from unity by at most 30%. Under this circumstance it appears justified to deduce the values (4.7) computed with F = 1, and to state that they agree as well as can be expected with those deduced by other authors from measurements of the one-photon inclusive cross-section.

We use the K.N.O. formalism generalized to the case of three non-overlapping phase-space regions[29] which, in our case, are those defined by the counters as follows:

for gamma-rays: the HV counters at 90° $\quad -0.2 \leq \eta_0 \leq +0.2$

for charged particles: the $\Sigma_1(B_1)$ counter $\quad -4.9 \leq \eta_1 \leq -3.1$ $(-4.7 \leq \eta_1 \leq -3.8)$

the $\Sigma_2(B_2)$ counter $\quad +3.1 \leq \eta_2 \leq +4.9$ $(+3.8 \leq \eta_2 \leq +4.7)$.

The ratio (F.1) is given by the expression

$$\left[\frac{M_1 \Sigma\Sigma(90°)}{\Sigma\Sigma}\right] = \frac{\phi_3(HV,\Sigma_1,\Sigma_2)}{\phi_2(\Sigma_1,\Sigma_2)}, \tag{F.2}$$

where

$$\phi_k(\alpha,\beta,\ldots) = \int_\alpha \bar{d}p_1 \int_\beta \bar{d}p_2 \ \ldots \int \bar{d}p_k \ \Phi^{(k)}(p_1,\ldots,p_k) \tag{F.3}$$

and $\Phi^{(k)}$ is the k-particle normalized inclusive cross-section. We recall now the relations

$$\phi_2(\Sigma_1,\Sigma_2) = f_2(\Sigma_1,\Sigma_2) + f_1(\Sigma_1)\cdot f_1(\Sigma_2)$$

$$\phi_3(HV,\Sigma_1,\Sigma_2) = f_3(HV,\Sigma_1,\Sigma_2) + f_1(HV)\cdot f_2(\Sigma_1,\Sigma_2) + \quad (F.4)$$
$$+ f_1(\Sigma_1)\cdot f_2(HV,\Sigma_2) + f_1(\Sigma_2)\cdot f_2(HV,\Sigma_1) +$$
$$+ f_1(HV)\cdot f_1(\Sigma_1)\cdot f_1(\Sigma_2)$$

where

$$f_1(\alpha) = \phi_1(\alpha)$$
$$f_2(\alpha,\beta) = \int_\alpha d\eta_1 \int_\beta d\eta_2 \; C(\eta_1,\eta_2) \quad (F.5)$$

with $C(\eta_1,\eta_2)$ given by (6.1). With the notation

$$\bar{R}(\alpha,\beta) = \frac{f_2(\alpha,\beta)}{f_1(\alpha)\cdot f_2(\beta)}$$
$$\bar{S}(\alpha,\beta,\gamma) = \frac{f_3(\alpha,\beta,\gamma)}{f_1(\alpha)\cdot f_1(\beta)\cdot f_1(\gamma)} \quad (F.6)$$

we obtain

$$\left[\frac{M_1\Sigma\Sigma(90°)}{\Sigma\Sigma}\right] = \phi_1(HV)\cdot F \quad (F.7)$$

where

$$F = 1 + \frac{\bar{R}(HV,\Sigma_1) + \bar{R}(HV,\Sigma_2) + \bar{S}(HV,\Sigma_1,\Sigma_2)}{1 + \bar{R}(\Sigma_1,\Sigma_2)} \; . \quad (F.8)$$

In conclusion the one gamma-ray inclusive cross-section $\phi_1(HV)$ that would be observed in the HV counters at 90° is obtained by dividing the ratio (F.1) by the numerical factor (F.8). This is expressed in terms of $\bar{R}$ and $\bar{S}$, where $\bar{R}$ differs from (6.3) only because numerator and denominator have been integrated over the phase-space volumes defined by the two counters.

The ratio $\bar{S}$ is similar to $\bar{R}$ but refers to triple coincidence. The pertinent values of $\bar{R}$ can be easily deduced from the results of various authors. Thus

$$\bar{R}(\Sigma_1,\Sigma_2) \simeq R(-4,+4)$$
$$\bar{R}(HV,\Sigma_1) \equiv \bar{R}(HV,\Sigma_2) \simeq R(0,\pm 4)$$

can be read from Fig. 22 [30]. One has

$$\bar{R}(\Sigma_1,\Sigma_2) \lesssim 0.05 \quad \bar{R}(HV,\Sigma_1) \lesssim 0.1 \; .$$

Measurements of $\bar{S}$ are not yet available, but one finds from all indications that it should be $\lesssim 1/3$ of $\bar{R}$.

In conclusion F should be not greater than 1.3 and for $|\eta_\alpha - \eta_\beta| >> \Delta\eta_\alpha, \Delta\eta_\beta$ it is practically independent of the dimensions of the counters, in particular the dimensions of Σ_1 and Σ_2 which determine the numerator as well as the denominator of (F.1) and appear in the numerator and denominator $\bar{R}$ and $\bar{S}$.

REFERENCES

1) E. Amaldi, M. Beneventano, B. Borgia, G.F. Dell, J.P. Dooher, P. Pistilli, H. Uto and L.C.L. Yuan, CERN/ISRC/70-19, 2 October 1970; CERN/ISRC/70-19 Rev., 1 November 1970; CERN/ISRC/70-19 Rev. 2, Part I: Search for high energy multigamma events; Part II: A few considerations concerning the search for multigamma ray events produced in p-p collisions; CERN/ISRC/70-19 Add, Revised proposal to the ISR: 27 May 1971; CERN/ISRC/72-22, 1 August 1972, Proposal for an experiment on multigamma (to NASA, NSF, AEC); Revision No. 4 of the Proposal to the CERN ISR, 12 January 1973.

2) M. Schein, D.M. Haskin and M.G. Glasser, Phys. Rev. 95, 855 (1954); 99, 643 (1955).
A. Debenedetti, C.M. Garelli, L. Tallone and M. Vigone, Nuovo Cimento 2, 220 (1955); 4, 115 (1956).
A. Jurak, M. Miesonicz, O. Stanisz and W. Walter, Bull. Acad. Polon. Sci. Cl. III 3, 369 (1955).
M. Koshiba and M.F. Kaplan, Phys. Rev. 100, 327 (1955).
L. Bardanti-Silva, C. Bonacini, C. De Pietri, I. Iori, G. Lovera, R. Petrilli-Fedeli and A. Roveri, Nuovo Cimento 3, 1465 (1956).

3) F.W. Büsser, L. Camilleri, L. Di Lella, G. Gladding, A. Placci, B.G. Pope, A.M. Smith, J.K. Yoh, E. Zavattini, B.J. Blumenfeld, L.M. Lederman, R.L. Cool, L. Litt and S.L. Segler, Phys. Letters 46B, 471 (1973); 48B, 371 (1974).

4) E. Amaldi, M. Beneventano, B. Borgia, G.F. Dell, J.P. Dooher, P. Pistilli, H. Uto and L.C.L. Yuan, Report on the exploratory tests for a search for multigamma events, 8 December 1971; CERN/ISRC/73-7, 17 March 1973; Progress report on the exploratory experiment on the production of multigamma events at the ISR presented by E. Amaldi to the Meeting of the ISR Committee, 12 June 1972.

5) J.S. Beale, F.W. Büsser, L. Camilleri, L. Di Lella, G. Gladding, A. Placci, B.G. Pope, A.M. Smith, B. Smith, J.K. Yoh, E. Zavattini, B.J. Blumenfeld, L.M. Lederman, R.L. Cool, L. Litt and S.L. Segler, Nuclear Instrum. Methods 117, 501 (1974).

6) C. Castagnoli, G. Cortini, C. Franzinetti, A. Manfredini and D. Moreno, Nuovo Cimento 10, 1539 (1953).

7) E. Longo and I. Sestili, Monte Carlo calculations of photon-initiated electromagnetic showers in lead glass, Istituto di Fisica G. Marconi, INFN Sezione di Roma, Nota Interna No. 587, 16 October 1974.

8) G. Neuhofer, F. Niebergall, J. Penzias, M. Regler, K.R. Schubert, P.E. Schumacher, W. Schmidt-Parzefall and K. Winter, Phys. Letters 37B, 438 (1971); 38B, 51 (1972).

9) K.R. Schubert, VII Rencontre de Moriond sur les interactions électromagnétiques, March 1972 (CNRS, Paris, 1972), vol. 2, p. 305.

10) See, for example, Chapter XI of the treatise by R. von Mieses (Edited and complemented by Gerringer), Mathematical theory of probability and statistics (Academic Press, New York and London, 1964).

11) P. Capiluppi, G. Giacomelli, A.M. Rossi, G. Vannini, A. Bertin, A. Bussière and R.J. Ellis, Nuclear Phys. B79, 189 (1974). The 22% is the sum of 4% K^+, 3% K^-, 14% p and 1% $\bar{p}$.

12) ISR Discussion Meeting between experimentalists and theorists No. 7, November 1973, CERN Internal report (ed. M. Jacob), Particle ratios reviewed by L. Leistam. The charged pions component decreases by increasing p_t.

13) ISR Discussion Meeting between experimentalists and theorists No. 10, May 1974, CERN Internal Report (ed. M. Jacob), British-Scandinavian Collaboration.

14) V.G. Grishin, G. Jancsò, S.P. Kuleshov, V.A. Matveev and A.N. Sijsakian, Lett. Nuovo Cimento 8, 590 (1973).

15) ISR Discussion Meeting between experimentalists and theorists No. 10, May 1974, CERN Internal Report (ed. M. Jacob). The ACHM and PSB results were presented by P. Dittman and R. Kephart.

16) G. Bellettini, Proc. 16th Internat. Conf. on High-Energy Physics, Batavia, 1972 (eds. J.D. Jackson and A. Robert) (NAL, Batavia, Ill., 1973), Vol. 1, p. 279.

17) H. Dibon, G. Flügge, Ch. Gottfried, B.M.K. Nefkens, G. Neuhofer, F. Niebergall, M. Regler, W. Schmidt-Parzefall, K.R. Schubert, P.E. Schumacher and K. Winter, Phys. Letters 44B, 313 (1973).

18) G.H. Thomas and B.R. Weber, ANL/HEP 7368.

19) We have adopted the notations used by Z. Koba, Multibody phenomena in strong interactions, *in* Proc. 1973 CERN-JINR School of Physics, Ebeltoft, Denmark, 17-30 June 1973, CERN 73-12 (1973), p. 170.

20) For an even more extensive discussion see L. Luminari, Doctoral Thesis, University of Rome, May 1974.

21) E.I. Feniberg, Phys. Reports 5, 238 (1972).

22) See, for example, A.N. Diddens and K. Schlüpmann, Particle production in proton-proton interactions, to be published in Landolt-Börnstein.

23) S.N. Ganguli and P.K. Malhotra, Phys. Letters 39B, 632 (1972).

24) M. Antinucci, A. Bertin, P. Capiluppi, M. D'Agostino-Bruno, A.M. Rossi, G. Vannini, G. Giacomelli and A. Bussière, Lett. Nuovo Cimento 6, 121 (1973).

25) See, for example, B. Rossi, High energy particles (Prentice Hall, New York, 1952).

26) CCR Collaboration, private communication.

27) Z. Koba, H.B. Nielson and P. Olesen, Nuclear Phys. 43B, 125 (1972).

28) J. Dooher, Grumman Aerospace Corporation Research Note RN 336, July 1972; appeared also as Appendix C of Revision No. 4 of the Proposal to CERN ISR, January 1973, by E. Amaldi et al. (see Ref. 1).

29) See, for example, Z. Koba, Multi-body phenomena in strong interactions, Proc. 1973 CERN-JINR School of Physics, Ebeltoft, 1973 (CERN 73-12, 1973), p. 171.

30) G. Bellettini, Results from the Pisa-Stony Brook ISR experiment, Proc. Int. Conf. on High Energy Collisions, Stony Brook, 1973 (ed. C. Quigg) (AIP Conf. Proc. No. 15, AEC CONF 730841, New York, 1973), p. 9.